

Computational Cosmology

Habilitationsschrift

zur Erlangung der *venia legendi*
für das Fach Astronomie & Astrophysik

eingereicht an der
Mathematisch-Naturwissenschaftlichen Fakultät
der Universität Potsdam

von
Dr. Alexander Knebe
(geboren am 31. Januar 1970 in Kiel)

Potsdam, im November 2008

Published online at the
Institutional Repository of the University of Potsdam:
URL <http://opus.kobv.de/ubp/volltexte/2010/4114/>
URN <urn:nbn:de:kobv:517-opus-41147>
<http://nbn-resolving.org/urn:nbn:de:kobv:517-opus-41147>

Populärwissenschaftliches Abstract zur Habilitationsschrift

Computational Cosmology,
vorgelegt von Dr. Alexander Knebe

Die Kosmologie ist heutzutage eines der spannendsten Arbeitsgebiete in der Astronomie und Astrophysik. Das vorherrschende (Urknall-)Modell in Verbindung mit den neuesten und präzisesten Beobachtungsdaten deutet darauf hin, daß wir in einem Universum leben, welches zu knapp 24% aus Dunkler Materie und zu 72% aus Dunkler Energie besteht; die sichtbare Materie macht gerade einmal 4% aus. Und auch wenn uns derzeit eindeutige bzw. direkte Beweise für die Existenz dieser beiden exotischen Bestandteile des Universums fehlen, so ist es uns dennoch möglich, die Entstehung von Galaxien, Galaxienhaufen und der großräumigen Struktur in solch einem Universum zu modellieren. Dabei bedienen sich Wissenschaftler Computersimulationen, welche die Strukturbildung in einem expandierenden Universum mittels Großrechner nachstellen; dieses Arbeitsgebiet wird Numerische Kosmologie bzw. “Computational Cosmology” bezeichnet und ist Inhalt der vorliegenden Habilitationsschrift.

Nach einer kurzen Einleitung in das Themengebiet werden die Techniken zur Durchführung solcher numerischen Simulationen vorgestellt. Die Techniken zur Lösung der relevanten (Differential-)Gleichungen zur Modellierung des “Universums im Computer” unterscheiden sich dabei teilweise drastisch voneinander (Teilchen- vs. Gitterverfahren), und es werden die verfahrenstechnischen Unterschiede herausgearbeitet. Und obwohl unterschiedliche Programme auf unterschiedlichen Methoden basieren, so sind die Unterschiede in den Endergebnissen doch (glücklicherweise) vernachlässigbar gering. Wir stellen desweiteren einen komplett neuen Code – basierend auf dem Gitterverfahren – vor, welcher einen Hauptbestandteil der vorliegenden Habilitation darstellt.

Im weiteren Verlauf der Arbeit werden diverse kosmologische Simulationen vorgestellt und ausgewertet. Dabei werden zum einen die Entstehung und Entwicklung von Satellitengalaxien – den (kleinen) Begleitern von Galaxien wie unserer Milchstraße und der Andromedagalaxie – als auch Alternativen zum oben eingeführten “Standardmodell” der Kosmologie untersucht. Es stellt sich dabei heraus, daß keine der (hier vorgeschlagenen) Alternativen eine bedrohliche Konkurrenz zu dem Standardmodell darstellt. Aber nichtsdestoweniger zeigen die Rechnungen, daß selbst so extreme Abänderungen wie z.B. modifizierte Newton’sche Dynamik (MOND) zu einem Universum führen können, welches dem beobachteten sehr nahe kommt.

Die Ergebnisse in Bezug auf die Dynamik der Satellitengalaxien zeigen auf, daß die Untersuchung der Trümmerfelder von durch Gezeitenkräfte zerriebenen Satellitengalaxien Rückschlüsse auf Eigenschaften des ursprünglichen Satelliten zulassen. Diese Tatsache wird bei der Aufschlüsselung der Entstehungsgeschichte unserer eigenen Milchstraße von erheblichem Nutzen sein. Trotzdem deuten die hier vorgestellten Ergebnisse auch darauf hin, daß dieser Zusammenhang nicht so eindeutig ist, wie er zuvor mit Hilfe kontrollierter Einzelsimulationen von Satellitengalaxien in analytischen “Mutterpotentialen” vorhergesagt wurde: Das Zusammenspiel zwischen den Satelliten und der Muttergalaxie sowie die Einbettung der Rechnungen in einen kosmologischen Rahmen sind von entscheidender Bedeutung.

Summary

“Computational Cosmology” is the modeling of structure formation in the Universe by means of numerical simulations. These simulations can be considered as the only “experiment” to verify theories of the origin and evolution of the Universe. Over the last 30 years great progress has been made in the development of computer codes that model the evolution of dark matter (as well as gas physics) on cosmic scales and new research discipline has established itself.

After a brief summary of cosmology we will introduce the concepts behind such simulations. We further present a novel computer code for numerical simulations of cosmic structure formation that utilizes adaptive grids to efficiently distribute the work and focus the computing power to regions of interests, respectively. In that regards we also investigate various (numerical) effects that influence the credibility of these simulations and elaborate on the procedure of how to setup their initial conditions. And as running a simulation is only the first step to modelling cosmological structure formation we additionally developed an object finder that maps the density field onto galaxies and galaxy clusters and hence provides the link to observations.

Despite the generally accepted success of the cold dark matter cosmology the model still inhibits a number of deviations from observations. Moreover, none of the putative dark matter particle candidates have yet been detected. Utilizing both the novel simulation code and the halo finder we perform and analyse various simulations of cosmic structure formation investigating alternative cosmologies. These include warm (rather than cold) dark matter, features in the power spectrum of the primordial density perturbations caused by non-standard inflation theories, and even modified Newtonian dynamics. We compare these alternatives to the currently accepted standard model and highlight the limitations on both sides; while those alternatives may cure some of the woes of the standard model they also inhibit difficulties on their own.

During the past decade simulation codes and computer hardware have advanced to such a stage where it became possible to resolve in detail the sub-halo populations of dark matter halos in a cosmological context. These results, coupled with the simultaneous increase in observational data have opened up a whole new window on the concordance cosmogony in the field that is now known as “Near-Field Cosmology”. We will present an in-depth study of the dynamics of subhaloes and the development of debris of tidally disrupted satellite galaxies.¹ Here we postulate a new population of subhaloes that once passed close to the centre of their host and now reside in the outer regions of it. We further show that interactions between satellites inside the radius of their hosts may not be negligible. And the recovery of host properties from the distribution and properties of tidally induced debris material is not as straightforward as expected from simulations of individual satellites in (semi-)analytical host potentials.

¹For the purposes of our studies, we treat “substructure haloes” (or subhaloes) and “satellite galaxies” as interchangeable. However, we note that the correspondence between dark matter substructures and luminous satellite galaxies is not a straightforward one.

Preface

The concept of this thesis is to present (part of) my cumulative work of the last decade in a thematically ordered fashion. While the key note of the research presented here is obviously computational cosmology it will be divided into the following sub-categories

- cosmological simulations (Section II),
- alternative cosmologies (Section III), and
- near-field cosmology (Section IV).

However, the thesis starts with a general introduction to cosmology in Section I where the currently accepted standard model alongside the terminology used throughout this thesis will be defined. The subsequent Sections are then summaries of my own contributions to the respective fields. To this extent I will give an introduction at the beginning of each Section motivating the scientific relevance and then present one particular highlight of each paper published by myself in that particular area. The papers that made it into this thesis are the following (ordered chronologically):

- (1) Knebe A., Green A., Binney J.J., 2001, *MNRAS* 325, 845
- (2) Knebe A., Islam R.R., Silk J., 2002, *MNRAS* 326, 109
- (3) Knebe A., Devriendt J.E.G., Mahmood A., Silk J., 2002, *MNRAS* 329, 813
- (4) Binney J.J., Knebe A., 2002, *MNRAS* 333, 378
- (5) Little B., Knebe A., Gibson B.K., 2003, *MNRAS* 341, 617
- (6) Knebe A., Devriendt J.E.G., Gibson B.K., Silk J., 2003, *MNRAS* 345, 1285
- (7) Dominguez A., Knebe A., 2003, *EpL* 4, 631
- (8) Knebe A., Dominguez A., 2003, *PASA* 20, 173
- (9) Knebe A., Gill S.P.D., Gibson B.K., 2004, *PASA* 21, 216
- (10) Knebe A., Gibson B.K., 2004, *MNRAS* 347, 1055
- (11) Knebe A., Gill S.P.D., Gibson B.K., Lewis G.F., Ibata R.A., Dopita M.A., 2004, *ApJ* 603, 7
- (12) Gill S.P.D., Knebe A., Gibson B.K., 2004, *MNRAS* 351, 399
- (13) Gill S.P.D., Knebe A., Gibson B.K., Dopita M.A., 2004, *MNRAS* 351, 410
- (14) Gill S.P.D., Knebe A., Gibson B.K., 2005, *MNRAS* 356, 1327
- (15) Knebe A., 2005, *PASA* 22, 184
- (16) Knebe A., Gill S.P.D., Kawata D., Gibson B.K., 2006, 357, 35
- (17) Power C.B., Knebe A., 2006, *MNRAS* 370, 691
- (18) Knebe A., Power C.B., Gill S.P.D., Gibson B.K., 2006, *MNRAS* 368, 1209
- (19) Warnick K., Knebe A., 2006, *MNRAS* 369, 1253
- (20) Knebe A., Dominguez A., Dominguez-Tenreiro R., 2006, *MNRAS* 371, 1959
- (21) Knebe A., Arnold B., Power C., Gibson B.K., 2008, *MNRAS* 386, 1029
- (22) Warnick K., Knebe A., Power C.B., 2008, *MNRAS* 385, 1859
- (23) Knebe A., Draganova N., Power C., Yepes G., Hoffman Y., Gottlöber S., Gibson B.K., 2008, *MNRAS* 386, L52
- (24) Knebe A., Yahagi H., Kase H., Lewis G.F., Gibson B.K., 2008, *MNRAS* 388, L34

This list is not exhaustive and the total number of peer-reviewed papers published by myself during the years 2001 - 2008 (i.e. after my PhD) is 33 with four more already submitted. The papers excluded from this thesis are mainly in-depth investigations of the properties of galaxies, galaxy clusters, superclusters, and the large-scale clustering patterns forming within the standard cold dark matter paradigm.

Contents

I	Introduction	1
I.1	Cosmology	2
I.2	Friedmann Equations	3
I.3	Structure Formation	4
I.3.1	The Nature of Dark Matter	4
I.3.2	Collisionless Matter	5
I.4	Λ CDM: Concordance Model of Cosmology	6
II	Cosmological Simulations	7
II.1	Introduction	8
II.1.1	The Necessity for Cosmological Simulations	8
II.1.2	The History of Cosmological Simulations	8
II.1.3	The State-of-the-Art of Cosmological Simulations	9
II.2	The N -body Concept	11
II.3	Newtonian Mechanics in Comoving Coordinates	12
II.4	Poisson Solver	14
II.4.1	Tree Codes	14
II.4.2	Particle-Mesh Codes	15
II.4.3	Hybrid Methods	17
II.4.4	Mass Resolution	17
II.4.5	Comparison	18
II.5	Numerical Issues	19
II.5.1	Two-Body Relaxation	19
II.5.2	Finite Box Size Effects	20
II.5.3	Hydrodynamics Approach to the Evolution of Cosmic Structure	20
II.6	MLAPM – Multi-Level-Adaptive-Particle-Mesh	23
II.6.1	Handling Adaptive Meshes	23
II.6.2	Generating Refinements	25
II.6.3	Mass Assignment Scheme	27
II.6.4	Solving Poisson’s Equation	27
II.7	Halo Finding	29
II.7.1	Friends-Of-Friends	29
II.7.2	DENMAX/SKID	29
II.7.3	Bound-Density-Maxima	30
II.7.4	MLAPM’s-Halo-Finder	30
II.8	Initial Conditions	34
II.8.1	Generating Cosmological Initial Conditions	34
II.8.2	The Reliability of Cosmological Initial Conditions	35

III	Alternative Cosmologies	37
III.1	Introduction	38
III.2	Warm Dark Matter	39
III.2.1	The Overabundance of Satellite Galaxies	39
III.2.2	The dynamics of subhaloes in WDM models	41
III.2.3	Top-Down Fragmentation of WDM Filaments	42
III.3	Bumpy Power Spectra	44
III.3.1	Mocking different Cosmologies	44
III.3.2	Bumpy Power Spectra vs. WDM	45
III.4	Modified Newtonian Dynamics	47
IV	Near-Field Cosmology	51
IV.1	Introduction	52
IV.1.1	The Simulations	53
IV.1.2	The Haloes	53
IV.2	Satellite Galaxies	53
IV.2.1	The Dynamics of Satellite Galaxies	54
IV.2.2	The Spatial Anisotropy of Satellite Galaxies	56
IV.2.3	The Radial Alignment of Satellite Galaxies	57
IV.2.4	Backsplash Galaxies: a new population	59
IV.2.5	The Importance of Satellite-Satellite Interactions	60
IV.2.6	The Sense of Rotation of Satellite Galaxies	62
IV.3	Debris from Satellite Galaxies	63
IV.3.1	Mapping Substructures	64
IV.3.2	Tidal Streams of Disrupting Subhaloes	65
V	Conclusions & Outlook	69
V.1	Conclusions	70
V.2	Outlook	72
	Bibliography	75

Part I

Introduction

I.1 Cosmology

Cosmology - the study of the formation and ultimate fate of structures and galaxies throughout the Universe - is without a doubt the dominant field of astrophysics today. And in the last few years theoretical and observational studies have begun to converge as we entered the era of “Precision Cosmology”. A picture has emerged in which contemporary structures have evolved by gravitational amplification of seed inhomogeneities that are likely of quantum origin. This picture ties together measurements of the cosmic background radiation, estimates of the primordial abundances of the light elements, measurements of the clustering of galaxies and, to a more limited extent, the characteristic properties of individual galaxies (e.g. Komatsu *et al.*, 2008).

There are several turning points to mention that mark the maturation of cosmology from mere speculations to a research discipline. It all began when Einstein formulated the theory of general relativity in 1915. It turned out that there are solutions to his equations that did not comply with the understanding of the Universe at that time, e.g. Friedmann found in 1922 that the Universe cannot be static. Only the pivotal discovery of the linear velocity-distance relation for galaxies by Edwin Hubble in 1929 changed that perspective. Nevertheless, there was still the prediction of a primordial singularity for an expanding Universe. Colloquially dubbed “Big Bang” by Fred Hoyle in 1949, it was in the year 1965 that Arno Penzias and Robert Wilson discovered what can be considered the “remnant fireball of the Big Bang”; they (accidentally) observed an “excess antenna temperature” at 4080 Mc/s (Penzias and Wilson, 1965). Already in the same volume of the *Astrophysical Journal* Dicke *et al.* (1965) ascribed a cosmological origin to this radiation, i.e. the cosmic microwave background radiation (CMBR). The CMBR stems from the epoch when matter and radiation no longer could be in thermal equilibrium due to the cooling arising from the expansion of the Universe: protons and electrons combined to hydrogen atoms and the Universe became transparent for (the CMBR) photons.

During the 1970’s scientists tried to piece together the jigsaw of how the big bang theory can give rise to non-linear structures such as galaxies, galaxy groups and clusters. And these years also saw the advent of computer simulations of cosmic structure formation to be elaborated upon in Section II. The required primordial density perturbations superimposed upon an otherwise homogenous and isotropic Universe were only discovered in 1992 by the COBE² satellite. COBE found anisotropies in the CMBR of the order $\Delta T/T \approx 10^{-5}$, just the right order of magnitude if the majority of the matter in the Universe was so-called “cold dark matter”.³

The following years saw the rise of a wealth of observations targetted at improved measurements of the cosmological parameters; parameters that describe the evolution of the Universe as a whole. And these observations converged to what has been called the “concordance model of cosmology” to be explained in greater detail in Section I.4.

²Cosmic Microwave Background Explorer

³Already at that time it was clear that the rotation curves of individual galaxies as well as the velocity dispersion of galaxies in clusters cannot be explained by luminous matter alone. Additional matter that only interacts via gravity was required to explain the inferred gravity.

I.2 Friedmann Equations

The central equations describing the evolution of the Universe as a whole were first formulated by Alexander Friedmann in the year 1922. They can be derived from Einstein's field equations of general relativity under the assumption of homogeneity and isotropy. In mathematical terms this comes down to using

$$G^{\mu\nu} + \Lambda g^{\mu\nu} = -\frac{8\pi G}{c^4} T^{\mu\nu} \quad (\text{I.1})$$

together with the (homogeneous and isotropic) Robertson-Walker metric

$$ds^2 = dt^2 - a^2(t) \left(\frac{dr^2}{1 - kr^2} + r^2(d\theta^2 + \sin\theta d\phi^2) \right), \quad (\text{I.2})$$

where $G^{\mu\nu}$ is the *Einstein tensor*, $T^{\mu\nu}$ the *energy-momentum tensor*, Λ the cosmological constant, $a(t)$ the cosmic expansion factor (which determines the overall scale of the spatial metric), and k the curvature parameter.

Under the further assumption that the Universe is filled with a perfect fluid (and hence constraining the energy-momentum tensor correspondingly) one arrives at the following set of two independent equations, the *Friedmann equations*:

$$\left(\frac{\dot{a}}{a}\right)^2 = \left(\frac{\dot{a}}{a}\right)_0^2 \left(\Omega_{r,0} a^{-4} + \Omega_{m,0} a^{-3} + \Omega_{k,0} a^{-2} + \Omega_{\Lambda,0} \right) \quad (\text{I.3})$$

$$\ddot{a} = \frac{4\pi G}{3} a(\rho - \rho_{\Lambda})$$

where the *density parameters* are defined as follows:

$$\begin{aligned} \Omega_{r,0} &= \frac{\rho_r}{\rho_{\text{crit}}} \\ \Omega_{m,0} &= \frac{\rho_m}{\rho_{\text{crit}}} \\ \Omega_{k,0} &= \frac{-k}{a_0^2 H_0^2} \\ \Omega_{\Lambda,0} &= \frac{\rho_{\Lambda}}{\rho_{\text{crit}}} \end{aligned} \quad (\text{I.4})$$

The normalisations used in the definitions of the density parameters are as follows

$$\begin{aligned} \rho_{\text{crit}} &= \frac{3H_0^2}{8\pi G} \\ \rho_{\Lambda} &= \frac{\Lambda}{8\pi G} \\ H &= \frac{\dot{a}}{a} \end{aligned} \quad (\text{I.5})$$

where ρ_{crit} is referred to as the *critical density* of the Universe (required to obtain a spatially flat universe – in the absence of ρ_{Λ}) and H_0 is today's value of the *Hubble parameter*.

The solution $a(t)$ to Eq. (I.3) describes the expansion/contraction of the Universe and sensitively depends on these parameters. The determination of these crucial values for cosmology needs to be done observationally and a lot of efforts during the past decade has been directed towards their confirmation.

I.3 Structure Formation

One of the underlying assumption in the derivation of the Friedmann Eq. (I.3) is the *cosmological principle*, i.e. that the Universe is homogenous and isotropic (cf. Robertson-Walker metric Eq. (I.2)). However, this is not what we observe! We see highly inhomogeneous structures such as galaxies and galaxy clusters alongside the filamentary structure of the Universe.

The just introduced density parameters determine how the Universe as a whole evolves in time. However, structure formation depends on a couple of more values. Small deviations from homogeneity and isotropy need to exist in the early Universe. They likely have their origin in quantum fluctuations and are produced in a phase shortly after the big-bang called *inflation*. These fluctuations are thought to be of Gaussian nature and can hence be described by a power spectrum. The overall amplitude of this power spectrum is yet another parameter to be fixed in order to have a credible model for cosmological structure formation. Further, the shape of the power spectrum of primordial density perturbation also depends on the nature of the (dark) matter. For instance, hot dark matter leads to a different structure formation scenario than cold dark matter: due to its relativistic nature, hot dark matter erases fluctuations on small scales and therefore has difficulties to form objects like galaxies whereas cold dark matter induces hierarchical structure formation by which small entities form first and subsequently merge to build larger and larger objects (e.g. Davis *et al.*, 1985). As we will later on return to the nature of dark matter (and actually question it in Section III.1) we are going to elaborate upon the differences in more detail now.

I.3.1 The Nature of Dark Matter

Cold dark matter (CDM) means that dark matter had negligible thermal velocities $kT \ll mc^2$ in the early universe. As mentioned in, for instance, Primack (2003), this assumption can be satisfied by two complementary sorts of particles:

1. dark matter particles are *WIMPs* (*Weakly Interacting Massive Particles*, such as the *neutralino*) with mass $m \approx 100\text{GeV}$ and a cross-section of $\sigma \approx 10^{-38}\text{cm}^2$,
2. dark matter particles are *axions* with mass $m \approx 10^{-5}\text{eV}$ and hence having non-relativistic velocities $kT \ll mc^2$, as they do not originate from a thermal mechanism in the early universe.

Other authors (e.g. Colín *et al.*, 2000) define a dark matter particle to be cold if and only if it has a mass of $m \gg 1\text{GeV}$ and the strength of its interaction is comparable to the strength of weak interaction.

The CDM model is the most favoured in structure formation scenarios first introduced by Peebles (1982) and entails (as already mentioned) hierarchical growth of structures.

Further, this model is in good agreement with several observations. It correctly predicts the abundances of galaxy clusters nearby and at $z \leq 1$. The power spectrum of (primordial) density perturbations is consistent with measurements from CMB anisotropies (Komatsu *et al.*, 2008) and with the flux power spectrum inferred from Ly α forest spectra (Croft *et al.*, 2002).

However, there also exist drawbacks that will be expanded upon later on in Section III.1.

Hot dark matter (HDM) has relativistic thermal velocities $kT \gg mc^2$. Hence, structures at significant scales up to tens of Mpc's are “washed out”. This model therefore entails fragmentation processes to form structures (cf. Doroshkevich *et al.*, 1974). As this model does not agree with, for instance, the clustering pattern of galaxies as observed (and simulated) it has been discarded already a long time ago (cf. Peebles, 1982; Bond and Szalay, 1983; White *et al.*, 1983). However, we need to mention that massive neutrinos are in fact hot dark matter particles. The discrepancy between hot dark matter models and observations therefore places constraints on the allowed mass range for neutrinos.

I.3.2 Collisionless Matter

The different kinds of dark matter have in common to be collisionless, as underlined by their estimated mean free path λ . Particle physics experiments lead to a WIMP-nucleon elastic-scattering cross section of at minimum $\sigma \approx 4 \times 10^{-43} \text{cm}^2$ at a WIMP mass of 60GeV (cf., e.g., Akerib *et al.*, 2005). Varying the mass m of a dark-matter particle between $1 \text{keV} \lesssim m \lesssim 100 \text{GeV}$ induces a number density n of dark matter between $1 \text{cm}^{-3} \lesssim n \lesssim 6 \cdot 10^{-8} \text{cm}^{-3}$. Thus, the mean free path of these particles

$$\lambda = \frac{1}{\sigma n} \in [10^{18}; 10^{25}] \text{Mpc.} \quad (\text{I.6})$$

is much larger than the Hubble radius

$$r_{\text{H}} = \frac{c}{H_0} \approx 4000 \text{Mpc}, \quad (\text{I.7})$$

where H_0 is today's value of the Hubble parameter (cf. Section I.4).

Even when increasing σ in Eq. (I.6) ten orders of magnitude would yield mean free paths being much greater than r_{H} . Hence, dark matter can be treated as a collisionless fluid with its phase-space evolution described by the collisionless Boltzmann equation.

I.4 Λ CDM: Concordance Model of Cosmology

Here we simply like to summarize the parameters and their values of the currently favoured (and commonly accepted) standard model of cosmology. The most recent combination of high-precision measurements of the cosmological parameters presented in Komatsu *et al.* (2008) yields

- the matter content $\Omega_m = 0.279$
- the cosmological constant $\Omega_\Lambda = 0.721$
- the Hubble parameter $H_0 = 70 \text{ km/sec/Mpc}$
- the amplitude of density perturbations $\sigma_8 = 0.817$

and this set of values is referred to as Λ CDM model.

Radiation (parameterized via Ω_r) is at a negligibly low level and hence can be discarded. Further, as the sum of all contributions as measured at today's time has to be unity (cf. Eq. (I.3)) the curvature term does not contribute, too.

We like to note that these are the *latest* measurements; the model changed over the years with minor adjustments of the parameters in one way or the other. Therefore, some of the work presented in this thesis may also refer to open cosmologies (i.e. OCDM, $\Omega_m < 1$ & $\Omega_\Lambda = 0$) and the “old” standard cold dark matter model (i.e. SCDM, $\Omega_m = 1$ & $\Omega_\Lambda = 0$).

Part II

Cosmological Simulations

This part represents a summary of the following publications:

- (1) Knebe A., Green A., Binney J.J., 2001, *MNRAS* 325, 845
- (2) Binney J.J., Knebe A., 2002, *MNRAS* 333, 378
- (3) Dominguez A., Knebe A., 2003, *EpL* 4, 631
- (4) Gill S.P.D., Knebe A., Gibson B.K., 2004, *MNRAS* 351, 399
- (5) Knebe A., Dominguez A., 2003, *PASA* 20, 173
- (6) Knebe A., 2005, *PASA* 22, 184
- (7) Power C.B., Knebe A., 2006, *MNRAS* 370, 691
- (8) Knebe A., Dominguez A., Dominguez-Tenreiro R., 2006, *MNRAS* 371, 1959

II.1 Introduction

As the major theme of this thesis is undoubtedly “computational cosmology” we decided to present the concepts behind this rather exciting and novel research field in considerable detail. All of the simulations presented later on in Section III and Section IV are though based upon the adaptive mesh refinement technique (cf. Section II.4.2, Section II.4.2 and Section II.6.2). However, we consider it important to highlight and stress the differences between various techniques and the respective codes available to (and used by) the astrophysical community for simulating cosmic structure formation.

II.1.1 The Necessity for Cosmological Simulations

Structure formation is generally believed to be a result of the gravitational amplification of primordial density perturbations. The amplitude of these initial perturbation though has to have the right value in order to match the clustering patterns observed today. While it is possible to follow the growth of structures to a certain extent using linear perturbation theory (e.g. Zel’dovich, 1970), such calculations are limited and cannot explain the wealth of observational data available to us; they break down on a scale where the (variance of the) density contrast

$$\delta = \frac{\rho(\vec{x}) - \langle \rho \rangle}{\langle \rho \rangle} \quad (\text{II.1})$$

approaches unity. Today’s structures exhibit δ -values in the range from voids with $\delta \approx -1$ to $\delta \approx 10^6$ in the central regions of galaxies and larger. This requires the need for computer simulations: the treatment of perturbations in the non-linear regime is a very complicated problem and the only exact way of doing it is by performing numerical simulations. As such simulations became more and more sophisticated their relevance for the field of cosmology has also increased. And today we are left with a research branch on its own, namely *computational cosmology* to be elaborated upon now.

II.1.2 The History of Cosmological Simulations

The Universe is believed to have started with a Big Bang in which – or more precisely: shortly after which – tiny fluctuations (in an otherwise homogeneous and isotropic space) were imprinted into the radiation and matter density field. To understand how the Universe evolved from that early stage into what we observe today (i.e. stars,

galaxies, galaxy clusters, ...) one needs to follow the evolution of those density fields using numerical methods as soon as they turn non-linear (i.e. $\sigma_\delta > 1$). Therefore, the approach to cosmological simulations is actually twofold: firstly, one needs to generate the initial conditions according to the cosmological structure formation model to be investigated (cf. Section II.8) and secondly, the initial density field (sampled by particles and hence the reference to N -body codes) needs to be evolved forward in time using a numerical integrator for the equations of interest (Sections II.2–II.4).

Algorithms have advanced considerably since the first N^2 particle-particle codes (Aarseth, 1963; Peebles, 1970; Groth *et al.*, 1977); we have seen the development of the tree-based gravity solvers (Barnes and Hut, 1986), mesh-based solvers (Klypin and Shandarin, 1983), then the two combined (Efstathiou *et al.*, 1985) and multiple strands of adaptive and deforming grid codes (Villumsen, 1989; Suisalu and Saar, 1995; Kravtsov *et al.*, 1997; Bryan and Norman, 1998; Knebe *et al.*, 2001). While they all push the limits of efficiency in computational resources, each code has its individual advantages and limitations. The result of such research has been highly reliable, cost effective codes.

In all such codes the evolution is simulated by following the trajectories of particles under their mutual gravity. These particles are supposed to sample the matter density field as accurately as possible and a cosmological simulation is nothing more (and nothing less) than a simple and effective tool for investigating non-linear gravitational evolution. There are two constraints on a cosmological simulation though: a) the correct initial conditions and b) the observation of galaxies, galaxy clusters, large-scale structure, voids, etc. Simulations are hence trying to bridge the gap between observations of the early Universe (i.e. anisotropies in the Cosmic Microwave Background observed as early as 300000 years after the Big Bang) and the Universe as we see it today.

II.1.3 The State-of-the-Art of Cosmological Simulations

Until now the methods have been continuously refined to allow for more and more particles while simultaneously resolving finer and finer structures. Today it is standard to run a cosmological simulation with millions of particles in a couple of days on large supercomputers or even clusters of PC's. These simulations can resolve the orbits of satellite galaxies within dark matter haloes spanning about five orders of magnitude in mass and spatial dimension (cf. Section IV).

Fig. 1 depicts the conceptual ideas behind (cosmological) simulations: starting from initial seed inhomogeneities superimposed onto a homogeneous and isotropic background the matter field is evolved forward in time. This evolution depends on the cosmological model under investigation and is performed using an integrator for the appropriate equations describing the physics under investigation. Snapshots of the simulation at various times are recorded and then analysed and compared to observational data to verify and falsify theories of structure formation and evolution.

In the following Section we present a brief explanation of the actual name “ N -body” code (Section II.2) before transferring the usual (Newtonian) equations of motion into a coordinate system that expands with the Universe in Section II.3. The heart and soul of every N -body code though is the part that solves Poisson's equation by one means or the other. We therefore present the general concepts behind the two most popular yet disparate methods to accomplish this task in Section II.4. Before introducing one

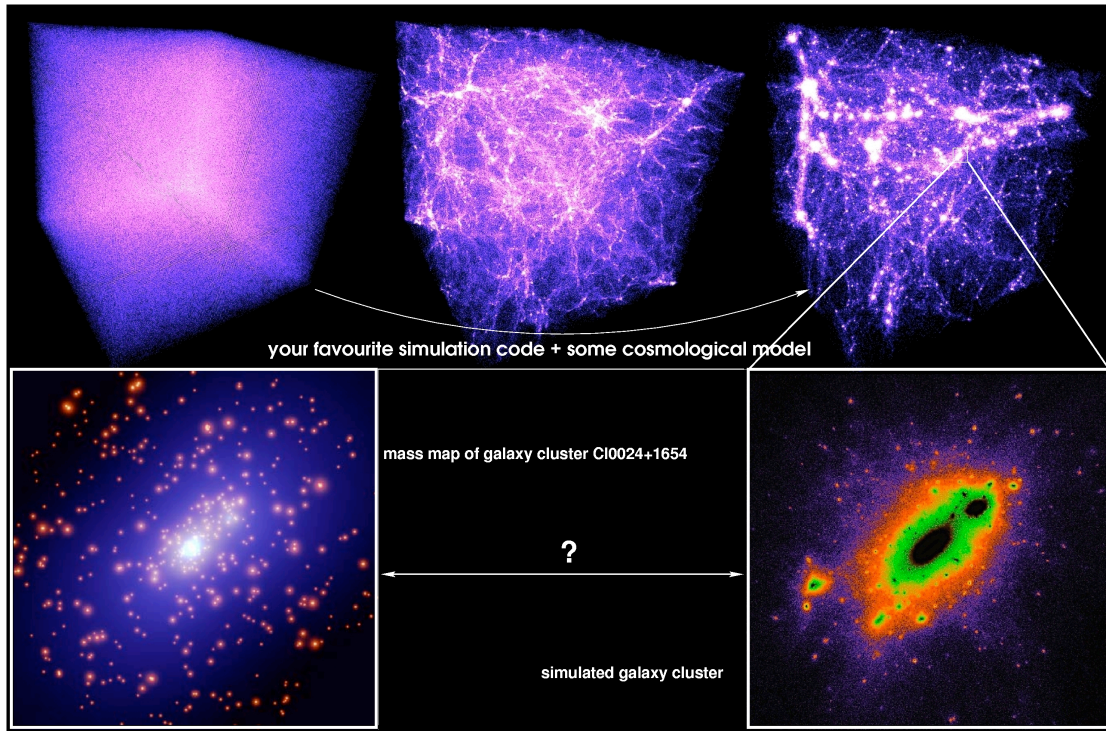


Fig. 1. Illustration of the idea driving N -body simulations. Initial conditions (upper left) are being evolved forward in time using a computer programme modeling gravity (and gas physics) under the assumption of a given cosmological model. The outputs over time are then compared to observational data and the cosmological model adjusted accordingly. Image credit (mass map of C10024+164): European Space Agency, NASA and Jean-Paul Kneib (Observatoire Midi-Pyrenees, France/Caltech, USA)

particular N -body in greater detail in Section II.6, we discuss some issues with such codes that are of mere numerical nature in Section II.5. The last Section II.8 then deals with the process of generating the initial conditions for cosmological simulations and its intrinsic complications.

II.2 The N -body Concept

As explained in Section I.3.2 dark matter is practically a collisionless fluid. When used to model the dynamics of such a collisionless system, an N -body code aims at simultaneously solving the collisionless Boltzmann equation (CBE)

$$\frac{\partial f}{\partial t} + \sum_{i=1}^3 \left(v_i \frac{\partial f}{\partial x_i} - \frac{\partial \Phi}{\partial x_i} \frac{\partial f}{\partial v_i} = 0 \right) \quad (\text{II.2})$$

and Poisson's equation

$$\nabla^2 \Phi(\vec{r}) = 4\pi G \rho(\vec{r}) , \quad (\text{II.3})$$

where the matter density $\rho(\vec{r})$ is given by

$$\rho(\vec{r}) = \int f d^3v . \quad (\text{II.4})$$

The CBE (II.2) is solved by the method of characteristics (e.g. Leeuwin *et al.*, 1993). Since the CBE states that f is constant along any trajectory $\{\vec{r}(t), \vec{v}(t)\}$, the trajectories obtained by time integration of N points $\{\vec{r}_i, \vec{v}_i\}$ sampled from the distribution function f at time $t = t_{\text{initial}}$ form a representative sample of f at each time t .

Hence the problem reduces to solving Poisson's Eq. (II.3) for a set of N particles and advancing them forward in time according to the equations of motion derived from the system's Hamiltonian \mathcal{H} : remember that Eq. (II.2) can be written as

$$\frac{\partial f}{\partial t} + [f, \mathcal{H}] = 0 . \quad (\text{II.5})$$

The details of the time-integration of the equations of motions are going to be explained below in Section II.3. The prime aspect of every N -body code is to solve Poisson's equation Eq. (II.3) and currently there are two commonly used approaches for deriving the potential from it:

- tree codes rely on a direct particle-particle summation, and
- Particle-Mesh (PM) codes utilize a numerical integration of Eq. (II.3) on a grid.

Both these techniques are going to be explained in Section II.4.

II.3 Newtonian Mechanics in Comoving Coordinates

Even though solving Poisson’s equation is central to every N -body code, it is also important to accurately update particle positions and velocities, i.e. integrating the equations of motion. And as the Universe is expanding it is convenient to introduce *comoving coordinates*:

$$\vec{x} = \frac{\vec{r}}{a(t)} \quad (\text{II.6})$$

where $a(t)$ is the cosmic expansion factor and the solution to the (first) Friedmann equation (I.3).

The (comoving) Lagrangian is given by (cf. Knebe *et al.*, 2001)

$$\mathcal{L} = \frac{1}{2}a^2\dot{x}^2 - \frac{\Phi}{a}, \quad (\text{II.7})$$

which leads to the canonical momentum

$$\vec{p} = a^2\dot{\vec{x}}. \quad (\text{II.8})$$

Hamilton’s equations are therefore

$$\begin{aligned} \frac{d\vec{x}}{dt} &= \frac{\vec{p}}{a^2} \\ \frac{d\vec{p}}{dt} &= -\frac{\nabla\Phi}{a}. \end{aligned} \quad (\text{II.9})$$

accompanied by the Poisson’s equation in comoving coordinates

$$\Delta\Phi = 4\pi Ga(\rho - \rho_b) \quad (\text{II.10})$$

where ρ_b is the cosmic background density (and hence Φ is the potential responsible for “peculiar accelerations”).

The equations-of-motion (II.9) can be discretized and integrated using a second-order accurate scheme as follows:

$$\begin{aligned} \vec{x}_{n+1/2} &= \vec{x}_n + \vec{p}_n \int_t^{t+\Delta t/2} \frac{dt}{a^2} \\ \vec{p}_{n+1} &= p_n - \nabla\Phi(x_{n+1/2}) \int_t^{t+\Delta t} \frac{dt}{a} \\ \vec{x}_{n+1} &= \vec{x}_{n+1/2} + \vec{p}_{n+1} \int_{t+\Delta t/2}^{t+\Delta t} \frac{dt}{a^2}, \end{aligned} \quad (\text{II.11})$$

where the integrals can be evaluated analytically as they depend only on the cosmology. This modified *leap-frog scheme* only needs to store one copy of the positions and velocities whereas other integrators as, for instance, Runge-Kutta consume more memory. Further, it has been shown that symplectic integrators⁴ such as Eq. (II.11) are better suited for Hamiltonian systems (Springel, 2005) as they are robust against non-

⁴Symplectic integrators preserve Poincare integral invariants, or in other words, preserve phase-space.

Hamiltonian perturbations introduced by, for instance, ordinary numerical integration methods.

II.4 Poisson Solver

As already mentioned in Section II.2 there are two complementary approaches for deriving the potential from Poisson's equation (II.3): a) tree codes rely on a direct particle-particle summation, and b) PM (**p**article-**m**esh) codes utilize a numerical integration of Eq. (II.3) on a grid.

II.4.1 Tree Codes

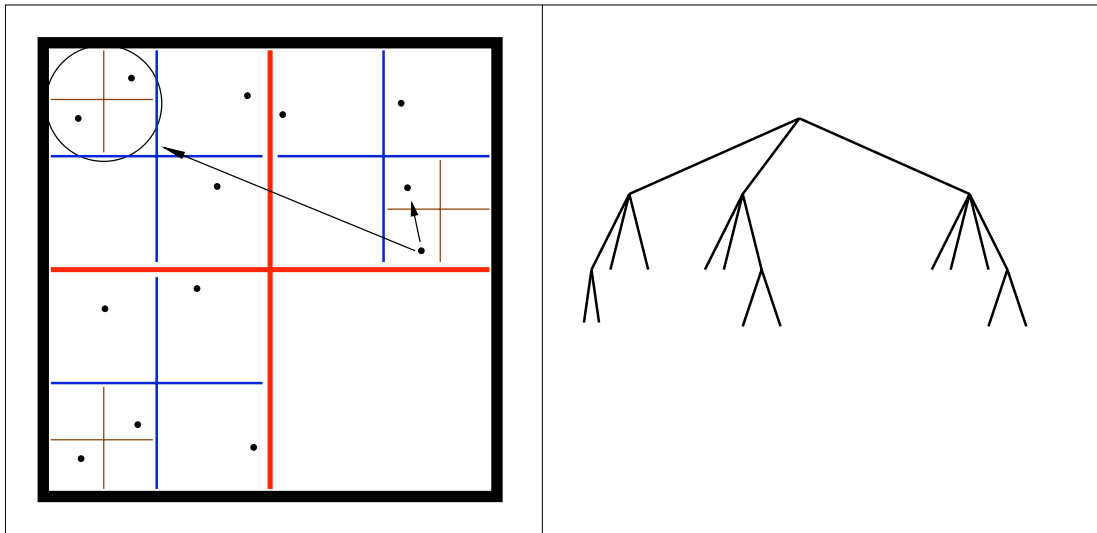


Fig. 2. Illustration of a tree code. The left panel shows the actual particle distribution and its cubical decomposition. The right panel is the tree corresponding to this distribution.

The Pre-Requisites

The **p**article-**p**article (PP) method upon which tree codes are based assumes that the particles are δ -functions and hence the density field (rhs of Poisson's Eq. (II.3)) reads as follows:

$$\rho(\vec{r}) = \sum_{i=1}^N m_i \delta(\vec{r} - \vec{r}_i) , \quad (\text{II.12})$$

where N is the total number of particles in use.

The Forces

Combining Eq. (II.12) with Eq. (II.3) the analytical solution for the force \vec{F} at particle position \vec{r}_i is given by:

$$\vec{F}(\vec{r}_i) = \sum_{j \neq i} \frac{m_i m_j}{|\vec{r}_i - \vec{r}_j|^2} \left(\frac{\vec{r}_i - \vec{r}_j}{|\vec{r}_i - \vec{r}_j|} \right) . \quad (\text{II.13})$$

But as we are interested in deriving the force at every single particle position, the PP method scales like N^2 (N summations, each over $(N - 1)$ particles). Therefore, a

(straightforward) PP summation does not appear to be feasible for evolving a set of N particles under their mutual gravity, not even on the largest supercomputers available nowadays! One needs to bypass the increase in computational time for large numbers of particles with a more sophisticated treatment when calculating the forces. One way of achieving this is to organize the particles in a tree-like structure: particles located "far away" from the actual particle (at which position we intend to calculate the force) can be lumped together as a single – but more massive – particle. This tunes down the number of calculations dramatically.

The idea of a tree code is sketched in Fig. 2. The particles are organized in a tree-like structure based upon a cubical decomposition of the computational domain. Consequentially, for each particle we "walk the tree" and add the forces from branchings that need no further unfolding into finer branches according to some pre-selected "opening criterion".

One publicly available tree code is called GADGET⁵ (**G**alaxies with **D**ark Matter and **G**as int**E**rac**T**) and I refer the reader to a more elaborate discussion of this technique to its reference paper by Springel *et al.* (2001) and Springel (2005).

Force Resolution – softening

In order to avoid the singularity for $\vec{r}_i = \vec{r}_j$ in Eq. (II.13) one needs to set a limit on the minimal allowed spatial separation between two particles. This can be achieved by introducing a (fixed) scale, i.e. the softening parameter ϵ :

$$\vec{F}(\vec{r}_i) = \sum_{j \neq i} \frac{m_i m_j}{|\vec{r}_i - \vec{r}_j|^2 + \epsilon^2} \left(\frac{\vec{r}_i - \vec{r}_j}{|\vec{r}_i - \vec{r}_j|} \right) \quad (\text{II.14})$$

This softening is closely related to the overall force resolution of the simulation and an elaborate discussion of it can be found in Dehnen (2001).

II.4.2 Particle-Mesh Codes

The Pre-Requisites

Another way for obtaining the forces is to numerically integrate Poisson's equation (II.3). This method, however, demands the introduction of a grid in order to define the density and hence the name **particle-mesh** (PM) method. The grid is usually of a regular (cubic) shape with $L \times L \times L$ cells where each cell is identified by the index triplet (i, j, k) . The forces are then calculated according to the following scheme:

1. assign all particles to the grid to get $\rho_{i,j,k}$
2. solve Poisson's equation $\nabla^2 \phi_{i,j,k} = 4\pi G \rho_{i,j,k}$
3. differentiate to get forces $F_{i,j,k} = -\nabla \phi_{i,j,k}$
4. interpolate $F_{i,j,k}$ back to particle positions

⁵GADGET can be downloaded from this web address <http://www.mpa-garching.mpg.de/gadget>

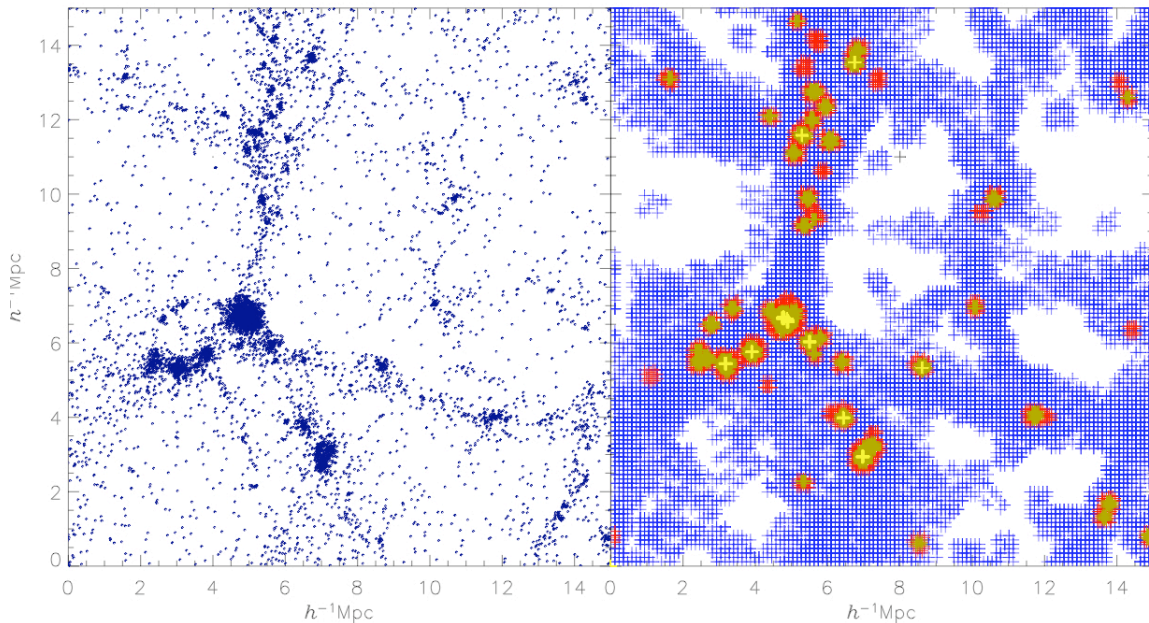


Fig. 3. An example for adaptive mesh refinement. The left panel shows the particle distribution at redshift $z = 0$ in a Λ CDM simulation. The right panel indicates the arbitrarily shaped grids invoked by the AMR code MLAPM to solve Poisson's equation. Note that the grid covering the whole computational domain is not shown for clarity.

The Forces

With this scheme most of the time is spent in step 2 and the most common way to solve Poisson's equation on a grid is to make use of FFT's (**F**ast-**F**ourier-**T**ransforms). The analytical solution to Poisson's equation is given by the integral

$$\Phi(\vec{r}) = \int G(\vec{r} - \vec{r}') \rho(\vec{r}') d\vec{r}' \quad (\text{II.15})$$

where $G(\vec{x}) = -\vec{x}/x^{3/2}$ is the Green's function of Poisson's equation. This integral can readily be evaluated in Fourier-space, i.e.

$$\hat{\Phi} = \hat{G} \hat{\rho} \quad (\text{II.16})$$

where $\hat{\Phi}$, \hat{G} , and $\hat{\rho}$ are the Fourier transforms of the respective variables.

The PM approach proves to be exceptionally fast outperforming any tree code.

There are of course other techniques than the use of FFT's available to numerically solve Poisson's equation but the utilisation of FFT's is the most common approach as it appears to be the fastest.

Force Resolution – adaptive mesh refinement

The most severe problem with the PM method is the lack of spatial resolution below two grid spacings. Whereas tree codes require the introduction of a softening length to avoid the force singularity for close encounters of particles, PM codes suffer from the opposite problem. Gravity is an attractive force and hence the particles flow from low density regions into high density regions amplifying primordial density fluctuations. This leads

to an excess of particles in certain cells whereas other cells are becoming more and more devoid of matter. But as the spacing of the grid introduces a (smoothing) scale particles closer than about two cell distances do not interact according to Eq. (II.15) anymore. We are left with the situation where we can not resolve structure formation on scales of (and below) roughly the cell spacing of the grid!

This is a major problem and the most obvious way to overcome it is to introduce finer grids in regions of high density. These grids though need to freely adapt to the actual particle distribution at all times and hence navigating such complex grids through computer memory is a very demanding task. One of the freely available adaptive mesh refinement (AMR) codes is MLAPM⁶ (Knebe *et al.*, 2001).

The mode of operation of this AMR technique can be viewed in Fig. 3 where a slice through a standard Λ CDM simulation is presented. The left panel shows the distribution of particles whereas the right panel indicates the adaptive meshes used to obtain a solution to Poisson's equation.

It needs to be stressed though that the use of irregularly shaped grids inhibits FFT's. Another technique for solving Poisson's equation needs to be sought such as, for instance, multi-grid relaxation (e.g. Brandt, 1977; Press *et al.*, 1992; Kravtsov *et al.*, 1997; Knebe *et al.*, 2001).

II.4.3 Hybrid Methods

There are, of course, various other techniques for simultaneously being time efficient and having a credible force resolution. One possibility is realized in the so-called P³M technique (i.e. Couchman, 1991) where a combination of PP and PM provides the necessary balance between accuracy and efficiency: the force as given by the plain PM calculation is augmented by a direct summation over all neighboring particles within the surrounding cells. This gives accurate forces down to the scale provided by the softening parameter ϵ again. Other examples, for instance, are Tree-PM (Bode and Ostriker, 2003) and moving mesh (Gnedin, 1995) codes, but the details are well beyond the scope of this thesis.

II.4.4 Mass Resolution

It still needs to be mentioned that a cosmological simulation in practice only simulates a certain fraction of the Universe. This is what people refer to as the *simulation box*. However, to account for the fact the Universe is actually infinite one uses periodic boundary conditions: particles leaving the box on one side immediately enter the box again on the other side.

Moreover, the size of the box also defines the mass resolution of the simulation. We are only using a certain number of particles within a fixed region of the Universe. And as the density of the Universe is determined by the cosmological model under investigation, each individual particle has a certain mass. This mass determines the *mass resolution* of that specific simulation. For instance, if we model the evolution of about 2 million particles in a box with side length $25h^{-1}\text{Mpc}$ using the Λ CDM cosmology ($\Omega_0 = 0.3$), each particle weighs about $6 \cdot 10^8 h^{-1} M_\odot$. Therefore we will not be able to properly resolve dwarf galaxies in that particular cosmological simulation ($M_{\text{dwarf}} \geq 10^7 h^{-1} M_\odot$).

⁶MLAPM can be downloaded from this web address <http://www.aip.de/People/AKnebe/MLAPM>

II.4.5 Comparison

It only appears natural to ask the question which method is superior and how they compare, respectively.

There is no straight forward answer as both methods have their (dis-)advantages. Tree codes are based upon the assumption that the Universe is filled with particles of a certain size related to the softening ϵ (cf. Section II.4.1). Adaptive mesh refinement codes use a smoothed density field (which in turn also introduces an effective particle size) to obtain the potential and hence the force field. In both cases it is important to bear in mind that particles are only to be understood as markers in phase-space and should not interact on a two-body basis, i.e. one always intends to integrate the collisionless Boltzmann equation (II.2). There are several studies investigating two-body interactions in such simulations and it can be confirmed that they are more prominent in tree codes (Binney and Knebe, 2002). But as long as one complies with certain constraints on the numerical parameters (cf. Power *et al.*, 2003) such effects can be minimized.

There are several studies comparing tree and AMR codes both in efficiency and accuracy (e.g. Frenk *et al.*, 1999; Knebe *et al.*, 2001; Heitmann *et al.*, 2007; Agertz *et al.*, 2007) but in the end it all comes down to a “question of taste”. Both techniques are well enough developed to successfully model the formation and evolution of cosmic structures.

II.5 Numerical Issues

II.5.1 Two-Body Relaxation

It is logically possible that two-body relaxation in simulations of cosmological clustering influences the final structure of massive clusters. It has therefore been a target of several investigations (e.g. Binney and Knebe, 2002; Diemand *et al.*, 2004; El-Zant, 2006). Convergence studies in which mass and spatial resolution are simultaneously increased, cannot eliminate this possibility. The standard way of determining the significance of two-body relaxation in a simulation is to include particles of more than one mass: if the simulation is collisionless, the final distributions of the particles will be independent of mass, whereas the more massive particles will tend to sink to the bottoms of potential wells if two-body relaxation is significant.

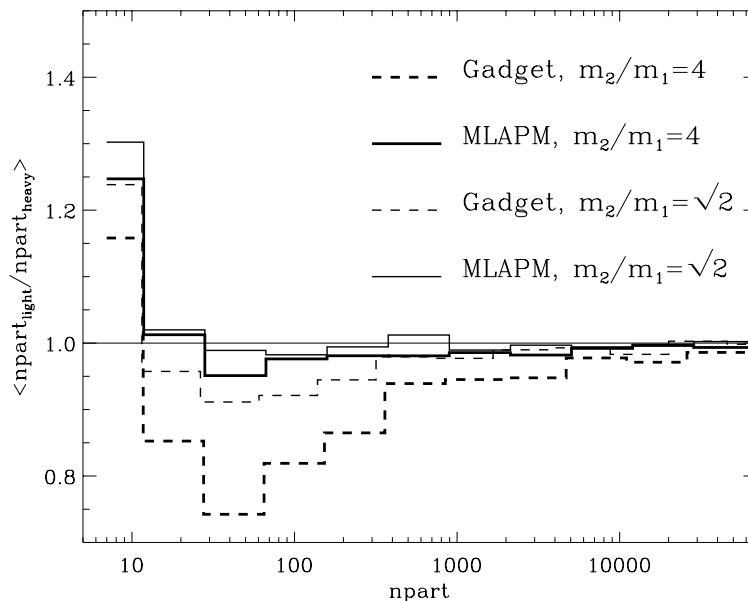


Fig. 4. Ratio of the numbers of light and heavy particles in haloes as a function of the total number of particles in the halo.

We performed simulations with both a spatially fixed softening length and adaptive softening using the publicly available codes GADGET (a tree code) and MLAPM (an adaptive mesh refinement code), respectively, where half of the particles have mass m_1 and the other half m_2 . The effects of two-body relaxation are detected in both the density profiles of haloes and the mass function of haloes. However, in the MLAPM simulations there is no evidence that two-particle relaxation enhances the fraction of heavy particles in clusters. The GADGET simulations show a clear tendency for clusters with more than a handful of particles to contain more massive than light particles as can be seen in Fig. 4. Further, this tendency increases in strength with the mass ratio m_2/m_1 , just as is expected if it is driven by two-particle relaxation.

This work has been published as “Two-Body Relaxation in Cosmological Simulations” (Binney J., Knebe A., 2002, MNRAS 333, 378).

II.5.2 Finite Box Size Effects

As explained in Section II.4.4 every cosmological simulation only follows the evolution of matter in a certain fraction of the volume of the actual universe (with periodic boundary conditions to account for infinity of space). But to what extent does the negligence of perturbations on scales larger than the simulation box affect structure formation?

We investigated the impact of a finite simulation box size on the structural and kinematic properties of cold dark matter haloes. Our approach involves generating a single realisation of the initial power spectrum of density perturbations and studying how truncation of this power spectrum on scales larger than $L_{\text{cut}} = 2\pi/k_{\text{cut}}$ affects the structure of dark matter haloes at $z = 0$. In particular, we have examined the cases of $L_{\text{cut}} = f_{\text{cut}}L_{\text{box}}$ with $f_{\text{cut}} = 1$ (i.e. no truncation), $1/2$, $1/3$ and $1/4$.

In common with previous studies, we found that the suppression of long wavelength perturbations reduces the strength of clustering, as measured by a suppression of the 2-point correlation function $\xi(r)$, and reduces the numbers of the most massive haloes, as reflected in the depletion of the high mass end of the mass function $n(M)$. Interestingly, we find that truncation has little impact on the internal properties of haloes. The masses of high mass haloes decrease in a systematic manner as L_{cut} is reduced, but the distribution of, for instance, concentrations is unaffected. On the other hand, the median spin parameter is $\sim 50\%$ lower in runs with $f_{\text{cut}} < 1$. We argue that this is an imprint of the linear growth phase of the halo's angular momentum by tidal torquing, and that the absence of any measurable trends in concentration (and only a minor influence of large-scale power on the shape) reflect the importance of virialisation and complex mass accretion histories for these quantities, respectively.

This work has been published as “The Impact of Box Size on the Properties of Dark Matter Haloes in Cosmological Simulations” (Power C.B., Knebe A., 2006, MNRAS 370, 691).

II.5.3 Hydrodynamics Approach to the Evolution of Cosmic Structure

The actual set of equations integrated by an N -body code (i.e. Eq. (II.9) and Eq. (II.10)) can be re-written as (cf. Knebe *et al.*, 2006)

$$\begin{aligned} \dot{x} &= \frac{1}{a}u, \\ \dot{u} &= w - Hu, \\ \nabla \cdot w &= -4\pi Ga \left[\frac{m}{a^3} \sum_i \delta^{(3)}(x - x_i) - \varrho_b \right], \\ \nabla \times w &= 0, \end{aligned} \tag{II.17}$$

where x is the comoving coordinate, u the peculiar velocity, m the particle mass, and w the peculiar gravitational acceleration.

If we now assume that the actual measure of the density field in an N -body code depends on a smoothing window $W(z)$, the microscopic field ϱ_{mic} relates to the measured (coarse-grained) field ϱ in the following way:

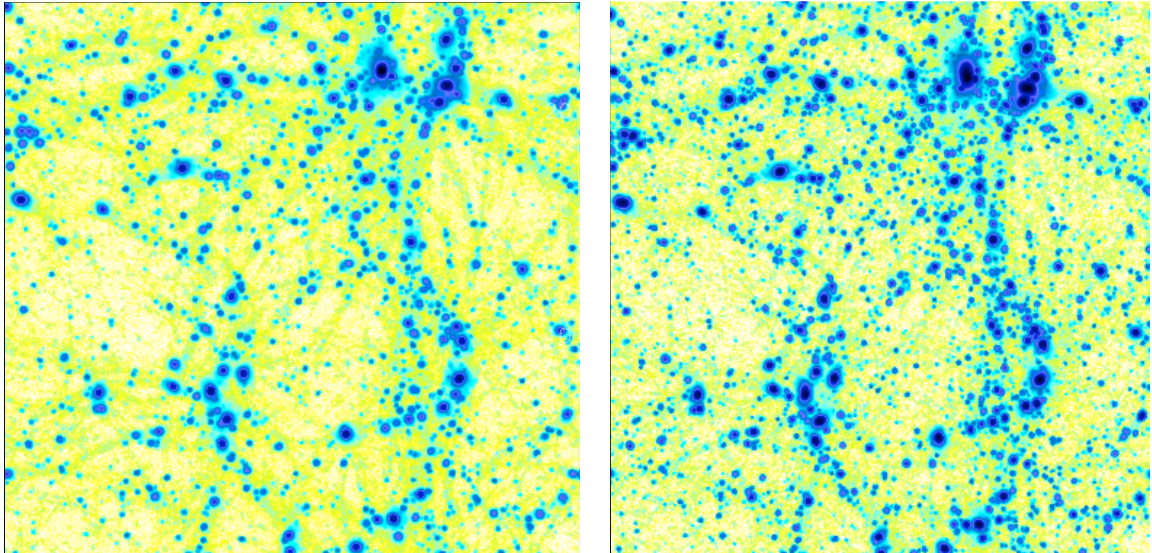


Fig. 5. Colour-coded density field of a Λ CDM simulation (left panel) and the corresponding hydrodynamic model (right panel).

$$\begin{aligned}\varrho_{mic}(x, t) &= \frac{m}{a(t)^3} \sum_i \delta^{(3)}(x - x_i(t)), \\ \varrho(x, t; L) &= \int \frac{dy}{L^3} W\left(\frac{|x - y|}{L}\right) \varrho_{mic}(y, t).\end{aligned}\tag{II.18}$$

The physical interpretation of the field $\varrho(\mathbf{x}; L)$ follows straightforwardly from the properties of the smoothing window: it is proportional to the number of particles contained within the coarsening cell of size $\approx L$ centered at \mathbf{x} . A microscopic peculiar-momentum density as well as a peculiar-acceleration field and the corresponding coarse-grained fields can be defined in the same way.

From these definitions and Eq. (II.17), it is straightforward to derive the evolution equations obeyed by the coarse-grained fields ϱ and u (from now on, $\partial/\partial t$ is taken at constant x and L , and ∇ means partial derivative with respect to x):

$$\begin{aligned}\frac{\partial \varrho}{\partial t} + 3H\varrho &= -\frac{1}{a}\nabla \cdot (\varrho u), \\ \frac{\partial(\varrho u)}{\partial t} + 4H\varrho u &= \varrho w - \frac{1}{a}\nabla \cdot (\varrho u u + \Pi),\end{aligned}\tag{II.19}$$

where a new second-rank tensor field has been defined (dyadic notation):

$$\begin{aligned}\Pi(\mathbf{x}, t; L) &= \int \frac{d\mathbf{y}}{L^3} W\left(\frac{|\mathbf{x} - \mathbf{y}|}{L}\right) \varrho_{mic}(\mathbf{y}, t) \\ &\quad [\mathbf{u}_{mic}(\mathbf{y}, t) - \mathbf{u}(\mathbf{x}, t; L)][\mathbf{u}_{mic}(\mathbf{y}, t) - \mathbf{u}(\mathbf{x}, t; L)].\end{aligned}\tag{II.20}$$

The peculiarities of the problem at hand (collisionless matter in the non-stationary state of structure formation) prevent the usual truncation of the hierarchy leading to the Euler or Navier-Stokes equations, respectively (see, e.g., Chapman and Cowling, 1991). The *small-size expansion* (SSE) is a specific truncation for this problem (Domínguez, 2000; Buchert and Domínguez, 2005), that starts from the physical assumption that the coupling to the small-scales is weak (this can be argued on the basis

that, in a hierarchical scenario, the smaller scales “virialize” earlier and thus “decouple” from the evolution of the larger scales). Then the fields Π and w are derived as a formal expansion in L : Keeping terms up to order L^2 , Eqs. II.19 become ($\partial_i = \partial/\partial x_i$; summation over the repeated index i is understood)

$$\begin{aligned} \frac{\partial \varrho}{\partial t} + 3H\varrho &= -\frac{1}{a}\nabla \cdot (\varrho u), \\ \frac{\partial(\varrho u)}{\partial t} + 4H\varrho u &= \varrho w^{\text{mf}} - \frac{1}{a}\nabla \cdot (\varrho u u) + \varrho C, \\ \nabla \cdot w^{\text{mf}} &= -4\pi G a (\varrho - \varrho_b), \\ \nabla \times w^{\text{mf}} &= 0, \end{aligned} \quad (\text{II.21})$$

with the additional acceleration

$$C = \frac{BL^2}{\varrho} \left[(\nabla \varrho \cdot \nabla) w^{\text{mf}} - \frac{1}{a} \nabla \cdot [\varrho (\partial_i u) (\partial_i u)] \right]. \quad (\text{II.22})$$

The constant B is determined by the smoothing window $W(z)$,

$$B = \frac{1}{3} \int d\mathbf{z} z^2 W(z) = \frac{4\pi}{3} \int_0^{+\infty} dz z^4 W(z). \quad (\text{II.23})$$

To order L^0 , Eq. (II.21) reduce to the “dust (pressureless) approximation” for cosmological structure formation (Sahni and Coles, 1995).

The dynamical evolution predicted by Eq. (II.21) can be implemented without much difficulties in a particle–mesh (PM) code of N -body simulation. For the details we refer the reader to the original paper by Knebe *et al.* (2006).

We now performed a series of cosmological N -body simulations which made use of this *hydrodynamic approach* to the evolution of structures. Comparing these simulations to usual N -body simulations, we find that

- the new (hydrodynamic) model entails a proliferation of low–mass halos, and
- dark matter halos have a higher degree of rotational support.

As an illustration we show in Fig. 5 a colour-coded density field of two “hydrodynamic” dark matter models in comparison to a Λ CDM model.

These results agree with the theoretical expectation about the qualitative behaviour of the “correction terms” (II.22) introduced by the hydrodynamic approach: these terms act as a drain of inflow kinetic energy and a source of vorticity by the small–scale tidal torques and shear stresses.

This work has been published as “Hydrodynamic Approach to the Evolution of Cosmic Structures II: Study of N-body Simulations at $z = 0$ ” (Knebe A., Dominguez A., Dominguez-Tenreiro R., 2006, MNRAS 371, 1959).

II.6 MLAPM – Multi-Level-Adaptive-Particle-Mesh

Most of the simulations and results presented in this thesis are based upon simulations done with a novel computer code that utilizes adaptive meshes in the solution process of Poisson’s equation (II.3). The code was developed from scratch and made publicly available to the community. We therefore consider it important to present the particulars of this code in sufficient detail within the context of this thesis.

The code we have developed, MLAPM, starts from a regular Cartesian grid and recursively refines cells such that subgrids can have arbitrary geometry (subject to each cell being cubical). MLAPM, which either uses a multigrid algorithm or a Fast-Fourier-Transform to solve Poisson’s equation, is in many ways similar to the Adaptive Refinement Tree (ART) code of Kravtsov *et al.* (1997) and RAMSES (Teyssier, 2002) which also utilize recursively placed refinements of arbitrary shape as the simulation evolves.

II.6.1 Handling Adaptive Meshes

MLAPM estimates the density on an arbitrarily shaped grid and then employs a finite-difference approximation to solve Poisson’s equation subject to periodic boundary conditions. If the density in any cell is found to exceed a certain threshold, which corresponds to ρ_{ref} of order 1 to 8 particles per cell, the cell is subdivided as described below. Cells obtained by this subdivision can be further subdivided. This sub-division process, which can generate grids of arbitrary geometry, is described in more detail in Section II.6.2.

To define and navigate such complex grids, several data structures are required, which we now describe. The general scheme closely follows the precepts of Brandt (1977). Functions are provided both for the creation and destruction of these structures.

With each cell we associate a data structure called a ‘node’, which stores the values for the centre of the cell of dynamically interesting quantities:

NODE	<ul style="list-style-type: none"> ○ density ○ potential ○ forces ○ pointer to first particle
------	---

Since there will be more nodes than particles, they need to be defined in a way that minimizes memory requirements. Moreover, so far as possible, we arrange for nodes that are adjacent physically to occupy adjacent locations in computer memory. This has the dual advantage of minimizing cache misses and of enabling neighbours to be found by incrementing or decrementing pointers. Hence we do not follow Kravtsov *et al.* (1997) in arranging nodes as fully-threaded oct-trees. Instead we gather nodes into x QUADS. An x QUAD is a line of nodes that follow each other parallel to the x -axis. With it we associate these numbers

x QUAD	<ul style="list-style-type: none"> ○ pointer to first node ○ x coordinate of the first node ○ number of nodes ○ pointer to next xQUAD
----------	---

Since the memory for the nodes described by this QUAD is allocated as one block, this information is sufficient to access directly any node in the QUAD and to determine its

x coordinate. The pointer to the next x QUAD similarly enables one to reach nodes further down the axis in a few steps.

Just as nodes are gathered into x QUADs, so x QUADs are gathered into y QUADs. Thus a y QUAD is a series of contiguous x QUADs and gives one access to a plane⁷ of nodes. With a y QUAD we associate these numbers

y QUAD	<ul style="list-style-type: none"> ○ pointer to first xQUAD ○ y coordinate of first xQUAD ○ length of yQUAD ○ pointer to next yQUAD
----------	--

A z QUAD is a similar linked list of y QUADs, so it contains these numbers

z QUAD	<ul style="list-style-type: none"> ○ pointer to first yQUAD ○ z coordinate of first yQUAD ○ length of zQUAD ○ pointer to next zQUAD
----------	--

Fig. 6 indicates how a two-dimensional, adaptive grid is organized using QUAD's. All (virtual) nodes of a grid are shown, with the nodes in use (refined region) represented by filled circles. Memory is assigned only for these nodes (and the supporting QUAD structures). As soon as a node is encountered that does not need to be refined, the x QUAD stops and its 'next'-pointer is set to the next x QUAD; if this is the last x QUAD, the pointer is set to NULL. The same scheme applies to the relation between x QUAD's and y QUAD's, and to the relation between y QUADs and z QUADs. In particular, when a series of x QUADs is contiguous in the sense that there is at least one x QUAD for every value of y in some range, the storage for the x QUADs with the smallest x coordinates at each y is allocated in a block. Similarly, storage for contiguous y QUADs with the smallest y coordinates at given z is allocated in a block.

Computation of the forces involves several sweeps through the nodes. In each such sweep one loops through the linked list of all z QUADs to locate each y QUAD, and within each y QUAD one runs through the list of x QUADs, and within each x QUAD one runs through the list of nodes. Consequently, when referencing a node one always knows which x QUAD, y QUAD and z QUAD it lies in. This information and the coherent storage of adjacent x and y QUADs allows one to find neighbours as follows. For example, suppose we want to find the neighbour that has y smaller by a grid spacing. Then we decrement by one the current value of the pointer in the loop over x QUADs to locate the x QUAD nearest the y -axis at the required value of y . Then we loop over the list of x QUADs at whose head this QUAD stands, until we find the x QUAD that contains the neighbour we are seeking.

The highest-level structure in MLAPM is a GRID. This gathers together a variety of information about a particular level of refinement:

⁷Brandt calls a y QUAD a CQUAD.

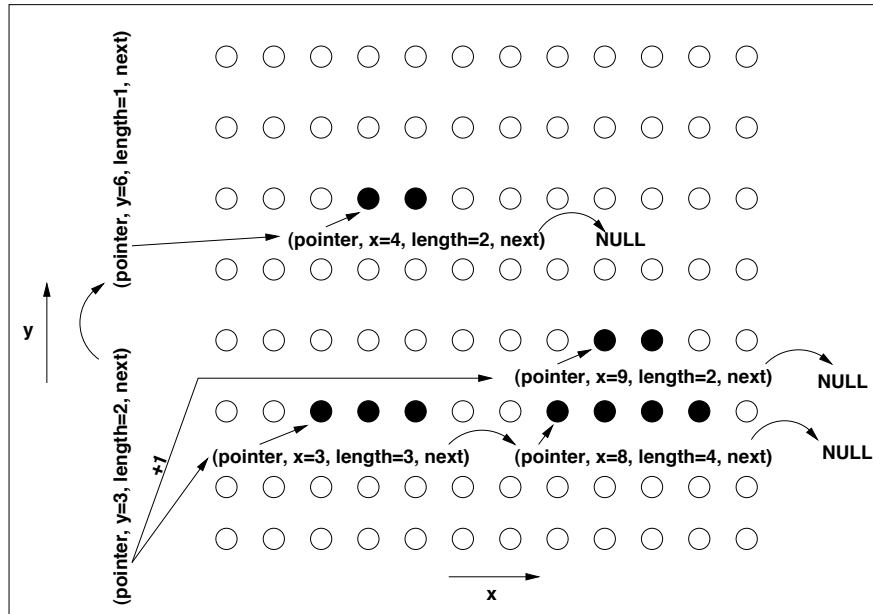


Fig. 6. QUAD structured grid used within MLAPM sketched for two dimensions. Circles mark nodes, open ones being virtual. QUADs are indicated by lists in brackets.

GRID	<ul style="list-style-type: none"> ○ pointer to first zQUAD ○ number of nodes per dimension ○ distance between adjacent nodes ○ critical density ○ mass to density conversion factor ○ residuals ○ cosmic expansion factor ○ ...
------	---

The crucial entries in this structure are the pointer to the first z QUAD and the number of (virtual) nodes. However, additional useful book-keeping data is stored here, such as the grid spacing, and the critical density for refinement.

The data structure associated with a particle is this

PARTICLE	<ul style="list-style-type: none"> ○ position ○ momentum ○ mass ○ pointer to next particle
----------	--

Each particle is assigned to a node, usually the finest node that contains it. The list of a nodes's particles is maintained as a standard linked list.

II.6.2 Generating Refinements

A node is refined if its density exceeds a predetermined threshold that varies from grid to grid, and de-refined whenever it falls below that value. However, around each high-density region some additional nodes are refined, to provide a ‘buffer zone’. These buffer zones ensure that the resolution of the grid changes only gradually even if the density is discontinuous. In detail, a node is refined if either its density, or the density of

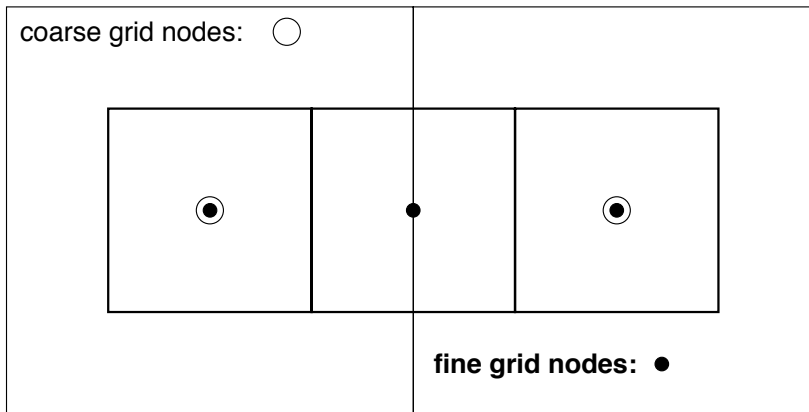


Fig. 7. Fine-grid cells often overlap more than one coarse-grid cell. Consequently, the fine-grid node at the centre may owe its existence to either of the two coarse-grid nodes exceeding the density threshold.

any of the 26 surrounding nodes exceeds the density threshold. Consequently, as MLAPM marches through the grid deciding whether to refine nodes, it is continually testing the density of nodes that lie ahead of its current position, since the current node must be refined if any of them lie above the density threshold. Careful programming is required to avoid wasting time by testing nodes twice. Notice that a refined node such as that shown in the centre of Fig. 7 can be called into existence by virtue of the coarse node to its right or to its left exceeding the density threshold, so we do not speak of ‘parent’ and ‘child’ nodes.

An important difference between our refinement scheme and that of the ART code, is that some of our refined nodes are cospatial with coarse nodes (see Fig. 7), whereas in the ART code all refined nodes are symmetrically distributed within the parent coarse node. Our refinement scheme is the natural one to adopt if one is simply solving partial differential equations: during the solution process the relevant values stored at each node (in our case density and potential) need to be interpolated between the grids which is done by a Taylor expansion about the centre of the node. For instance, for a prolongation of the coarse node density to the fine node this reads as follows

$$\rho(x_{\text{fine}}) = \rho(x_{\text{coarse}}) + \rho'(x_{\text{coarse}})(x_{\text{fine}} - x_{\text{coarse}}), \quad (\text{II.24})$$

where $\rho'(x_{\text{coarse}})$ is determined as a finite-difference between the neighbouring nodes to $\rho(x_{\text{coarse}})$. If the fine and coarse nodes are co-spatial (i.e. $x_{\text{fine}} = x_{\text{coarse}}$) we simply copy the coarse value over to the fine node; this scheme therefore ensures to best preserve peaks in the density field as opposed to always having $x_{\text{fine}} \neq x_{\text{coarse}}$ as is the case for codes that symmetrically distribute fine cells within the volume of the coarse cell. When particles are involved, it does lead to additional complexity, however, because with our scheme refined nodes that are not cospatial with coarse nodes have cells that overlap the cells of more than one coarse node – see Fig. 7.

The edges of refinements always include cospatial nodes of the parent grid (e.g., Fig. 7). Nodes that lie on the boundary of a refinement have a different role from ones in the interior. First they carry the boundary conditions subject to which Poisson’s equation is solved in the interior of the refined grid. That is, the potential on a refinement’s boundary nodes is obtained by interpolation from the embedding coarse grid and held

constant as the potential at interior points is adjusted towards a solution of Poisson’s equation as described in Section II.6.4. The second role of boundary nodes is to carry values used in the determination of the forces on particles in the refinement – the determination of these forces involves both numerical differentiation and interpolation.

II.6.3 Mass Assignment Scheme

Generally, each particle is placed in the linked list of the finest node within whose cell it lies. Exceptions to this rule occur when a particle enters a refinement during a call to the routine performing the integrating of the equations-of-motions (cf. Section II.3) and on the boundaries of refinements, where refined nodes exist only to provide values of the potential and forces. These nodes do not acquire particles.

After testing the nearest-grid-point (NGP), cloud-in-cell (CIC) and triangular-shaped-cloud (TSC) mass-assignment schemes (Hockney and Eastwood, 1988) we adopted the TSC mass-assignment scheme. In both the CIC and TSC schemes a particle contributes to the density in more than one node. Particular care has to be exercised at the edges of refinements if the integral of the density is to equal the total mass of the particles. A particle in the interior of a refinement only contributes to the density at refined nodes. When the density at cospatial coarse nodes is required, it is set equal to a weighted mean of the densities on a number of nearby fine nodes. Brandt (1977) calls this operation of taking a weighted mean “restriction”. The operator that accomplishes it has to be matched to the mass-assignment scheme, so that one obtains the same coarse-grid densities by restriction from a fine grid as one would have obtained if there had been no refinement and particles had been assigned to the coarse grid.

The restriction operator is also matched to an interpolation operator that is used to estimate quantities on a fine grid from their values on the embedding coarse grid. Brandt calls this the “prolongation” operator. The matching is such that if values are prolonged from coarse to fine and then restricted back to the coarse grid, they do not change.

Intricate book-keeping is required when particles are transferred between grids on the creation of a refinement.

II.6.4 Solving Poisson’s Equation

Poisson’s equation is solved using a variant of the multigrid technique (Brandt, 1977; Press *et al.*, 1992). In essence one relaxes a trial potential to an approximate solution of Poisson’s equation by repeatedly updating the potential according to

$$\Phi_{i,j,k} = \frac{1}{6}(\Phi_{i+1,j,k} + \Phi_{i-1,j,k} + \Phi_{i,j+1,k} + \Phi_{i,j-1,k} + \Phi_{i,j,k+1} + \Phi_{i,j,k-1} - \rho_{i,j,k}\Delta^2), \quad (\text{II.25})$$

where Δ is the grid spacing. There are several possible orderings of the points (i, j, k) at which these updates are made. We use ‘red-black’ ordering, so called because it involves first updating Φ on every other node on the grid, as on the red squares of a chess board, and then updating the other half of the nodes, equivalent to the black squares on a chess board.

This algorithm rapidly eliminates errors in the trial potential that fluctuate on the scale of the grid, but eliminates errors with longer-range fluctuations much more slowly. The

multigrid technique involves using a coarser grid to seek a correction in the event that convergence is slow.

Once we have a solution on the domain grid⁸, we prolong it to any refinements and iterate on the refinements until convergence (see below). Each refinement poses an independent boundary-value problem. Fortunately, the trial potential only deviates from the true one on the finest scales because it is obtained by prolongation of a coarse-grid solution of the same problem. So convergence is in practice rapid. Any further refinements are handled in the same way.

The potential on any grid is deemed to have converged when the residual

$$e = \nabla^2\Phi - \rho \quad (\text{II.26})$$

is smaller than a fraction, ~ 0.1 , of the estimated truncation error

$$\tau = \wp \left[\nabla^2(\mathfrak{R}\Phi) \right] - (\nabla^2\Phi), \quad (\text{II.27})$$

where \wp and \mathfrak{R} are the prolongation and restriction operators, respectively. Thus, τ is essentially the difference between evaluating the Laplacian operator on the current grid and on the next coarser grid.

Forces at each node are evaluated from centred differences of the potential and propagated to the locations of particles by the TSC scheme to ensure exact momentum conservation within any given refinement (Hockney and Eastwood, 1988). The forces $\nabla\Phi$ obtained in this way are then used with the integration of the equations-of-motion as specified in Section II.3, Eq. (II.11).q

A more elaborate description of MLAPM can be found in “Multi-Level Adaptive Particle Mesh (MLAPM): a C code for cosmological simulations” (Knebe A., Green A., Binney J.J., 2001, MNRAS 325, 845).

⁸Please note that the latest version of MLAPM/ has the option to obtain the solution on the domain grid via a Fast-Fourier-Transform (FFT) method.

II.7 Halo Finding

Performing a cosmological simulation is only one step in the process of understanding structure formation by means of computer simulations; the ensembles of millions of (dark) matter particles generated by the actual run still require interpreting and then comparison to the real Universe. This necessitates access to analysis tools to map the phase-space which is being sampled by the particles onto “real” objects in the Universe; traditionally this has been accomplished through the use of “halo finders”. Halo finders mine simulation data to find locally over-dense gravitationally bound systems, which are then attributed to the dark haloes we currently believe surround galaxies. Such tools have led to critical insights into our understanding of the origin and evolution of structure and galaxies. To take advantage of sophisticated simulation codes and to optimise their predictive power one needs an equally sophisticated halo finder.

Over the years, halo finding algorithms have paralleled the development of their partner N -body codes. We briefly outline the major halo finders currently in use.

II.7.1 Friends-Of-Friends

The Friends-of-Friends (FOF) (Davis *et al.*, 1985; Frenk *et al.*, 1988) algorithm uses spatial information to locate haloes. Specifying a linking length b_{link} the finder links all pairs of particles with separation equal to or less than b_{link} and calls these pairs “friends”. Haloes are defined by groups of friends (friends-of-friends) that have at least one of these friendship connections. Two such advantages of this algorithm are its ease of interpretation and its avoidance of assumption concerning the halo shape. The greatest disadvantage is its simple choice of linking length which can lead to a connection of two separate objects via so-called linking “bridges”. Moreover, as structure formation is hierarchical, each halo contains substructure and thus the need for different linking lengths to identify “haloes-within-haloes”. There have been many variants to this scheme which attempt to overcome some of these limitations (Suto *et al.*, 1992; Sugihara and Suto, 1992; van Kampen, 1995; Okamoto and Habe, 1999; Klypin *et al.*, 1999a).

II.7.2 DENMAX/SKID

DENMAX (Bertschinger and Gelb, 1991; Gelb and Bertschinger, 1994) and SKID (Weinberg *et al.*, 1997) are similar methods in that they both calculate a density field from the particle distribution, then gradually move the particles in the direction of the local density gradient ending with small groups of particles around each local density maximum. The FOF method is then used to associate these small groups with individual haloes. A further check is employed to ensure that the grouped particles are gravitationally bound. The two methods differ through their calculation of the density field. DENMAX uses a grid while SKID applies an adaptive smoothing kernel similar to that employed in Smoothed Particle Hydrodynamics techniques (Lucy, 1977; Gingold and Monaghan, 1977; Monaghan, 1992). The effectiveness of these methods is limited by the method used to determine the density field (Goetz *et al.*, 1998).

II.7.3 Bound-Density-Maxima

A similar technique to the above is the Bound Density Maxima (BDM) method (Klypin and Holtzman, 1997; Klypin *et al.*, 1999a). In this scheme a smoothed density is derived by smearing out the particle distribution on a scale r_{smooth} of order the force resolution of the N -body code used to generate the data: randomly placed “seed spheres” with radius r_{smooth} are shifted to their local centre-of-mass in an iterative procedure until convergence is reached. Hence, as with DENMAX and SKID, this process finds local maxima in the density field. Bullock *et al.* (2001) further refined the BDM technique by first generating a set of possible centres, ranking the particles with respect to their local density and then implementing modifications which allow for credible identification of haloes-within-haloes. The Bullock *et al.* (2001) adaptation to BDM excels at finding halo substructure.

II.7.4 MLAPM’s-Halo-Finder

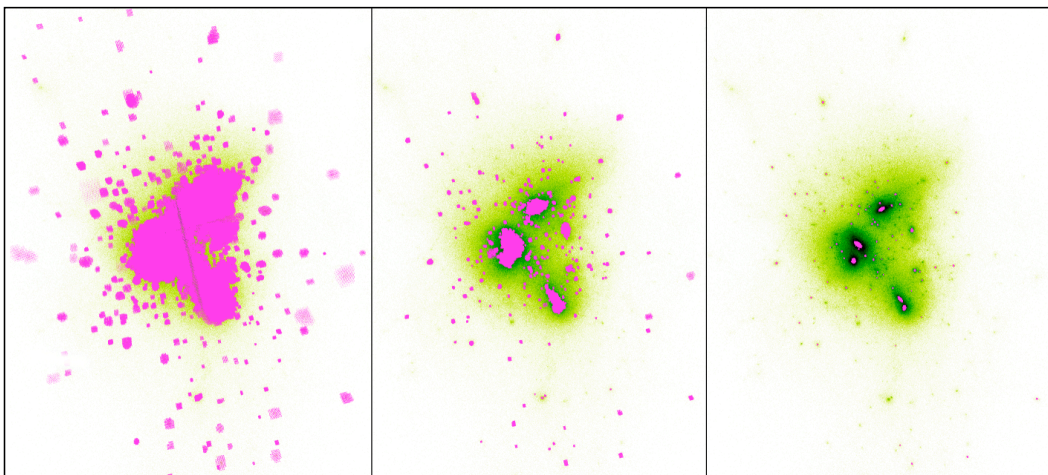


Fig. 8. This panel shows a series of 3 consecutive refinement levels of MLAPM’s grid structure starting at the 5th refinement level superimposed upon the density projection of the particle distribution (cf. also Fig. 3).

Prospective Halo Centres The general goal of a halo finder is to identify gravitationally bound objects. As all haloes are centered about local over-density peaks they are usually found simply by using the spatial information provided by the particle distribution. Thus, the haloes are located as peaks in the density field of the simulation. To locate objects in this fashion, the halo finder is required in some way to reproduce the work of the N -body code in the calculation of the density field or the location of its peaks. When locating haloes like this, the major limitation will always be the appropriate reconstruction of the density field. With that in mind we introduced MLAPM’s-Halo-Finder, MHF hereafter.

MHF essentially uses the adaptive grids of the original simulation code MLAPM to locate the centres of prospective haloes. As previously mentioned in Section II.6, MLAPM’s adaptive refinement meshes follow the density distribution *by construction*. Grid structure naturally “surrounds” the haloes as they are simply manifestations of over-densities, a view which can best be appreciated through inspection of Fig. 8. In this

figure, the refinement grids of MLAPM are superimposed over the projected density of the particle distribution. The left image is the 5th refinement level, with the 6th and 7th levels shown in the middle and right panel, respectively. We emphasise that the grids get successively smaller and are subsets of other grids on lower refinement levels. The advantage of reconstructing and using these grids to locate haloes is that they naturally follow the density field with the accuracy of the N -body code. No additional scaling length is required, in contrast with techniques such as FOF. Therefore, MHF avoids one of the major complications inherent to most halo finding schemes as a natural consequence of its construction.

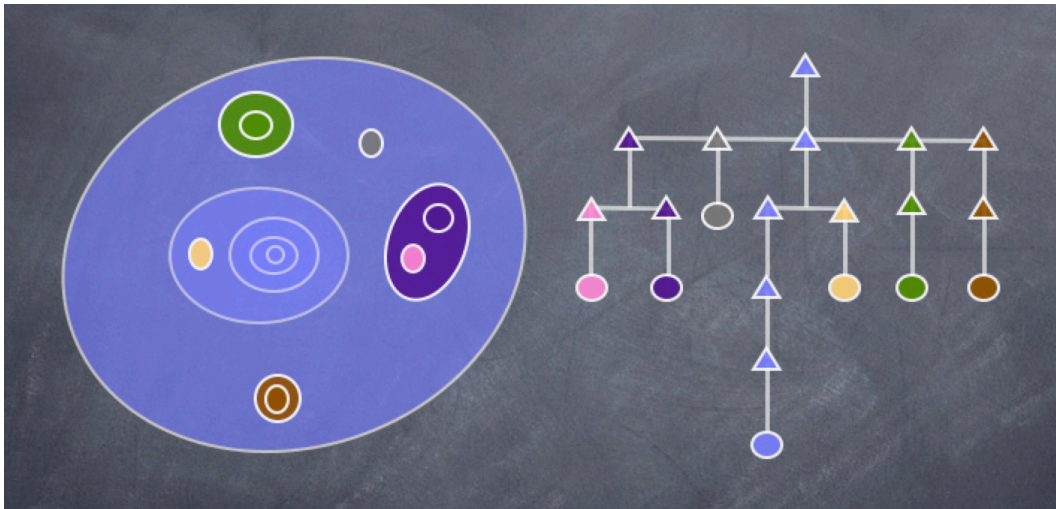


Fig. 9. This figure illustrates the restructuring of the nested MLAPM grids into to the “grid tree”. The left side represents an idealised refinement grid structure, while the right side shows the re-ordering of these grids into a “grid tree”. Note that each branch of the grid tree represents a single dark matter halo within the simulation.

Gathering Halo Particles An initial guess for particles belonging to a (sub-)halo in a cosmological simulation is based upon the adaptive mesh hierarchy of the simulation code MLAPM. The adaptive meshes are organized into a tree structure where the end leaf of each branch is one of the prospective halo centres. The situation is sketched in Fig. 9. We now need to remember that one of the features of MLAPM is to link particles to the finest node surrounding it (cf. Section II.6.1). Therefore, to obtain a first set of particles “belonging” to a given centre we collect all particles starting at the end-leaf moving up the tree to a point where the branch merges with another branch. That “intersection” with another halo marks the point where two centres share a larger (lower density) grid, i.e. they are embedded within a lower isodensity contour. Not to miss any particles that possibly belong to a halo we also collect all the particles from that parent branch that are within half the distance to the next closest more massive branch.

Unbinding Procedure Once we know the prospective centres for haloes and have a list of particles possibly belonging to that halo we test whether the particles are gravitationally bound to it or not.

In order to remove the unbound particles we have to obtain the (local) escape velocity $v_{\text{esc}}(r)$ at each particle position. As v_{esc} is directly related to the (local) value of the potential we integrate Poisson's equation (under the assumption of spherical symmetry):

$$\Delta\phi(r) = \frac{1}{r} \frac{d}{dr} \left(r^2 \frac{d\phi}{dr} \right) = 4\pi G \rho(r) \quad (\text{II.28})$$

The first integral reads as follows

$$r^2 \frac{d\phi}{dr} - \left[r^2 \frac{d\phi}{dr} \right]_{r=0} = 4\pi G \int_0^r \rho(r') r'^2 dr' = GM(< r) \quad (\text{II.29})$$

This equation shows that $d\phi/dr \propto M(< r)/r^2$ and hence $r^2 d\phi/dr \rightarrow 0$ for $r \rightarrow 0$. We are therefore left with the following first-order differential equation for $\phi(r)$:

$$\frac{d\phi}{dr} = G \frac{M(< r)}{r^2} \quad (\text{II.30})$$

Another integration leaves us with

$$\phi(r) = G \int_0^r \frac{M(< r')}{r'^2} dr' + \phi_0 \quad (\text{II.31})$$

This time we need to calculate ϕ_0 . We do this by requiring $\phi(\infty) = 0$:

$$\begin{aligned} \phi(\infty) &= G \int_0^\infty \frac{M(< r')}{r'^2} dr' + \phi_0 \\ &= G \int_0^{r_{\text{vir}}} \frac{M(< r')}{r'^2} dr' + G \int_{r_{\text{vir}}}^\infty \frac{M(< r')}{r'^2} dr' + \phi_0 \\ &= G \int_0^{r_{\text{vir}}} \frac{M(< r')}{r'^2} dr' + GM_{\text{vir}} \int_0^{r_{\text{vir}}} \frac{1}{r'^2} dr' + \phi_0 \\ &= G \int_0^{r_{\text{vir}}} \frac{M(< r')}{r'^2} dr' + G \frac{M_{\text{vir}}}{r} + \phi_0 \end{aligned} \quad (\text{II.32})$$

and hence

$$\phi_0 = - \left(G \int_0^{r_{\text{vir}}} \frac{M(< r')}{r'^2} dr' + G \frac{M_{\text{vir}}}{r} \right) \quad (\text{II.33})$$

Note that we assume that the halo is truncated at r_{vir} when evaluating the integral $\int_{r_{\text{vir}}}^\infty \frac{M(< r')}{r'^2} dr'$.

Unbound particles are removed iteratively where we integrate Eq. (II.31) along a list of radially ordered particles; the same holds for obtaining ϕ_0 that has to be re-evaluated prior to a new iteration.

MHF in Action A visual impression of MHF can be viewed in Fig. 10. Here we show the colour-coded density field of a dark matter halo (left panel) and the subhaloes identified by MHF (right panel). Note that the host halo itself (which is in fact the whole object shown on the left) is not marked in the right panel for clarity. This figure nicely demonstrates the capabilities of MHF: our halo finder is proficient in locating even the smallest subhaloes without the need to fine-tune any technical parameters. We further like to mention that MHF also works on-the-fly when performing a simulation

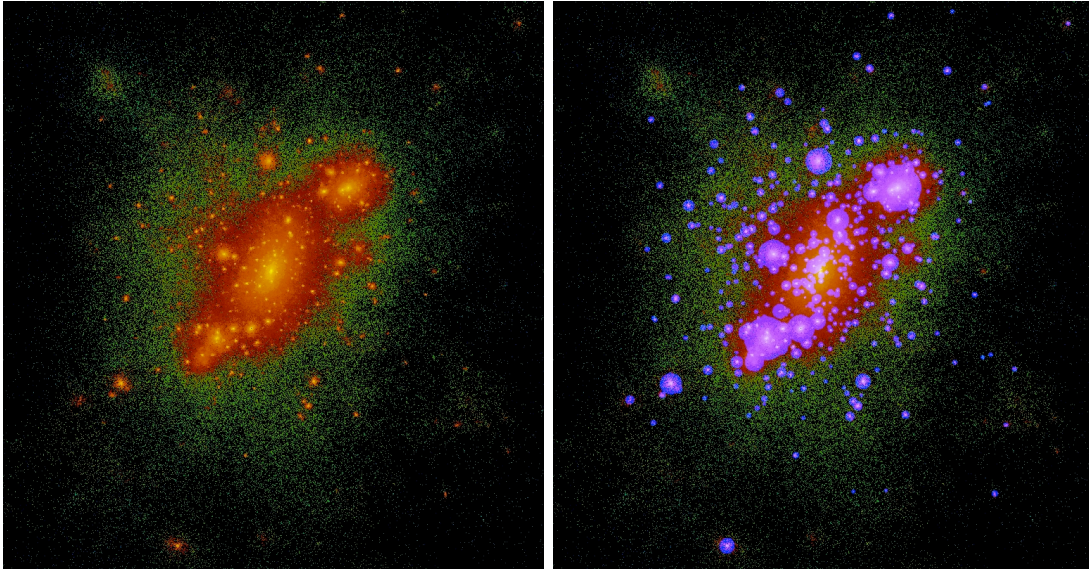


Fig. 10. MHF in action: the left panel shows the colour-coded density field of a particular host haloes while the right panel additionally marks the positions and radii of all identified subhaloes. Note that the host is not marked for clarity.

with MLAPM; whenever the user requests to store an output file of the simulation the code automatically generates a halo catalogue, too.

This work has been published as “The evolution substructure I: a new identification method” (Gill S.P.D., Knebe A., Gibson B.K., 2004, MNRAS 351, 399).

II.8 Initial Conditions

Before actually starting a cosmological simulation one needs to generate the appropriate initial conditions. In Layman’s terms this means to convert the observed fluctuations in the cosmic microwave background radiation into density perturbations and generate a particle distribution with the corresponding statistical properties. This is fairly straightforward under the assumption that the fluctuations are of Gaussian nature; in that case one single function is sufficient to describe the perturbations, namely the power spectrum of matter perturbations $P(k)$. In this Section we are going to explain how to perform this task and present a study that checks the credibility of the initial conditions obtained this way.

II.8.1 Generating Cosmological Initial Conditions

The commonly used way for setting up initial conditions for a cosmological simulation is to make use of the Zeldovich approximation to move particles from a Lagrangian point \vec{q} to an Eulerian point \vec{x} (e.g. Efstathiou *et al.*, 1985):

$$\vec{x} = \vec{q} - D(t)\vec{S}(\vec{q}) , \quad (\text{II.34})$$

where $D(t)$ describes the growing mode of linear fluctuations and $\vec{S}(\vec{q})$ is the “displacement field”. This method is not restricted to a cosmological scenario nor to the Zeldovich approximation: it is very general, relying only on the continuity equation for the transport of particles in the limit $D(t) \rightarrow 0$. The initial Lagrangian coordinates \vec{q} are usually chosen to form a regular, three-dimensional lattice although there are other possible point-particle realizations yielding a homogeneous and isotropic density field on large scales (i.e. glass-like initial condition, White, 1996).

For the runs presented in this study we used the code described in Klypin and Holtzman (1997) to set up the initial conditions

$$\vec{S}(\vec{q}) = \nabla_q \Phi(\vec{q}), \quad \Phi(\vec{q}) = \sum_{\vec{k}} a_{\vec{k}} \cos(\vec{k} \cdot \vec{q}) + b_{\vec{k}} \sin(\vec{k} \cdot \vec{q}) , \quad (\text{II.35})$$

where the Fourier coefficients $a_{\vec{k}}$ and $b_{\vec{k}}$ are related to a pre-calculated input power spectrum of density fluctuations, $P(k)$, as follows:

$$a_{\vec{k}} = R_1 \frac{1}{k^2} \sqrt{P(k)}, \quad b_{\vec{k}} = R_2 \frac{1}{k^2} \sqrt{P(k)}. \quad (\text{II.36})$$

R_1, R_2 are (Gaussian) random numbers with mean zero and dispersion unity. The factor $1/k^2$ is (the Fourier transform of) the Green’s function of Poisson’s equation⁹ and $\Phi(\vec{q})$ can therefore be understood as the gravitational potential created by a Gaussian stochastic density field whose power spectrum agrees with the input $P(k)$; the power spectrum $P(k)$ measures the strength of each individual k -mode contributing to the density field. However, to fully preserve the random nature both amplitudes (sine- and cosine-wave) are to be picked from a Gaussian distribution.

Eq. (II.35) can be rewritten introducing complex numbers:

⁹Actually, $-1/k^2$ is the correct Green’s function, but the factor -1 can be dropped as R_1 and R_2 scatter around zero.

$$\Phi(\vec{q}) = \sum_{\vec{k}} A_{\vec{k}} \exp(i[\vec{k} \cdot \vec{q} + \theta_{\vec{k}}]), \quad A_{\vec{k}} \exp(i\theta_{\vec{k}}) := \frac{1}{2}[a_{\vec{k}} + a_{-\vec{k}} - i(b_{\vec{k}} - b_{-\vec{k}})]. \quad (\text{II.37})$$

Both $A_{\vec{k}}$ and $\theta_{\vec{k}}$ need to be drawn from appropriate random distributions. However, the ICs of cosmological relevance are ergodic for $A_{\vec{k}}$ with $k \gg k_{min}$, making their random nature irrelevant: spatial regions of size much smaller than the simulation box already work as many different realizations inside the box for those amplitudes. Thus, cosmic variance enters through the random nature of the phases $\theta_{\vec{k}}$ and of the amplitudes $A_{\vec{k}}$ for $k \approx k_{min}$.

II.8.2 The Reliability of Cosmological Initial Conditions

In order to check the credibility of the initial conditions generated in above outlined way we create ten random realizations of the same power spectrum $P(k)$ by using different random seeds when drawing R_1, R_2 in Eq. (II.36). The input power spectrum $P(k)$ was calculated using the CMBFAST code (Seljak and Zaldarriaga, 1996), and all parameters (e.g. box size, number of particles, force resolution, integration steps, etc.) were fixed except for the seed for generating the random sequence providing the R -values¹⁰.

These initial conditions for N -body simulations were tested with respect to their correlation properties. Recent claims by Baertschiger *et al.* (2002) throw doubts on the ability of this method to clearly reproduce the analytical input correlations: Baertschiger *et al.* (2002) claim that the power spectrum $P(k)$ and the mass variance $\sigma_M(r)$ as recovered from the initial conditions deviate from the expected behavior.

Our estimator for the mass variance distributes a certain number of spheres with radius r at random in the simulation volume and compares the number of particles inside those spheres to the expected mean value

$$\sigma_{M,\text{est}}^2(r) = \frac{1}{\langle N_r \rangle^2} \sum_{i=1}^{N_s} \frac{(N_i(r) - \langle N_r \rangle)^2}{N_s - 1}. \quad (\text{II.38})$$

N_s is the total number of spheres with radius r and $\langle N_r \rangle = \langle \rho \rangle 4\pi r^3 / 3m_p$ is the mean number of particles in such a sphere.

We first thoroughly tested our estimator Eq. (II.38) by confirming the scaling relations predicted for simple particles distribution as for instance a Poisson distribution and a shuffled lattice. The result can be viewed in the left panel of Fig. 11. The estimator has then been applied to the set of ten initial conditions alluded to above with the result presented in the right panel of Fig. 11. The solid line in that plot is the analytical curve as derived from a simple integration of the initial input power spectrum

$$\sigma_M^2(r) = \frac{1}{2\pi^2} \int_0^{+\infty} P(k) \hat{W}^2(kr) k^2 dk, \quad \hat{W}(x) = \frac{3}{x^3} (\sin x - x \cos x). \quad (\text{II.39})$$

Contrary to the findings of Baertschiger *et al.* (2002), we observe that the initial conditions agree, from approximately the scale of the particle Nyquist frequency out to nearly half the box size, with the analytical predictions. The faster drop of $\langle \sigma_{M,\text{est}}^2(r) \rangle_{\text{set}}$ for scales approaching the box size is simply the effect of the finite (periodical) box. As

¹⁰An appropriate routine might be **GASDEV** from Numerical Recipes (Press *et al.*, 1992).

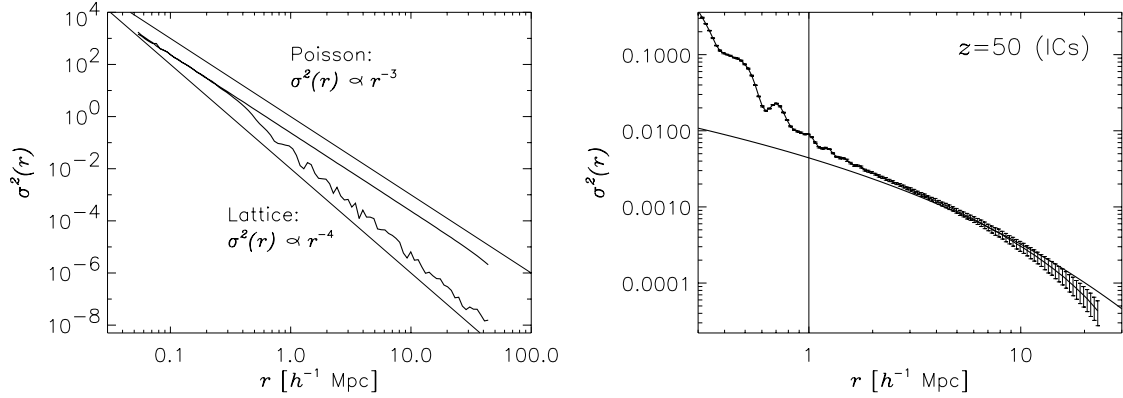


Fig. 11. Reliability check for our $\sigma_{M,\text{est}}^2(r)$ estimator Eq. (II.38) (left panel). The solid lines have the slopes of the analytical expectations (all amplitudes are arbitrary). (right panel).

soon as the volume of the sphere comes close to the actual box size (which happens for $r \approx B/2$) one finds nearly all particles in the sphere due to the periodic boundary conditions. Hence the variance $\sigma_{M,\text{est}}^2(r)$ drops faster than predicted by Eq. (II.39). And the larger amplitude of $\sigma_{M,\text{est}}^2(r)$ for small scales is indeed a reflection of the discreteness of the initial conditions. But in any case Fig. 11 is a rather convincing argument that the mass variance in the initial conditions does agree with the CDM type fluctuations as described by the input power spectrum $P(k)$.

This work has been published as “On the reliability of initial conditions for dissipationless cosmological simulations” (Knebe A., Dominguez A., 2003, PASA 20, 173) and as a comment on “On the problem of initial conditions in cosmological N-body simulations” (Dominguez A., Knebe A., 2003, EpL 4, 631).

Part III

Alternative Cosmologies

This part represents a summary of the following publications:

- (1) Knebe A., Islam R.R., Silk J., 2002, *MNRAS* 326, 109
- (2) Knebe A., Devriendt J.E.G., Mahmood A., Silk J., 2002, *MNRAS* 329, 813
- (3) Little B., Knebe A., Gibson B.K., 2003, *MNRAS* 341, 617
- (4) Knebe A., Devriendt J.E.G., Gibson B.K., Silk J., 2003, *MNRAS* 345, 1285
- (5) Knebe A., Gibson B.K., 2004, *MNRAS* 347, 1055
- (6) Knebe A., Arnold B., Power C., Gibson B.K., 2008, *MNRAS* 386, 1029

III.1 Introduction

The currently favoured Λ CDM model of cosmological structure formation (cf. Section I.4) has proven to be extremely successful at describing the clustering of matter on intermediate to large scales (e.g. Springel *et al.*, 2005; Spergel *et al.*, 2007; Komatsu *et al.*, 2008). In contrast, it has been argued that the predictions of the Λ CDM model are at odds with observations on the scales of galaxies, on the basis of cosmological N -body simulations. The major discrepancies can be summarized as follows

- Cold dark matter haloes are predicted to have “cuspy” density profiles with inner logarithmic slopes of approximately -1.2 (e.g. Navarro *et al.*, 2004; Tasitsiomi *et al.*, 2004; Diemand *et al.*, 2005; Reed *et al.*, 2005), whereas high resolution observations of low surface brightness galaxies appear to require haloes with constant density cores (e.g. Gentile *et al.*, 2007; McGaugh *et al.*, 2007).
- Furthermore, CDM haloes are predicted to contain a wealth of substructure, which we might expect to observe as satellite galaxies within galactic haloes, in sharp contrast to the observed abundance of satellites around our Galaxy and others (Klypin *et al.*, 1999b; Moore *et al.*, 1999).
- Implied by point 1., the very inner regions of simulated CDM haloes are too dense, which leads to too efficient baryonic cooling. This results into simulated galactic disks with too low angular momentum (Steinmetz and Navarro, 1999).

Suggested solutions to these problems have included allowing the dark matter to be collisional (i.e. *self-interacting*) rather than collisionless (Spergel and Steinhardt, 2000; Bento *et al.*, 2000), allowing it to be warm rather than cold (Bode *et al.*, 2001; Avila-Reese *et al.*, 2001; Knebe *et al.*, 2002), or introducing non-standard modifications to an otherwise unperturbed CDM power spectrum (e.g. Bullock, 2001; Little *et al.*, 2003). In this part we are going to explore some of these alternative structure formation scenarios and compare them against the Λ CDM paradigm.

III.2 Warm Dark Matter

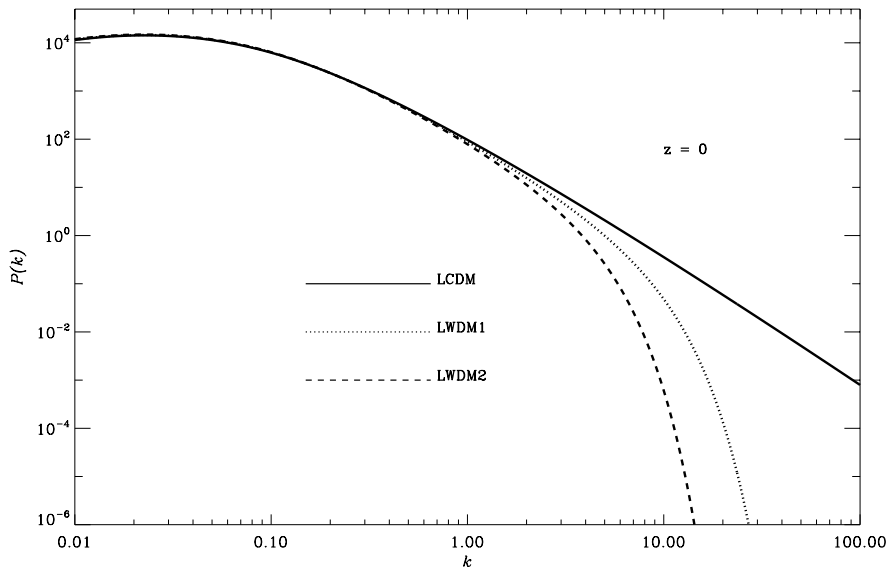


Fig. 12. Power spectra of cold vs. warm dark matter models. Λ WDM1 corresponds to a warmon mass of 1.5keV and Λ WDM2 to 0.5keV.

Arguably one of the most promising (and least intrusive) modification to the (cold) dark matter paradigm is to allow the dark matter particle to be warm (i.e. warm dark matter, WDM hereafter). In such a case, warm dark matter particles will have a relatively high thermal velocity dispersion at the era of decoupling and therefore a non-negligible *free-streaming scale* λ_{fs} . This modification results in a change to the primordial matter power spectrum, corresponding to a damping of density perturbations on scales below a *filtering scale* λ_f (which is related to the free-streaming scale λ_{fs}), which in turn is related to a filtering mass M_f (Bardeen *et al.*, 1986; Bode *et al.*, 2001; Avila-Reese *et al.*, 2001; Knebe *et al.*, 2002).

As an illustration we present two such warm dark matter power spectra in comparison to the Λ CDM model in Fig. 12 where Λ WDM1 corresponds to a warmon mass of 1.5keV and Λ WDM2 to 0.5keV. The following Sections III.2.1–III.2.3 now take a closer look at properties of dark matter haloes forming in simulations of WDM cosmic structure formation. The simulations have been performed using identical phase information when generating the initial conditions (cf. Section II.8) to allow for a direct cross-comparison of objects.

III.2.1 The Overabundance of Satellite Galaxies

As WDM was “designed” to reduce small scale power in the simulation it comes at no surprise that we find a depletion of subhaloes in this model. This can be viewed in Fig. 13 where we show the grey-scaled density field of two host haloes. While the upper panel shows those two objects in the CDM simulation we notice the clear trend for the number of substructures to decrease with decreasing warmon mass (the middle panel shows the Λ WDM1 and the lower panel the Λ WDM2 model). In terms of the

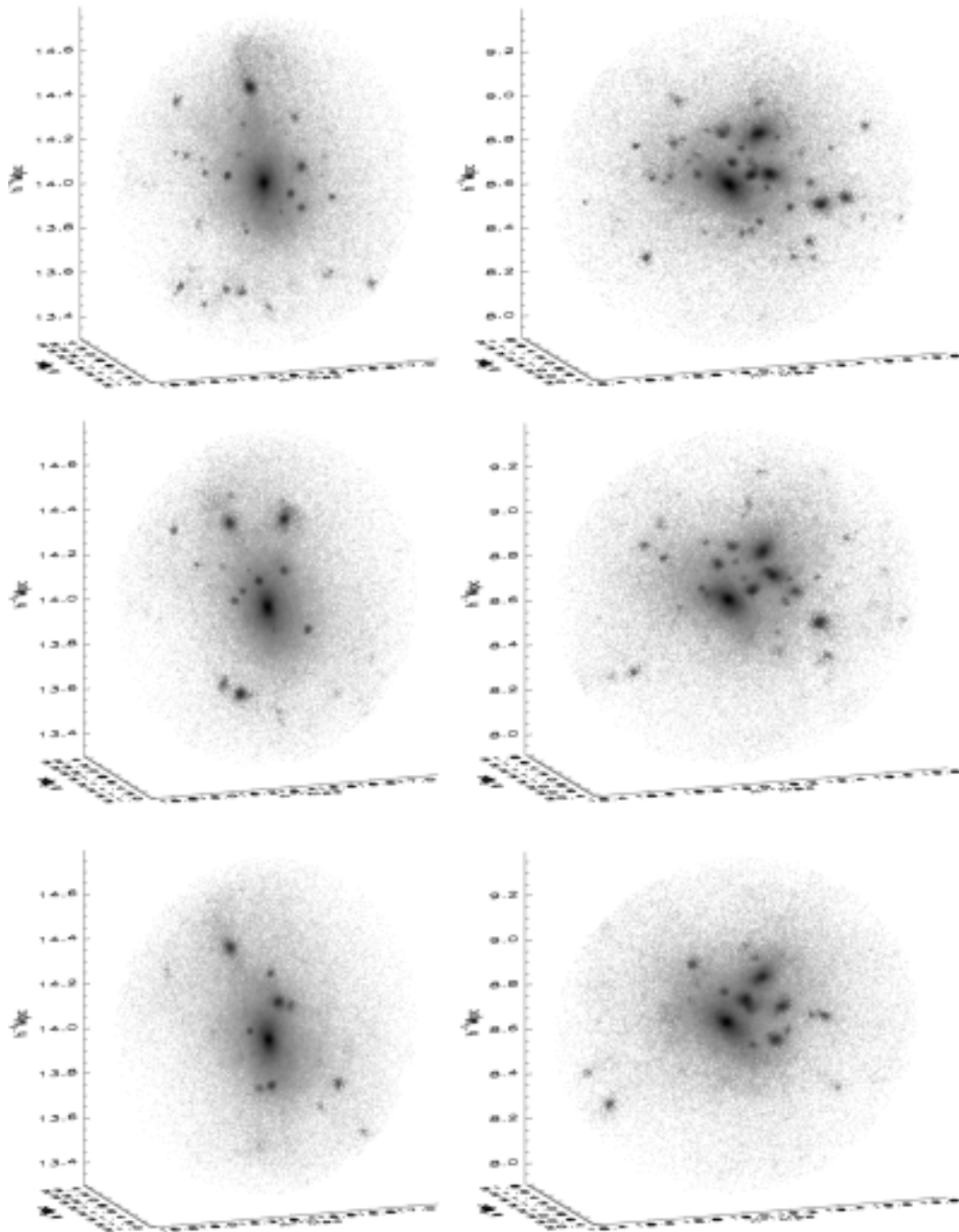


Fig. 13. Grey scaled density field of two galactic haloes (left and right column, respectively) identified at $z=0$. The upper row shows the Λ CDM model whereas the middle and bottom row are taken from the AWDM1 and AWDM2 model, respectively.

number of subhaloes WDM models are therefore in better agreement with observations. However, we also note (though not shown here) that WDM has little influence on the shape of the density profile which still inhibits the “cuspy” nature in the central parts. The only difference being the concentration of haloes which is lowered in WDM. This is also the explanation for the depletion of subhaloes: they have lower concentration and are hence more prone to tidal disruption.

This work has been published as “Merger Histories in WDM Structure Formation Scenarios” (Knebe A., Devriendt J.E.G., Mahmood A., Silk J., 2002, MNRAS 329, 813).

III.2.2 The dynamics of subhaloes in WDM models

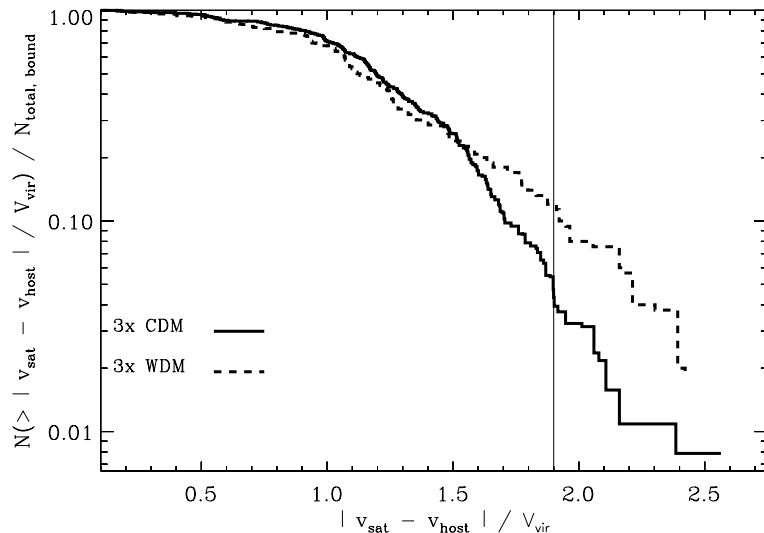


Fig. 14. Cumulative distribution of relative velocities between all subhaloes and their respective host. The thin vertical line is representative of the collisional speed of the “Bullet” cluster.

Aside from the actual number of subhaloes are there other apparent differences in the subhalo populations of CDM and WDM host haloes?

In Fig. 14 we plot the cumulative distribution of relative velocities ($V_{\text{sat}} - V_{\text{host}}$) for all interior subhaloes, where V_{sat} and V_{host} are the centre-of-mass velocities of all particles inside the virial radius of the subhalo and the host, respectively. Relative velocities have been normalised to the circular velocity V_{vir} of the host at the virial radius. If we compute this quantity for the “Bullet cluster” (Markevitch, 2006) using the estimate of the mass deduced from weak lensing (Clowe *et al.*, 2004), the normalised collision speed $(V_{\text{sat}} - V_{\text{host}})/V_{\text{vir}}$ is approximately 1.9 (and shown as a thin vertical line). We need to stress that the Bullet Cluster (1E0657-56) is on ongoing merger and poses a challenge to CDM as the relative speed of the encounter is extremely large and there are not that many high-velocity encounters predicted within the CDM paradigm (Hayashi and White, 2006).

Fig. 14 now reveals that $\sim 6\%$ of subhaloes in the CDM model have normalised relative velocities in excess of 1.9, compared to $\sim 10\%$ in the WDM model. In other words, the probability of a high-speed encounter is greater in the WDM model than in the CDM

model.

This work has been published as “The dynamics of subhaloes in warm dark matter models” (Knebe A., Arnold B., Power C., Gibson B.K., 2008, MNRAS 386, 1029).

III.2.3 Top-Down Fragmentation of WDM Filaments

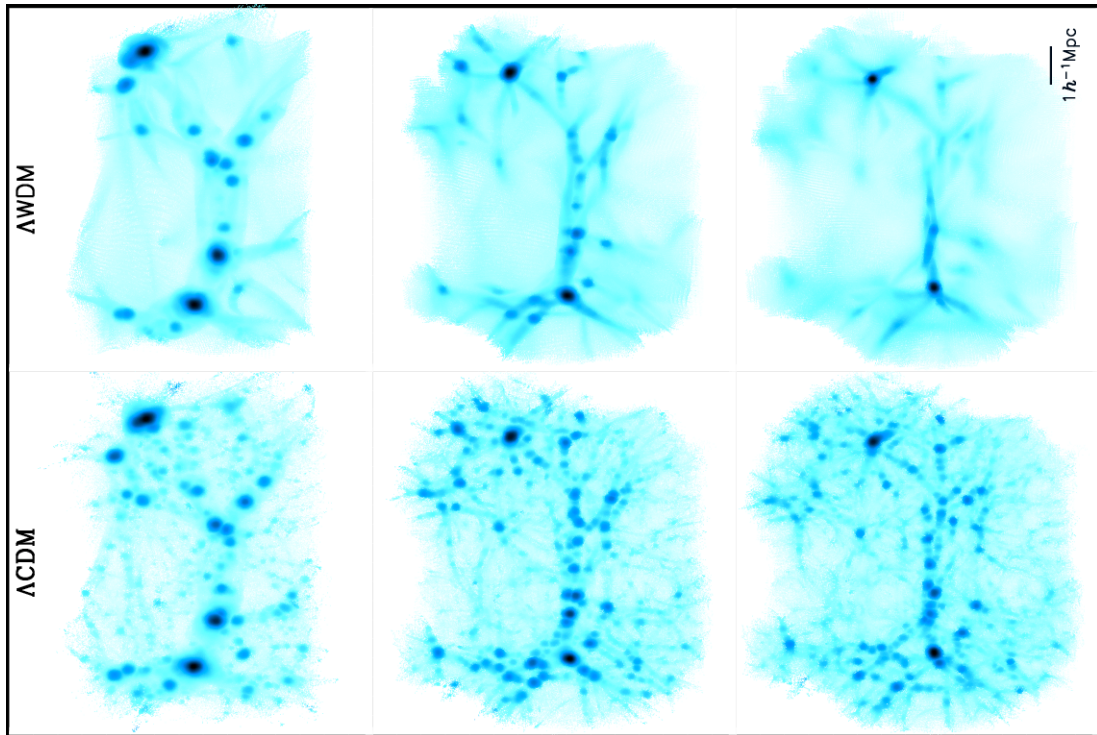


Fig. 15. Gray-scaled image of the logarithm of the density field around the filament at redshifts $z = 1$ (left column), $z = 3$ (middle column) and $z = 5$ (right panel) for Λ WDM2 (upper row) and Λ CDM (lower row).

As outlined in Section I.3 structure formation proceeds substantially different for cold and hot dark matter. Now, warm dark matter is somewhat in-between and it therefore only appears natural to ask whether objects primarily form top-down (as in HDM) or bottom-up (as in CDM).

While we investigated the hierarchical structure formation of WDM haloes in a previous study (Knebe *et al.*, 2002), we now set the focus upon the emergence of objects in filaments. To this extent we simulated one particular filament with high spatial and mass resolution in CDM and WDM. Fig. 15 shows the particle distribution for both models with each particle being grey-scaled proportionally to the logarithm of the local (over-)density. A striking feature of Fig. 15 is the marked granularity of the density field in the CDM model at all redshifts in contrast with WDM. This reflects the lack of filtering of power on small scales in CDM as opposed to WDM. However, while the WDM filament is obviously different from its CDM counterpart at redshift $z=5$, they are similar at $z=1$. This similarity is all the more remarkable that the logarithmic scale used to plot the density fields shown in Fig. 15 artificially enhances the density

contrast, thus highlighting differences between the two universes that would have gone unnoticed had the scale been linear.

A further difference of note is the *appearance* of individual (low-mass) haloes during the course of the WDM filament evolution, whereas dense objects only seem to be merging in the CDM filament, therefore *decreasing* steadily in number. This is a clear indication of a top-down fragmentation of the filament into smaller entities opposite to hierarchical structure formation in CDM.

We need to mention at this point that these results have recently been challenged by Wang and White (2007) who claim that it is intrinsically difficult to simulate any kind of structure formation in hot/warm dark matter models. However, we believe that the final verdict is still out there and will investigate and check their claims, respectively.

This work has been published as “Top-Down Fragmentation of WDM Filaments” (Knebe A., Devriendt J.E.G., Gibson B.K., Silk J., 2003, MNRAS 345, 1285).

III.3 Bumpy Power Spectra

Several mechanisms have been proposed that could generate “features” in the primordial spectrum during the epoch of inflation. Among these are models with Broken Scale Invariance (BSI) (Lesgourgues *et al.*, 1998), and particularly BSI due to phase transitions during inflation (Barriga *et al.*, 2001). Other inflationary models include resonant production of particles (Chung *et al.*, 2000) and non-vacuum initial states as the quantum mechanical origin for inflationary perturbations (Martin *et al.*, 2000). Broad features can also be introduced into the power spectrum by including a running spectral index in slow-roll inflationary models (e.g. Hannestad *et al.*, 2001). After inflation, other effects such as pressure-induced oscillations¹¹ in the matter radiation fluid before decoupling also leave an imprint in the overall matter transfer function towards small scales mainly in the form of successive crests and troughs (Eisenstein and Hu, 1998). These features will therefore also be part of the cosmological matter power spectrum after matter-radiation equality. We therefore investigated the effects of such features onto structure formation by means of cosmological simulations again.

III.3.1 Mocking different Cosmologies

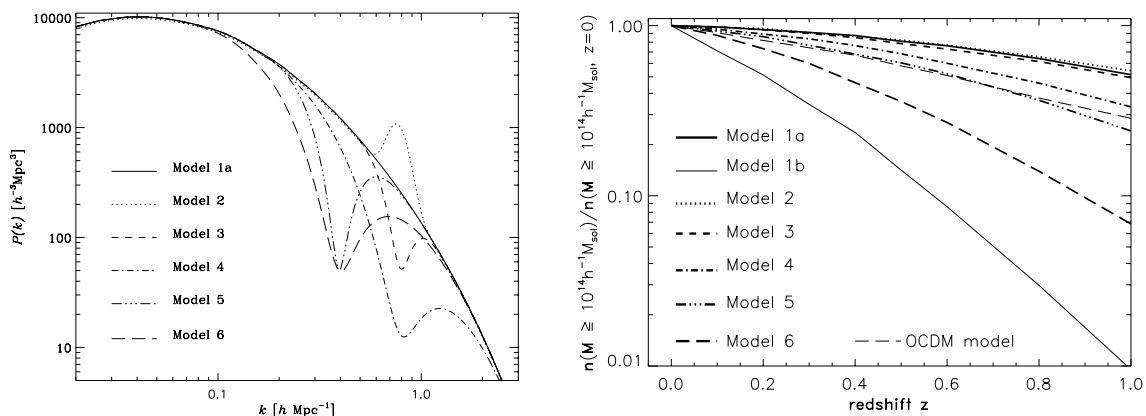


Fig. 16. CDM input spectra containing several features (left panel) and the evolution of the abundance of haloes more massive than $10^{14} h^{-1} M_{\odot}$ normalised to unity at redshift $z = 0$ in those models (right panel).

In the left panel of Fig. 16 we present a series of artificially generated “bumps” and “dips” into an otherwise unperturbed matter power spectrum $P(k)$ (solid line). One particular interesting quantity to investigate is the abundance evolution of galaxy clusters which can be viewed in the right panel of Fig. 16. It has been used throughout the literature to put constraints on the matter content of the Universe and the density parameter Ω_m , respectively (e.g. Bahcall *et al.*, 1997, 1999). We note that the abundance in Fig. 16 has been normalized to unity at redshift $z = 0$ as we are mainly interested in comparing the evolution rather than the absolute value.

¹¹This is also recorded in the oscillatory nature of the spectrum of the cosmic microwave background fluctuations.

This figure indicates that the evolution of the abundance of galaxy clusters is not a reliable measure of Ω_m if there are features on scales of a few Mpc in the primordial power spectrum. Conversely, if we know the cosmological model parameters from other measurements, the cluster abundance evolution permits us to probe features in the power spectrum that are in the nonlinear regime at the present epoch, and hence difficult to discern directly from current epoch measurements.

This work has been published as “Bumpy Power Spectra and Galaxy Clusters” (Knebe A., Islam R.R., Silk J., 2001, MNRAS 326, 109).

III.3.2 Bumpy Power Spectra vs. WDM

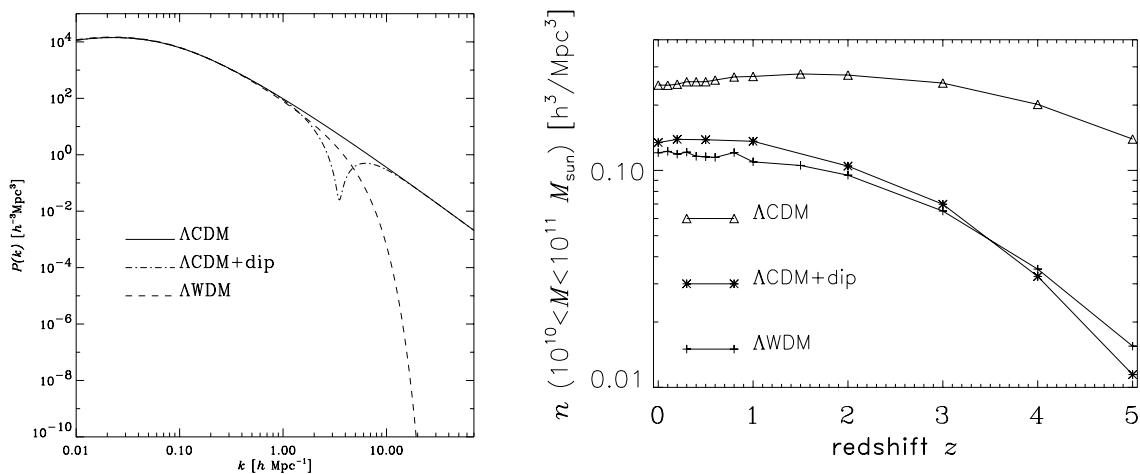


Fig. 17. Input power spectra for WDM vs. Bump simulations (left panel) and the evolution of halo abundance for particle groups with mass M in the range $[10^{10} h^{-1} M_{\odot}, 10^{11} h^{-1} M_{\odot}]$ (right panel).

We may even go one step further and interpret WDM has some kind of dip in the matter power spectrum $P(k)$. Both, dips (cf. Fig. 16) and WDM (cf. Fig. 12) reduce the power and hence may have comparable effects when it comes to, for instance, the number of satellite galaxies.

For the dip model presented in the left panel of Fig. 17 we are using the same prescription to introduce a feature into an otherwise unperturbed CDM power spectrum as for the simulations presented in Section III.3.1. The power taken away from the standard Λ CDM model via the dip agrees with the lack of power in the Λ WDM model to the extent that the integral

$$\sigma^2 = \frac{1}{2\pi^2} \int_0^{k=16h\text{Mpc}^{-1}} P(k) k^2 dk \quad (\text{III.1})$$

is identical for the Λ WDM and dip model ($k = 16h\text{Mpc}^{-1}$ is the point for which the dip meets the unperturbed Λ CDM power spectrum again). The power in the dip model only drops in a narrow interval around k_0 with the width of that interval controlled by the parameter σ_{mod} . A visualization of the three power spectra used in this study is given in Fig. 17 (left panel).

In the right panel of Fig. 17 we highlight the number density evolution of objects in the mass range $10^{10}h^{-1}M_{\odot} < M < 10^{11}h^{-1}M_{\odot}$ by plotting the abundance evolution for particle groups within that range out to redshift $z = 5$. Again, the behavior for WDM and the Dip model are very similar, but we see the trend for a steeper and faster evolution in the latter.

We further showed (though not presented here) that some of the large-scale clustering patterns of this new dip model follow more closely the usual CDM scenario while simultaneously suppressing small scale structures (within galactic haloes) even more efficiently than WDM. The analysis in the original paper (Little *et al.*, 2003) shows that the dip model appears to be a viable alternative to WDM but it is based on different physics. Where WDM requires the introduction of a new particle species the dip model is based on a non-standard inflationary period. If we are looking for an alternative to the currently challenged standard Λ CDM structure formation scenario, neither the Λ WDM nor the new dip model can be ruled out based on the analysis presented in Little *et al.* (2003). They both make very similar predictions.

This work has been published as “Warm Dark Matter vs. Bumpy Power Spectra” (Little B., Knebe A., Gibson B.K., 2003, MNRAS 341, 617).

III.4 Modified Newtonian Dynamics

Some of the problems alluded to in the introduction of Section III.1, as for instance the overabundance of satellites, can be resolved with modifications such as introducing a filtering-scale (or “dips” produced during non-standard inflationary epochs) in the power spectrum of primordial density perturbations (e.g. WDM), self-interactions of dark matter, etc., but none of the proposed solutions have been able to rectify *all* shortcomings of Λ CDM simultaneously.

Therefore, there might be alternative solutions worthy of exploration, one of which is to abandon dark matter completely and to adopt the equations of MODified Newtonian Dynamics (MOND; Milgrom 1983; Milgrom (1983); Bekenstein and Milgrom (1984)). It has already been shown by other authors that this simple idea might explain many properties of galaxies without the need of non-baryonic matter (e.g. Begeman *et al.*, 1991; Milgrom, 1994; Sanders, 1996; McGaugh and de Blok, 1998; Scarpa *et al.*, 2003). MOND is also successful in describing the dynamics of galaxy groups and clusters (Sanders, 1999; Milgrom, 1998), globular clusters (Scarpa *et al.*, 2003) and, to a limited extent, gravitational lensing (Mortlock and Turner, 2001; Qin *et al.*, 1995). A recent review of MOND is given by Sanders and McGaugh (2002) which also summarizes (most of) the successes alluded to above.

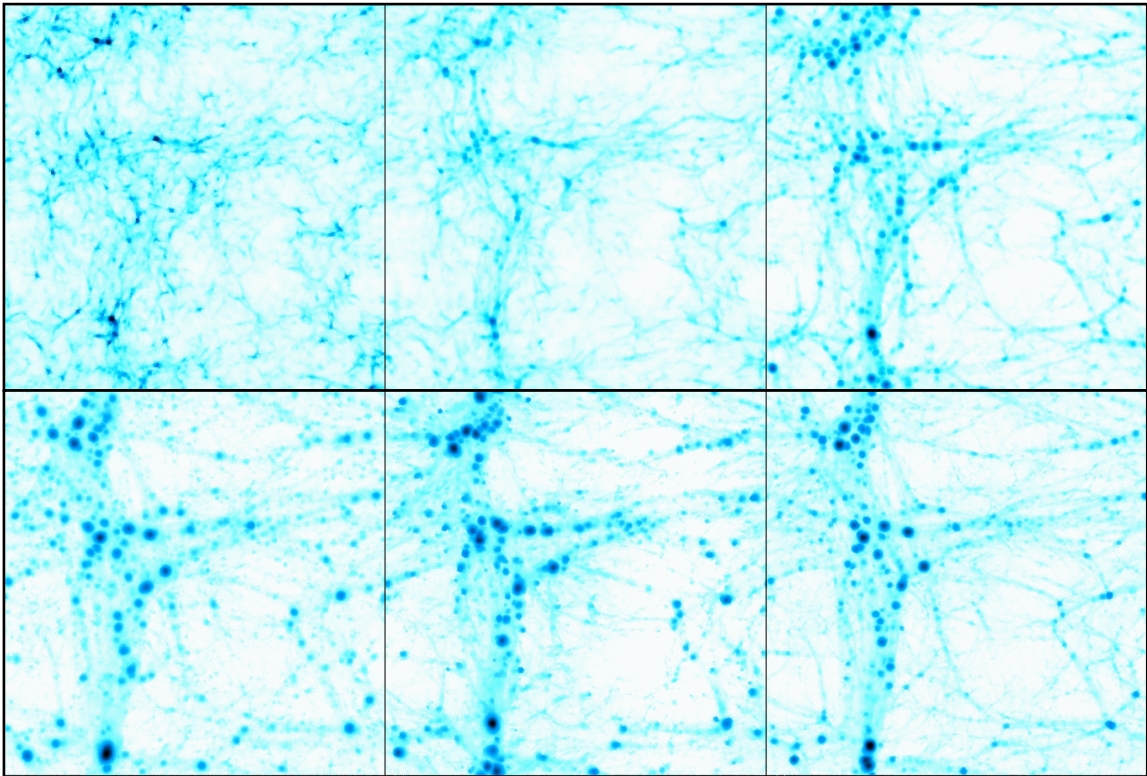


Fig. 18. Comparison of the large-scale density field of the three models under investigation at redshift $z = 0$ (bottom) and $z = 5$ (top). The left column shows the Λ CDM simulation, the middle column the MONDian cosmological simulation and the right one the fiducial OCBMond model.

Here we present a series of high-resolution N -body simulations in which the equations of motion have been changed to account for MODified Newtonian Dynamics (MOND).

For the technical details and equations involved we refer the reader to the original paper by Knebe and Gibson (2004).

We showed that a low- Ω_0 MONDian model with an appropriate choice for the normalisation σ_8 can lead to similar clustering properties at redshift $z = 0$ as the commonly accepted (standard) Λ CDM model. However, such a model shows no significant structures at high redshift with only very few objects present beyond $z > 3$ that can be readily ascribed to the low Ω_0 value adopted. The agreement with Λ CDM at redshift $z = 0$ is driven by the more rapid structure evolution in MOND. This agreement can be viewed in Fig. 18 where we show for three simulations, i.e.

- a standard Λ CDM model,
- an open, low- Ω_0 model with the same $\sigma_8 = 0.9$ as Λ CDM,
- an open, low- Ω_0 model with MOND and adjusted $\sigma_8^{\text{MOND}} = 0.4 \ll \sigma_8$.

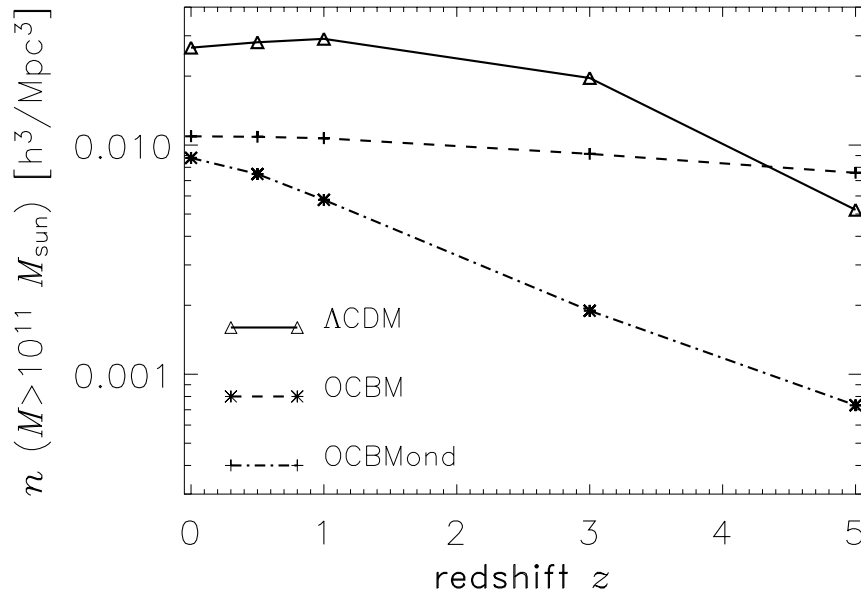


Fig. 19. Redshift evolution of the abundance of haloes with mass $M > 10^{11} h^{-1} M_{\odot}$.

a projection of the whole simulation with each individual particle grey-scaled according to the local density at redshift $z = 0$ and $z = 5$. This figure indicates that the MOND simulation (middle column) looks fairly similar to both the Λ CDM model (left column) and the OCBM model (right column) in terms of the locations of high density peaks (dark areas), filaments and the large-scale structure, respectively. One should bear in mind though that the MONDian simulation was started with a much lower σ_8^{MOND} normalisation than the other two runs. This is in fact reflected in the upper panels showing the density field at redshift $z = 5$; the MOND simulation is less evolved.

As in the previous Sections, the evolution of the abundance of objects proves to be again a discriminator for the different cosmological models. To this extent, Fig. 19

shows the (integral) abundance evolution of objects with mass $M > 10^{11} h^{-1} M_{\odot}$. The Λ CDM model undoubtedly experiences very little evolution from $z \sim 5$ to today whereas both other models show a very steep evolution. The discrepancy between the MOND model and the other two models at redshift $z = 5$ can, however, be ascribed to the lower initial σ_8^{MOND} value again; the MOND model was set up with much smaller initial density perturbation which only grew to a comparable level of clustering via the effects of MOND. This is again in agreement with the findings of Sanders (2001) who showed that the collapse of spherically symmetric overdensities becomes MOND dominated for redshifts $z \lesssim 5$ and hence starts to outrun Newtonian models (cf. Fig. 5 in Sanders 2001).

This work has been published as “Galactic Haloes in MONDian Cosmological Simulations” (Knebe A., Gibson B.K., 2004, MNRAS 347, 1055).

Part IV

Near-Field Cosmology

This part represents a summary of the following publications:

- (1) Knebe A., Gill S.P.D., Gibson B.K., 2004, *PASA* 21, 216
- (2) Knebe A., Gill S.P.D., Gibson B.K., Lewis G.F., Ibata R.A., Dopita M.A., 2004, *ApJ* 603, 7
- (3) Gill S.P.D., Knebe A., Gibson B.K., Dopita M.A., 2004, *MNRAS* 351, 410
- (4) Gill S.P.D., Knebe A., Gibson B.K., 2005, *MNRAS* 356, 1327
- (5) Knebe A., Gill S.P.D., Kawata D., Gibson B.K., 2006, 357, 35
- (6) Knebe A., Power C.B., Gill S.P.D., Gibson B.K., 2006, *MNRAS* 368, 1209
- (7) Warnick K., Knebe A., 2006, *MNRAS* 369, 1253
- (8) Warnick K., Knebe A., Power C.B., 2008, *MNRAS* 385, 1859
- (9) Knebe A., Draganova N., Power C., Yepes G., Hoffman Y., Gottlöber S., Gibson B.K., 2008, *MNRAS* 386, L52
- (10) Knebe A., Yahagi H., Kase H., Lewis G.F., Gibson B.K., 2008, *MNRAS* 388, L34

IV.1 Introduction

There is mounting evidence that the Cold Dark Matter (CDM) structure formation scenario provides the most accurate description of our Universe. Observations point towards a “standard” Λ CDM Universe comprised of 28% dark matter, 68% dark energy, and luminous baryonic matter (i.e. galaxies, stars, gas, and dust) at a mere 4% (cf. Spergel et al., 2007; Komatsu *et al.*, 2008, , and Section I.4). This so-called “concordance model” induces hierarchical structure formation whereby small objects form first and subsequently merge to form progressively larger objects (White and Rees, 1978; Davis *et al.*, 1985, cf. also Section I.3).

Even though CDM appears to have problems with, for instance, the abundance of satellite galaxies orbiting within a galactic dark matter host halo, there are indications from gravitational lensing experiments that these (missing) objects are in fact needed to reconcile observations with theory (Dalal and Kochanek, 2002; Dahle *et al.*, 2003). Hence, if the (overabundant) satellite population predicted by CDM really does exist, it is imperative to understand the orbital evolution of these objects and their deviation from the background dark matter distribution. Moreover, a new astrophysical discipline called “galactic archaeology” has emerged which tries to decipher the formation history of our very own Milky Way by utilizing the debris fields of tidally destroyed satellite galaxies (cf. Helmi and de Zeeuw, 2000). While such disrupted satellites may no longer be detectable in real space, they will still be identifiable in the “integrals-of-motion-space” due to the conservation of angular momentum and energy. Large observational projects (e.g. RAVE (Radial Velocity Experiment, Steinmetz *et al.* (2006)) and GAIA¹²) are being initiated to survey millions of stars in phase-space for exactly this purpose.

In order to test (and possibly confirm) the underlying Λ CDM model utilizing these “galactic building blocks”, more predictions regarding their properties are necessary which can be verified by observations. And this is the driving agent for the science presented in this Part of the thesis.

¹²http://www.esa.int/esaSC/120377_index_0_m.html

IV.1.1 The Simulations

Our analysis is based on a suite of in total 25 high-resolution N -body simulations. Eight of them were carried out using the publicly available adaptive mesh refinement code **MLAPM** (Knebe *et al.*, 2001) and first presented in Gill *et al.* (2004a). Another one was simulated with the ART code and corresponds to the Milky Way type halo “Box20” introduced in Prada *et al.* (2006). For the analysis of the radial alignment signal presented in Section IV.2.3 we augmented these nine hosts with 16 more haloes taking from various other (re-)simulations (Knollmann *et al.*, in preparation; Knebe *et al.* (2008a); Knebe *et al.* (2008b)) in order to span a host halo mass range from $10^{12}h^{-1}M_{\odot}$ to $10^{15}h^{-1}M_{\odot}$. While the particulars of the simulations obviously vary amongst the runs, they are all based upon the Λ CDM model (with only little variation in the actual parameters as given by the first and third year WMAP analysis, Spergel *et al.* (2003, 2007)). Further, all these hosts contain of order millions of dark matter particles and the time-sampling of the outputs is sufficient to closely follow the orbital evolution (and tidal disruption) of their subhalo populations. For the very details we refer the reader to the respective publication.

IV.1.2 The Haloes

The host haloes (as well as all substructure objects down to 20 particles) are identified using our novel open source halo finder **MHF**¹³ (**MLAPM**’s-halo-finder; Gill *et al.*, 2004a, see also Section II.7.4). **MHF** is based upon the adaptive grid hierarchy of **MLAPM** and acts with exactly the same resolution as the N -body code itself; it is therefore free of any bias and spurious mismatch between simulation data and halo finding precision arising from numerical effects. For every halo (either host or satellite) we calculate a suite of canonical properties based upon the particles within the virial/truncation radius. The virial radius R_{vir} is defined as the point where the density profile (measured in terms of the cosmological background density ρ_b) drops below the virial overdensity Δ_{vir} , i.e. $M(< R_{\text{vir}})/(4\pi R_{\text{vir}}^3/3) = \Delta_{\text{vir}}\rho_b$. This threshold Δ_{vir} is based upon the dissipationless spherical top-hat collapse model and is a function of time for the given cosmological model. For $z = 0$ it amounts to $\Delta_{\text{vir}} = 340$. This prescription does no longer apply to subhaloes where the point R_{vir} will not be reached due to the embedding of the satellite within the mass distribution of the host, i.e. the density profile will show a rise again at a certain point. In that case, we use this “upturn point” and truncate the object ignoring all particles outside of the corresponding sphere. For a more elaborate discussion of this process and the halo finder in particular, we refer the reader to Gill *et al.* (2004b).

IV.2 Satellite Galaxies

Within the cold dark matter paradigm haloes constantly grow in mass through slow accretion and violent mergers (cf. Section I.3) and hence satellite galaxies can be considered the “galactic building blocks”. While a self-consistent cosmological modeling of both hosts and satellites has long been recognised as optimal, the required mass and

¹³**MHF** (and **MLAPM**) can be downloaded from the following web page <http://www.aip.de/People/aknebe/MLAPM>

force resolution can be difficult to accommodate (hence the use of static host potentials in most previous studies, Ibata *et al.* (cf. 2003); Helmi (cf. 2004); Peñarrubia *et al.* (cf. 2006)).

The first fully self-consistent simulations targeting the subject were performed by Tormen (1997) and Tormen *et al.* (1998). Both studies were landmark efforts, but lacked the temporal, spatial, and mass resolution necessary to explore a wide range of environmental effects. Unable to follow the satellite distribution within the host’s virial radius, satellites were instead tracked only up to and including the point of “accretion”. This allowed an analysis of the infall pattern, rather than the orbital evolution of the satellites. Ghigna *et al.* (1998) also investigated the dynamics of satellite galaxies in live dark matter host haloes. Although greatly increasing the mass and spatial resolution, they still lacked the temporal resolution to explicitly track the satellite orbits. Instead, the orbits were approximated using a spherical static potential. More recently, Taffoni *et al.* (2003) used N -body simulations coupled with semi-analytical tools to explore the evolution of dark matter satellites inside more massive haloes. However, they focus their efforts on the interplay between dynamical friction and tidal mass loss in determining the final fate of the satellites. Kravtsov *et al.* (2004) also mainly concentrate on the mass loss history of satellites using fully self-consistent cosmological N -body simulations.

In the following Sections we investigate the evolution of substructure and the orbital parameters of satellites using high spatial, mass, *and* temporal resolution.

IV.2.1 The Dynamics of Satellite Galaxies

The work described in this sub-section focuses upon a detailed analysis of the temporal and spatial properties of satellite galaxies residing within host dark matter haloes and is based upon eight cluster sized dark matter haloes. To date, typical satellite properties such as orbital parameters and mass loss under the influence of the host halo have primarily been investigated using *static* potentials for the dark matter host halo (e.g. Johnston *et al.*, 1996; Hayashi *et al.*, 2003). We stress that each of these studies have provided invaluable insights into the physical processes involved in satellite disruption; our goal was to augment these studies by relaxing the assumption of a static host potential, in deference to the fact that realistic dark matter haloes are not necessarily axis-symmetric. Haloes constantly grow in mass through slow accretion and violent mergers, possessing rather triaxial shapes (e.g. Frenk *et al.*, 1988; Warren *et al.*, 1992; Kasun and Evrard, 2005; Bailin and Steinmetz, 2005; Allgood *et al.*, 2006; Macciò *et al.*, 2007; Bett *et al.*, 2007; Gottlöber and Yepes, 2007).

As an example of the results obtained we show in Fig. 20 the eccentricity of each satellite (represented by the crosses) versus the number of orbits the satellite has completed. There is a clear trend for eccentricity to decrease as the number of orbits of a satellite increases. This is also demonstrated by the histogram, which is not the “binned” result of the crosses, but is instead the average eccentricity for all satellites that had $\geq N_{\text{orbits}}$ orbits

$$\langle e \rangle(N_{\text{orbits}}) = \frac{1}{N_{\text{sat}}(\geq N_{\text{orbits}})} \sum_{i=1}^{N_{\text{sat}}(\geq N_{\text{orbits}})} e_i(N_{\text{orbits}}) . \quad (\text{IV.1})$$

Here, $e_i(N_{\text{orbits}})$ is the eccentricity of satellite i after N_{orbits} orbits and $N_{\text{sat}}(\geq N_{\text{orbits}})$ is the number of satellites with equal or more than N_{orbits} orbits.

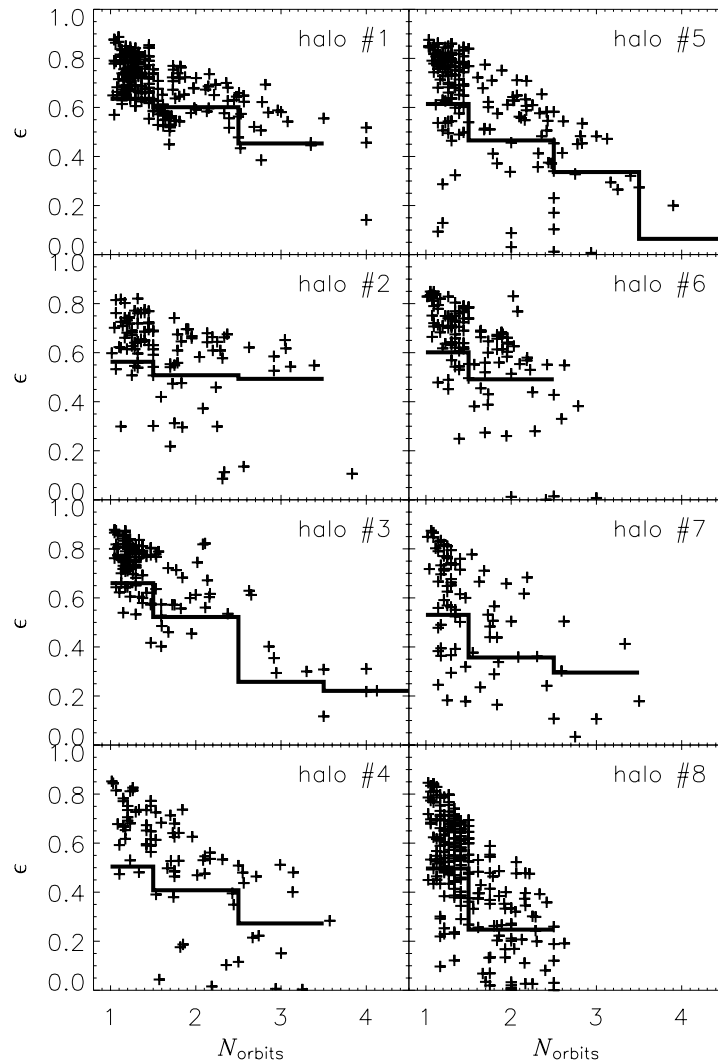


Fig. 20. The final orbital eccentricity plotted against the number of orbits completed for each surviving satellite (pluses). The histograms show the averaged eccentricity.

For example, a satellite that has had 3 orbits contributes its respective value of eccentricity to the average eccentricity in the bins for 1, 2, and 3 orbits. This histogram shows a trend indicative of orbit circularisation with time. Before the work of Hashimoto *et al.* (2002) one would have been quick to interpret this result as dynamical friction circularising the orbits, however, they suggested otherwise. To confirm this, we selected the satellites at differing pericentre, as dynamical friction is proportional to the local density of the background field, and thus has its strongest influence at pericentre. Having done this, we saw no significant change in the above trend. Further, when we used the analytical predictions of Taffoni *et al.* (2003) we found that very few satellites in the population presented could be affected by dynamical friction. Therefore, we do not attribute the circularising of the orbits to dynamical friction. One mechanism which could be responsible for the circularising of the orbits is the secular growth in the host halo's mass. In response to this increase in host mass the velocity and hence the orbit of the satellite changes.

This work has been published as “The evolution of galaxy cluster substructure II: linking dynamics to environment” (Gill S.P.D., Knebe A., Gibson B.K., Dopita M.A., 2004, MNRAS 351, 410).

IV.2.2 The Spatial Anisotropy of Satellite Galaxies

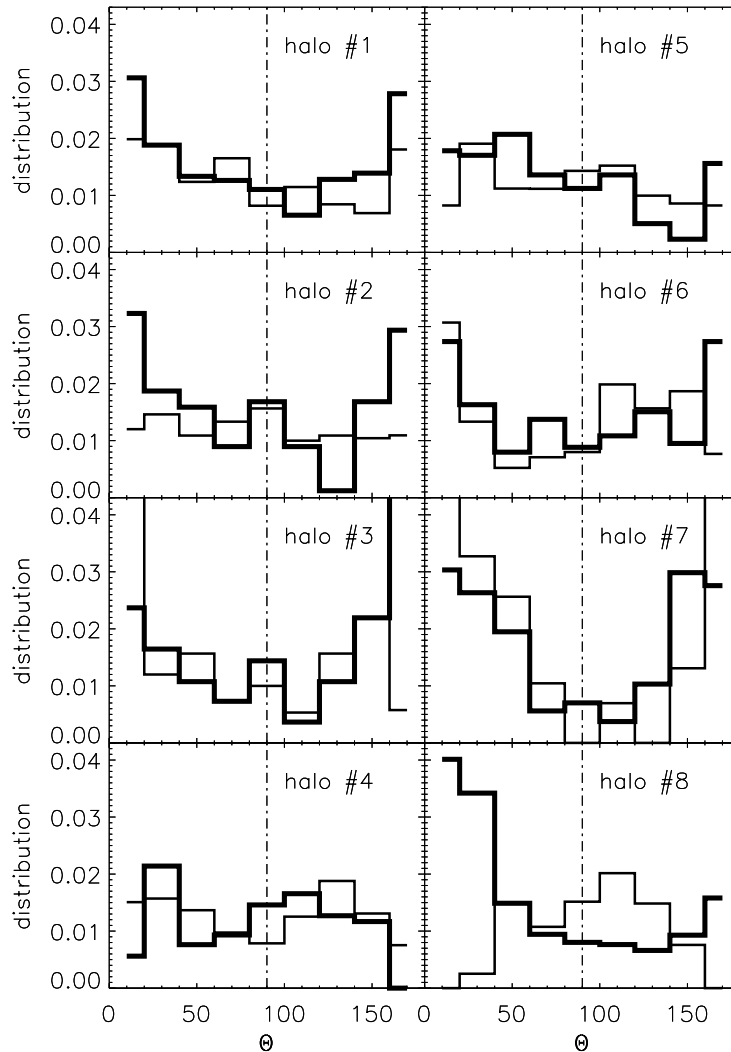


Fig. 21. Normalized distribution of angles between the position vector $\vec{R}_{\text{sat}}^{\text{apo}}$ of the satellites measured at the last apocenter and the major axis $\vec{E}_{1,\text{host}}$ of the host halo.

Observations of the distribution of bright elliptical galaxies within the Virgo galaxy cluster show a remarkable collinear arrangement (West and Blakeslee, 2000). Moreover, this axis also appears to be part of a filamentary bridge connecting Virgo and the rich cluster Abell 1367. Moreover, even on smaller scales – in galactic systems – there are clear observational indications that the distribution of the orbits of satellite galaxies is biased towards the galactic pole (Holmberg, 1969) giving an anisotropic distribution.

Zaritsky *et al.* (1997) found that satellites of (isolated) disk galaxies are scattered asymmetrically about the parent galaxy and aligned preferentially with the disk minor axis.

Using the same set of simulations as already presented in Section IV.2.1 we now probe the alignment of the satellites' positions with the shape and orientation of the host halo. To this extent, Fig. 21 presents the (normalized) distribution of angles between $\vec{R}_{\text{sat}}^{\text{apo}}$ and $\vec{E}_{1,\text{host}}$, i.e. the vector to the satellite's last apocentre and the major axis of the host halo. This graph shows that there is a clear trend in at least six of the eight host haloes studied for the two vectors to be aligned (the distribution peaks at 0° and 180° , respectively) meaning that the orbits of the satellites are preferentially found along the major axis of the host. We like to stress that only satellite galaxies that at least had one or more complete orbits were taken into account in Fig. 21; the figure is *not* based upon the infall pattern of satellites as investigated by, for instance, Tormen (1997). We also need to stress that the distributions presented in that figure are normalized, i.e. they are corrected for the bias introduced by plotting them as a function of the angle θ rather than $\cos\theta$.

This work has been published as "Anisotropy in the Distribution of Satellite Galaxy Orbits" (Knebe A., Gill S.P.D., Gibson B.K., Lewis G.F., Ibata R.A., Dopita M.A., 2004, ApJ 603, 7).

IV.2.3 The Radial Alignment of Satellite Galaxies

Another property of the satellite population that has caught the interest of observers and simulators (aside from the aforementioned spatial anisotropy) is the radial alignment of their primary axes of subhaloes with respect to the direction towards the host. The first evidence for this effect was reported for the Coma cluster, where it was observed that the projected major axes of cluster members preferentially align with the direction to the cluster centre (Hawley and Peebles, 1975; Thompson, 1976). Such a correlation between satellite elongation and radius vector has further been confirmed by statistical analysis of the SDSS data (Pereira and Kuhn, 2005; Agustsson and Brainerd, 2006; Wang and White, 2007; Faltenbacher *et al.*, 2008). The radial alignment of subhalo shapes towards the centre of their host has also been measured for the subhalo population in cosmological simulations (Kuhlen *et al.*, 2007; Faltenbacher *et al.*, 2007; Pereira *et al.*, 2008).

In this sub-section we provide evidence that the radial alignment of subhaloes in cosmological simulations does not depend on the mass of their host dark matter halo. Further, the strength of the observed signal is only recovered when measuring the (projected) 2D shape of subhaloes at about 10-20% of their virial radii.

To measure the radial alignment of subhaloes, we use the eigenvector \vec{E}_1 which corresponds to the direction of the major axis of the subhalo. We quantify the radial alignment of subhaloes as the angle between the major axis \vec{E}_1 of each subhalo and the radius vector of the subhalo in the reference frame of the host:

$$\cos\theta = \frac{\vec{R}_{\text{sat}} * \vec{E}_{1,\text{sat}}}{|\vec{R}_{\text{sat}}| |\vec{E}_{1,\text{sat}}|} \quad (\text{IV.2})$$

The (normalized) distribution $P(\cos\theta)$ of $\cos\theta$ measuring the fraction of subhaloes in

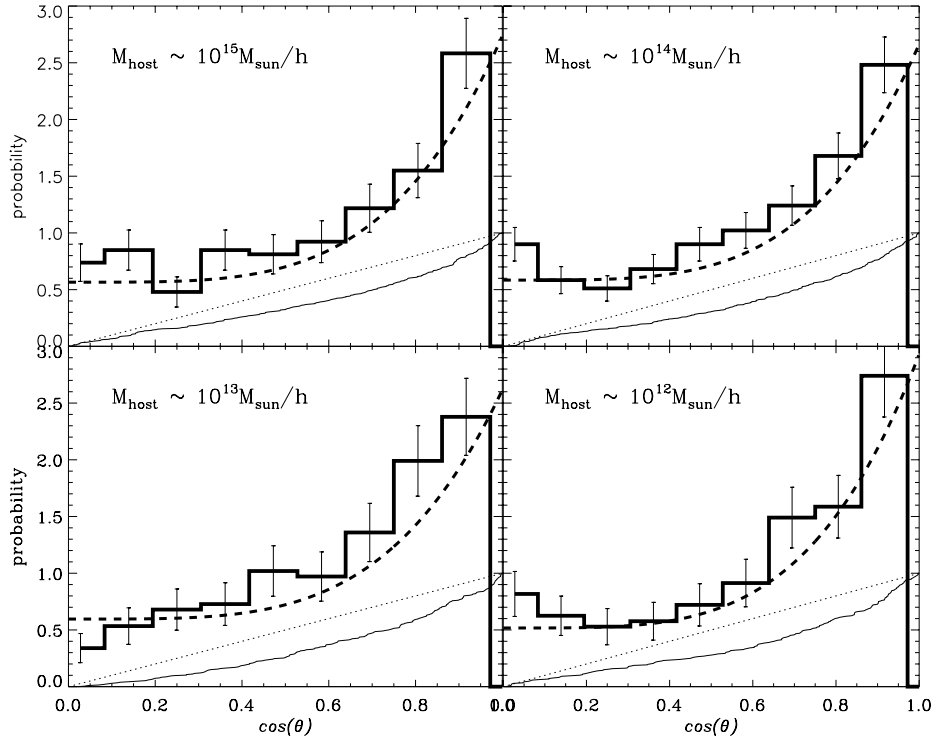


Fig. 22. Distribution of subhalo radial alignment. The histograms are the differential distribution (with Poissonian error bars) with the best function of the form $P(\cos \theta) \propto \cos^4 \theta$ shown as dashed line. The continuous line represents the cumulative probability distribution $P(< \cos \theta)$; the dotted line is the (cumulative) isotropic distribution. Only subhaloes with $N_p > 200$ and $b/a < 0.9$ are considered.

the respective bin can be viewed in Fig. 22 where we find a positive radial alignment signal different from isotropy, in agreement with Kuhlen *et al.* (2007), Faltenbacher *et al.* (2007) and Pereira *et al.* (2008). We further note that the signal does *not* depend on the mass of the host halo.

Fig. 23 now presents the orientation correlation in 2D projection using different percentages of inner particles for the determination of the subhaloes’ shape. We observe a drop in the signal’s strength when restricting to the central parts: considering only the inner 10-20% of particles we recover the observed correlation noted by Pereira and Kuhn (2005).

We like to note that the host haloes used in Figs. 22 and 23 are different. These two studies are based upon two different collaborations each with access to different cosmological simulations. The former utilizes a set of 5 objects in each mass bin whereas the latter combines the information from 40 cluster sized objects.

This work has been published as “On the relation between radial alignment of dark matter subhaloes and host mass in cosmological simulations” (Knebe A., Draganova N., Power C., Yepes G., Hoffman Y., Gottlöber S., Gibson B.K., 2008, MNRAS 386, L52) and “The radial alignment of dark matter subhaloes: from simulations to observations” (Knebe A., Yahagi H., Kase H., Lewis G.F., Gibson B.K., 2008, MNRAS Letter, in press).

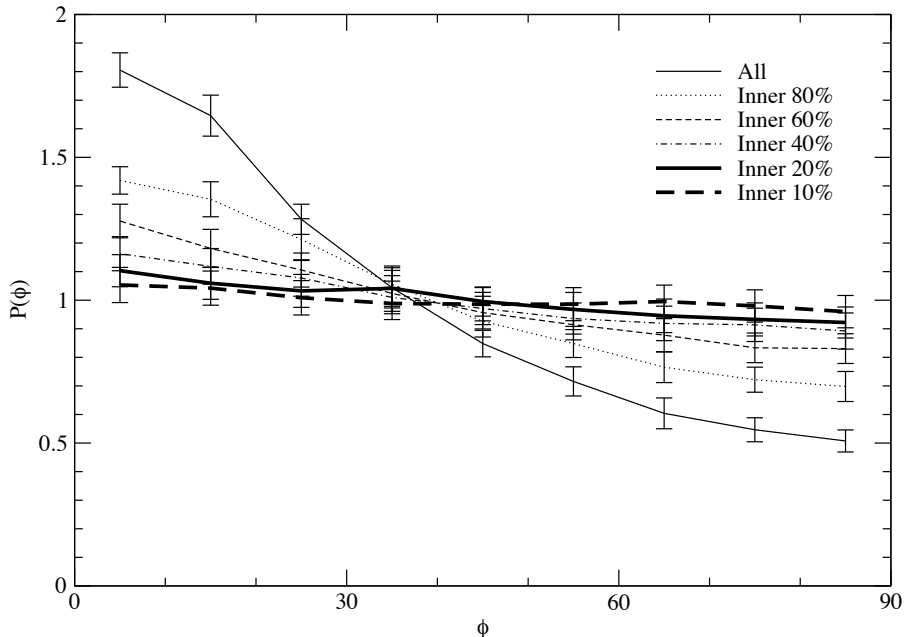


Fig. 23. Correlation of angle between major axes of subhaloes and position of the subhaloes from the center of their host in 2D projection. Each line shows the correlation using major axes derived from a fraction of particles. The different lines represent shape measures at different mass thresholds. Error bars indicate the projection variation.

IV.2.4 Backsplash Galaxies: a new population

The relationship between galaxy morphology and local environment (i.e. the morphology-density relation) was first noticed by Hubble and Humason (1931), where they reported that field and cluster galaxy populations differ. However, the origin of this morphology-density relationship is still not fully understood with several large and small scale mechanisms proposed to explain their existence, including ram pressure stripping (Gunn and Gott, 1972), tidal stripping/star formation (Merritt, 1983, 1984), starvation (Larson *et al.*, 1980), galaxy merger and harassment (Icke, 1985; Moore *et al.*, 1996) and dynamics (Tsuchiya and Shimada, 2000).

We demonstrate in Fig. 24 that a rich population of galaxies exist beyond the virial radius most of which have previously spent time near the cluster centre. In this figure we plot for all of our simulated dark matter host haloes the minimum distance D_{\min} a subhalo reached to the host's centre throughout its history versus its current distance $D_{z=0}$. Both distances have been normalised by the host's present day virial radius R_{vir} . The number of backplash galaxies with $D_{\min} < R_{\text{vir}}$ and $D_{z=0} > R_{\text{vir}}$ is significant and should be accounted for when interpreting the galaxy morphology-density relationship. These galaxies penetrate deep within the cluster potential, as deep as their bound counterparts. Hence, they should be sampling the large and small-scale transformation mechanisms alluded to above.

Please note that we stacked the data for eight cluster-sized host systems in the preparation of Fig. 24. Nevertheless, we confirm in a different study that the backplash population also exists for galactic host systems (Warnick and Knebe, 2006).

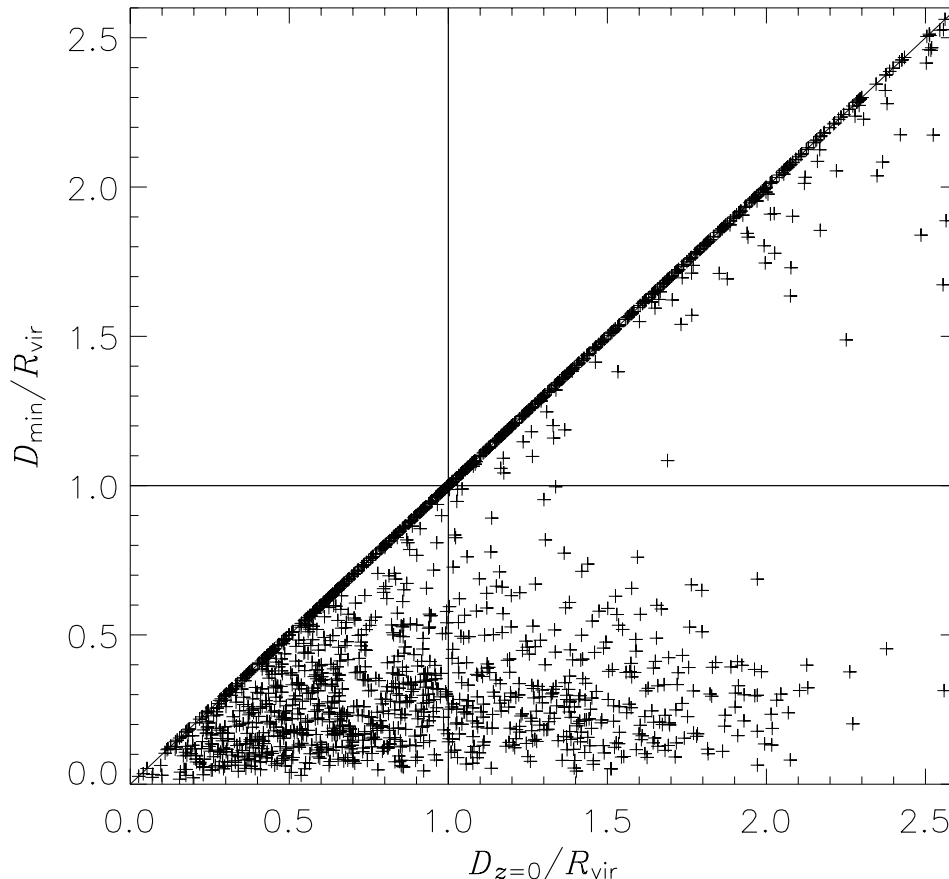


Fig. 24. Minimum distance for all satellite galaxies versus current distance in terms of the host’s virial radius. The population in the upper right corner consists of substructure orbiting within satellites, i.e. sub-subhaloes. This figure clearly indicates that there is a distinct population of “backsplash” satellites, i.e. $D_{\min} < R_{\text{vir}}$ and $D_{z=0} > R_{\text{vir}}$ in the lower right corner.

This work has been published as “The evolution of galaxy cluster substructure III: the outskirts of clusters” (Gill S.P.D., Knebe A., Gibson B.K., 2005, MNRAS 356, 1327).

IV.2.5 The Importance of Satellite-Satellite Interactions

It has been understood for some time that the structure of a galaxy can be affected by tidal interactions with its close neighbour(s) (e.g. Gunn and Gott, 1972); tell-tale signs such as tidal tails and disturbed morphologies provide a visible record of these encounters. Around our own Galaxy, there is substantial evidence for its tidal interaction with the Small and Large Magellanic Clouds (SMC and LMC), the consequences of which have been studied in detail (e.g. Lin *et al.*, 1995; Oh *et al.*, 1995; Gardiner and Noguchi, 1996; Yoshizawa and Noguchi, 2003; Bekki and Chiba, 2005; Mastropietro *et al.*, 2005; Connors *et al.*, 2006). What yet remained less well understood and studied is the interaction of satellite galaxies with other satellites orbiting within the same host. We therefore quantified the importance of satellite-satellite encounters and

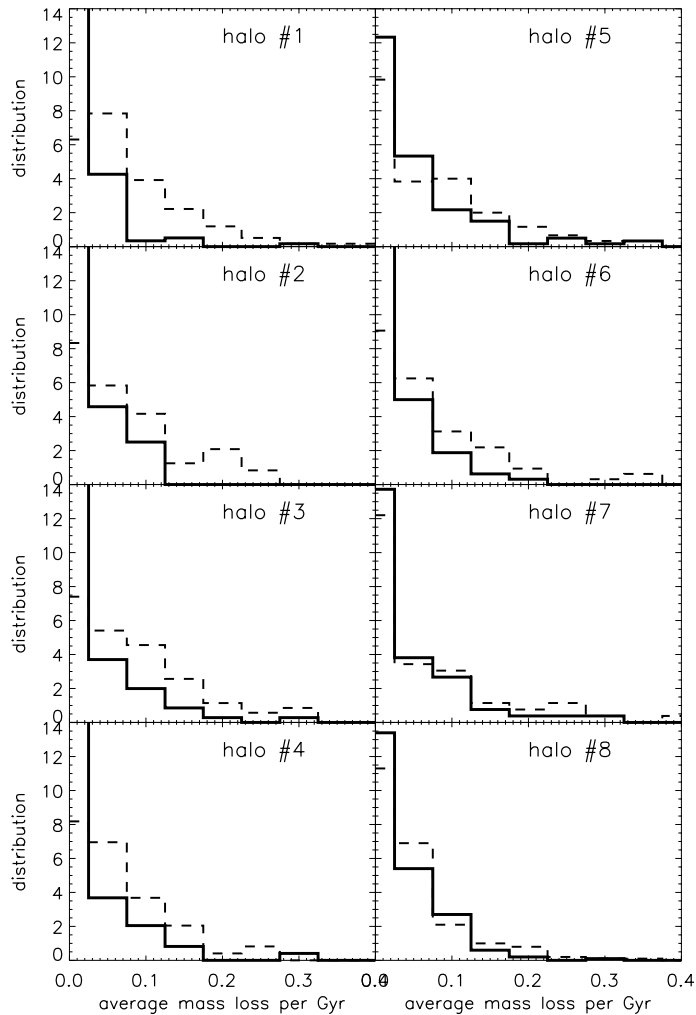


Fig. 25. Frequency distribution of the average (fractional) mass loss per Gyr. The thick solid line shows mass loss due to satellite interactions and the dashed line due to the influence of the host alone.

assessed their impact upon mass loss from the substructure population.

In Fig. 25 we show the distribution of the average mass loss per Gyr induced by either tidal interactions with the host (dashed line) and encounters with other satellites (solid line). These two contributions to the total mass loss have been calculated using a novel method based upon a decomposition of the integral force experienced by each satellite into the contribution from the host and all other companion satellites (cf. please refer to the original paper for more details).

This figure demonstrates that the mass loss induced by encounters between satellite galaxies can be as important as the tidal stripping of mass by the host potential, at least in dynamically young host systems (halo #8, note that the host haloes are ordered by their age with halo #1 being the oldest).

This work has been published as “Interactions of Satellite Galaxies in Cosmological Dark Matter Haloes” (Knebe A., Gill S.P.D., Gibson B.K., 2004, PASA 21, 216) and

“The importance of interactions for mass loss from satellite galaxies in cold dark matter haloes” (Knebe A., Power C., Gill S.P.D., Gibson B.K., 2006, *MNRAS* 368, 741).

IV.2.6 The Sense of Rotation of Satellite Galaxies

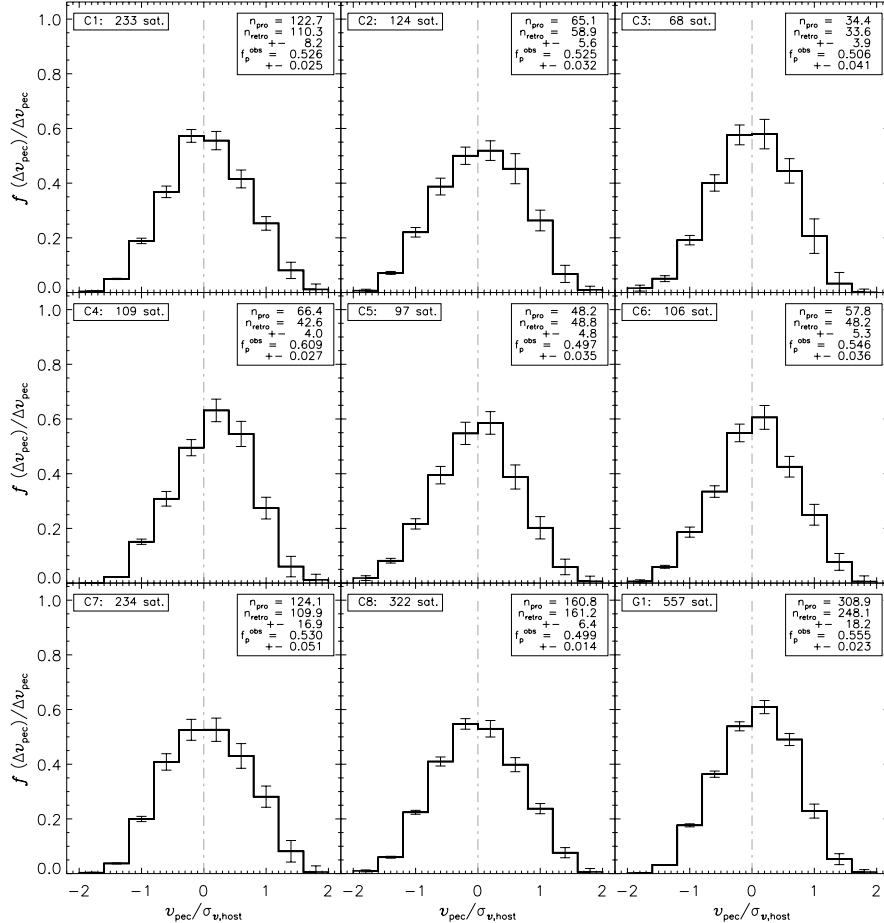


Fig. 26. The peculiar velocity distribution (normalised to the hosts’ velocity dispersion $\sigma_{v,\text{host}}$). Here velocities are defined to be positive, if the observer classifies the satellite as prograde, negative velocities mean retrograde motion.

Host dark matter haloes usually carry a small internal angular momentum, which is established by the transfer of angular momentum from infalling matter via tidal torques (Peebles, 1969; Barnes and Efstathiou, 1987). However, Gardner (2001) as well as Vitvitska *et al.* (2002) proposed another explanation for the origin of the angular momentum in galaxies and their dark matter haloes: they claim that haloes obtain their spin through the cumulative acquisition of angular momentum from satellite accretion. These two descriptions are certainly linked together and mutually dependent, respectively. A detailed analysis of the orbits of satellite haloes shows that they are directly connected to the infall pattern of satellites along the surrounding filaments (cf. Knebe *et al.*, 2004). Those subhaloes falling into the host at early times establish the angular

momentum of the inner regions of the primary halo (cf. Vitvitska *et al.*, 2002) and are channelled into the host along the same direction as those merging at later times. This leads to the speculation that satellites are preferentially co-rotating with the host, which is going to be investigated in Fig. 26.

In Fig. 26 we present the results for the (differential) peculiar velocity distribution of subhaloes when viewed in 2D projection. We used one hundred random lines of sight and the velocities are normalised by the hosts' velocity dispersion. All satellites to the left of the vertical dash-dotted “zero” line have been classified as retrograde while all satellites to the right are observed to be prograde. In addition, the mean number of prograde and retrograde orbits (along with the 1σ deviation) is given for every host halo in the upper right corner of every panel. We get a mean observed prograde fraction of 53.3% ($\pm 3.3\%$). The individual observed prograde fractions f_p^{obs} for each dark matter host are given in the inset panels of the respective plot of Fig. 26.

Despite the weakness of the signal this is a new prediction of CDM structure formation that can be verified observationally.

This work has been published as “The sense of rotation of subhaloes in cosmological dark matter haloes” (Warnick K., Knebe A., 2006, MNRAS 369, 1209).

IV.3 Debris from Satellite Galaxies

The tidal disruption of satellite galaxies is characteristic of the hierarchical merging scenario. As a satellite galaxy orbits within the gravitational potential of its more massive host, it is subject to a tidal field that may vary both in space and time. The gravitational force acting on the satellite strips a stream of tidal debris from it, and in some cases tidal forces may be sufficient to lead to the complete disruption of the system. This tidal debris tends to form two distinct arms – a *leading* arm ahead of the satellite and a *trailing* arm following the satellite.

Observationally, large scale surveys have uncovered strong evidence for several tidal streams around the Milky Way (see e.g. Belokurov *et al.*, 2006; Grillmair, 2006; Powell *et al.*, 2006, for recent observations). The well-known Magellanic stream is an example of a gaseous stream, arising from the tidal interaction of the Magellanic Clouds with our Galaxy (e.g. Bekki and Chiba, 2005; Mastrogiuseppe *et al.*, 2005; Connors *et al.*, 2006). The tidal stream associated with the Sagittarius dwarf (Ibata *et al.*, 1994) has been studied extensively (e.g. Johnston *et al.*, 1995; Helmi and White, 2001; Majewski *et al.*, 2003; Martínez-Delgado *et al.*, 2004; Johnston *et al.*, 2005, and many others), as has the Monoceros stream (Newberg *et al.*, 2002; Yanny *et al.*, 2003). Further, Ibata *et al.* (2001) have found evidence for a giant stream around M31, while deep photometric observations by Brown *et al.* (2006) suggest that this tidal stream and the spheroid of M31 have similar properties and hence may have a common origin. And even beyond our Local Group, Pohlen *et al.* (2004) and Wehner *et al.* (2006) have found evidence for tidal features around a number of distant galaxies, while the recent study of Cortese *et al.* (2007) has uncovered evidence for the tidal stripping of material from a spiral galaxy that is in the process of disruption in the galaxy cluster Abell 2667.

While previous studies of individual satellites disrupting in analytical host potentials via means of controlled N -body experiments hinted at simple and direct links between, for instance, flattening of the host and dispersion of the debris field (e.g., Ibata *et al.*,

2003; Helmi, 2004; Peñarrubia *et al.*, 2006), the situation is vastly more complicated in “live” host haloes. Already Peñarrubia *et al.* (2006) pointed out that there is only hope to recover *present-day* properties of the host due to the adiabatic response of the stream to changes in the host potential, we actually go one step further: even the current state of the host will be difficult to obtain given the complexity of interactions responsible for the emergence of debris fields. There are multiple processes driving these effects and so while we note tentative correlations, we require further simulations to help us understand what is happening. This will represent the focus of the following Sections.

IV.3.1 Mapping Substructures

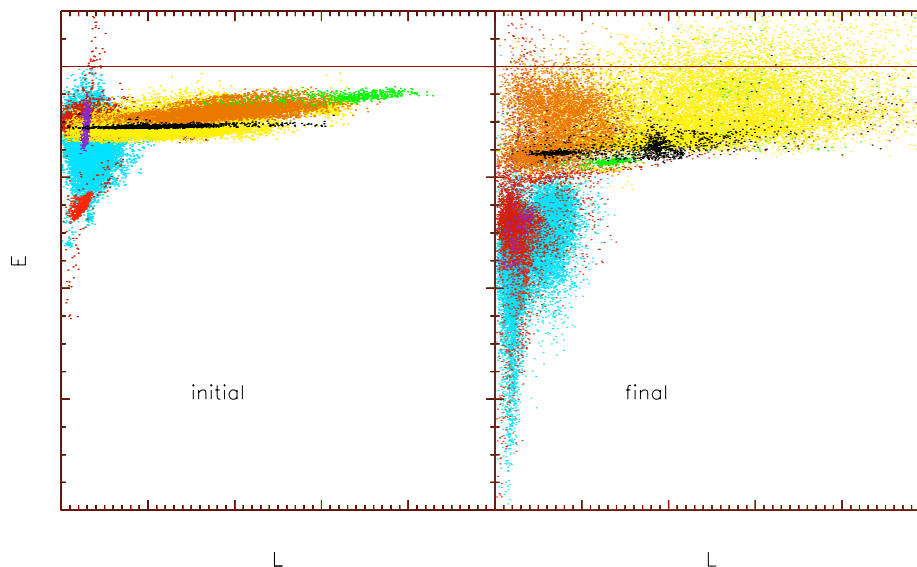


Fig. 27. The distribution of satellite particles in the $E - L$ plane for one of the cluster sized host haloes. The left panel shows the distributions at the time the respective satellite galaxy enters the virial radius of the host whereas the right panel presents the distributions at $z = 0$. Different colours represent particles of different satellites.

We present in Fig. 27 the evolution for eight different (tidally disrupting) satellites in the so-called integrals-of-motions space, i.e. energy E vs. angular momentum L . Each satellite is represented by an individual colour. The satellites shown in Fig. 27 are all taken from a self-consistent cosmological simulation of a galaxy cluster of mass $M \approx 10^{14} h^{-1} M_{\odot}$ and represent a fair sample of all available satellites, i.e. their masses cover a range from from $M \sim 5 \times 10^{10} h^{-1} M_{\odot}$ to $M \sim 4 \times 10^{12} h^{-1} M_{\odot}$ and they are on different orbits. The left panel of Fig. 27 shows the distributions at the time the respective satellite enters the virial radius of the host, whereas the right panel displays the distributions at $z = 0$.

Fig. 27 allows us to gauge the “drift” of satellites in integral-space. We note that, compared to Fig. 4 of Helmi and de Zeeuw (2000), the integrals-of-motion are hardly conserved in our “live” model, neither for high nor low mass streamers. The distributions rather show a large scatter, and have been significantly “re-shaped” over time. In addition, the mean values of E and L are also moved after the evolution. For instance, the “red” satellite drifts in time over to the initial position of the “cyan” satellite.

One encouraging result implied from Fig. 27, however, is that even though the integrals-of-motion are changing over time (mainly due to the constant growth of mass of the host halo, Knebe *et al.* (cf. 2005)), *satellites still appear coherent in the $E - L$ plane*. Hence, the integral-space analysis pioneered by Helmi and de Zeeuw (2000) still proves to be a useful diagnostic to identify streams. We further like to stress that observations only provide us with the snapshot of the distribution at today’s time, i.e. the right hand panel of Fig. 27 and hence measuring “evolution” is beyond the scope of, for instance, RAVE (Steinmetz *et al.*, 2006) and GAIA.

This work has been published as “Mapping Substructures in Dark Matter Haloes” (Knebe A., Gill S.P.D., Kawata D., Gibson B.K., 2005, MNRAS 357, 35).

IV.3.2 Tidal Streams of Disrupting Subhaloes

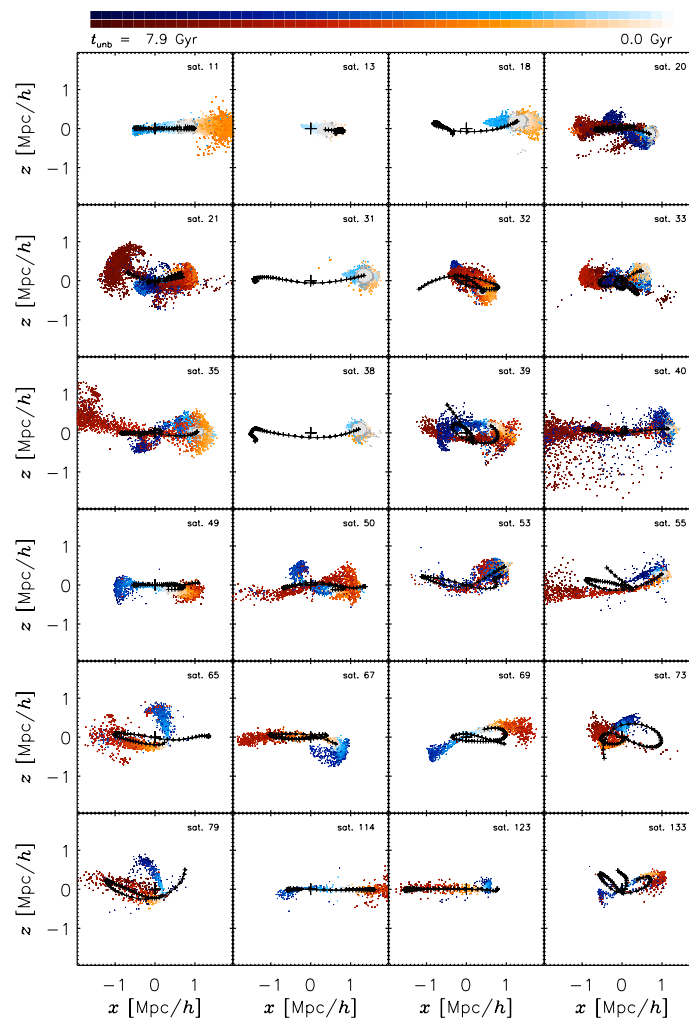


Fig. 28. Classifying stream particles according to age and leading/trailing arm. Shown are the particles of a representative sample of subhalo galaxies orbiting in one of our host haloes viewed edge-on with respects to the best fit debris plane. The black line represents the path of the orbit. Grey particles are still bound to the subhalo, red particles are marking the trailing, blue ones the leading arm. The colours vary from dark to bright, indicating the age of the respective stream.

In order to study leading and trailing debris arms we devised an automated method to identify (and separate) these two arms and hence get a handle on their combined as well as individual properties. A number of examples are given in Fig. 28 where we show the orbits of a sample of satellites (crosses) and their respective debris fields. This figure nicely demonstrates how well our method for tracking debris fields works and we will now present one particular result. The particulars of this method are given in Warnick *et al.* (2008).

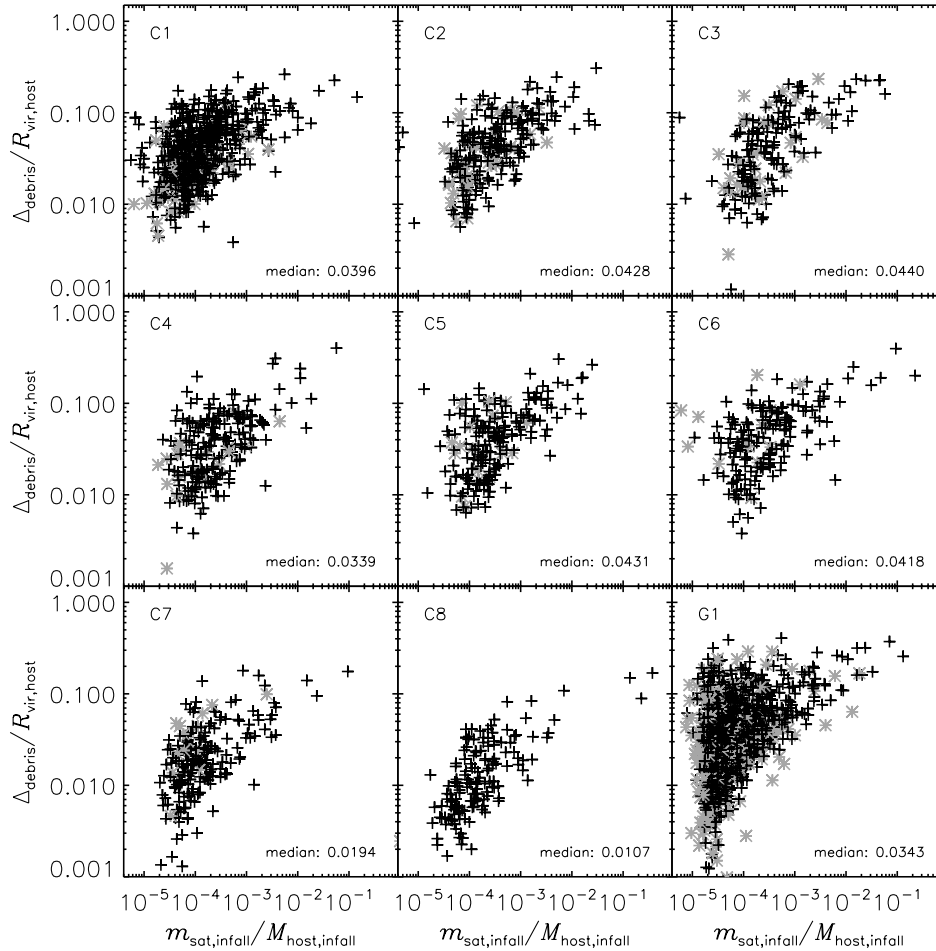


Fig. 29. The deviation of debris particles from the best fitting *debris plane* (normalised to the virial radius of the respective host) as a function of infall mass for subhaloes with at least one orbit. Backsplash subhaloes are marked with grey asterisks and the median values of the distributions are shown in the lower right corners.

Our analysis of the tidal arms reveals that there is a relation between the scatter of stream particles about the best-fit debris plane and the infall mass of the progenitor subhalo. This allows us to reconstruct the infall mass from the spread of its tidal debris in space: for Fig. 29 we fit a plane to the detected debris field and then determine the deviation of the debris field from this best-fit plane and plot it against the original infall mass of the satellite (prior to disruption). We observe a correlation between infall mass and debris deviation. Thus, by measuring the deviation of debris from the debris plane

itself, it is possible for an observer to predict the most probable mass of the subhalo it originates from.

This work has been published as “Tidal Streams of Disrupting Subhaloes in Cosmological Dark Matter Haloes” (Warnick K., Knebe A., Power C.B., 2008, MNRAS 385, 1859).

Part V

Conclusions & Outlook

V.1 Conclusions

During the past thirty years, numerical simulations of cosmic structure formation have become a powerful theoretical tool to accompany, interpret, and sometimes to lead cosmological observations. We presented a (more or less) thorough introduction into this exciting discipline of “Computational Cosmology”. After a primer on the technical details and numerical methods (Section II) simulations have been presented that looked into the differences between the standard Λ CDM model and alternative cosmologies (Section III) as well as an in-depth study of the dynamics and disruption of satellite galaxies – the building blocks of cosmic structures (Section IV).

In each of these sub-categories we can draw individual conclusions to be summarized below.

Numerical Simulations We presented a novel solver for the integration of the equations-of-motion of dark matter particles under their mutual gravity as described by Poisson’s equation. This solver is based upon arbitrarily shaped adaptive meshes and hence automatically adapts to the problem at hand. We further highlighted the differences to other codes in the field that utilize tree-structures to increase the computational speed for obtaining the relevant forces via direct summation.

However, performing the simulation is only the first step in the study of cosmic structure formation by means of computer simulations. One also needs to identify objects (galaxies, galaxy cluster, filaments, etc.) in them to be able to compare the results against observations. To this extent we also developed a new “halo finder” that is essentially parameter free. Both these codes (i.e. the simulation code `MLAPM` and the halo finder `MHF`) have been made publically available to the community and our main achievements/results can be summarized as follows.

- We developed an adaptive mesh gravity solver for cosmology.
- We developed a novel halo finder to be used with such simulations.
- Despite the diversity in numerical methods most of the codes used to simulate structure formation agree with each other.
- Each method though has its strengths and weaknesses and we showed that, for instance, two-body scattering is more prominent in tree-codes than in adaptive-mesh-refinement codes.

Alternative Cosmologies We tested whether we can solve to so-called “CDM crisis”, considering even the most extreme alternatives to dark matter (i.e. modified Newtonian dynamics (MOND), Milgrom (1983)). While most of the suggested solutions are (minor) modifications to the cold dark matter paradigm and include warm dark matter as well as effects from non-standard inflationary periods, MOND abandons the need for dark matter completely by adjusting the law of gravity. The main results from these studies can be summarized as follows.

- None of the studied alternatives is capable of simultaneously rectifying all shortcomings of CDM.
- Warm dark matter greatly reduces the number of subhaloes.

- Warm dark matter haloes have lower concentrations.
- The likelihood of high-speed encounters akin to the “Bullet” cluster is greater in WDM than in CDM.
- Non-standard inflationary theories may lead to (bumpy) features in the power spectrum of primordial density fluctuations and such “bumps” may mock different cosmologies.
- MONDian cosmological simulations show that it is in fact possible to arrive at a universe akin to the observed one with a different temporal evolution though.

Despite our efforts to solve the “CDM crisis” by merely tweaking the properties of dark matter we believe that only when all the governing physics (dark matter and gas) is included in the theoretical modeling we will have a fair chance of understanding how galaxies formed and evolved and will possibly resolve the CDM crisis. This refers to the fact that our simulations are pure dark matter simulations whereas it is rather obvious that on those scales for which the CDM crisis is apparent the physics of gases can and should not be neglected. This last point is the main driver for further code development to be elaborated upon in the Outlook below.

Near-Field Cosmology Within the hierarchical structure formation scenario induced by cold dark matter the smallest entities, i.e. satellite galaxies, are the building blocks of all larger structures. It therefore appears mandatory to study their formation, evolution and tidal disruption in greater detail. Only recently it became possible to address this task not only observationally but also computationally. And as it combines our knowledge of (large-scale) cosmology and small scale structures it has been dubbed “Near-Field Cosmology” (Freeman and Bland-Hawthorn, 2002). Utilizing a large suite of (dark matter only) simulations of individual halos we explored the dynamics of subhaloes in great detail. The main results obtained are as follows.

- Subhaloes are radially aligned, i.e. their major axis points towards the centre of the host halo they orbit in.
- Subhaloes are anisotropically distributed, i.e. they are preferentially found along the major axis of their host halo.
- Subhaloes tend to be on orbits co-rotating with their host.
- Satellite-satellite interactions can lead to significant contributions to mass loss.
- Tidal debris fields from disrupting satellite galaxies are a powerful tool for studying the formation history of their host halos.
- We found a correlation between properties of the debris field and the initial mass (and orbital eccentricity) of the satellite.
- We developed a technique to separate the leading and trailing debris arm.
- Even in “live” host halos debris fields can be identified as coherent structures in the integrals-of-motion space.

- However, the relation between host and debris properties is more complex than derived from controlled experiments of individual satellites disrupting in analytical (static) host potentials: we found little correlation of debris fields and host halo properties.

V.2 Outlook

Amongst many of the unanswered and open questions that emerged during the investigation of cosmic structure formation by means of numerical simulation that could only be in part presented in this thesis, we like to draw the attention to a small subset of the problems planned to be addressed in the near future.

The subhalo-satellite galaxy connection For the purposes of the studies presented in this thesis, we treated “substructure haloes” (or subhaloes) and “satellite galaxies” as interchangeable. However, the correspondence between dark matter substructures and luminous satellite galaxies is not a straightforward one. And despite great advances in refining numerical techniques allowing for an ever-increasing resolution of the problem under investigation, the implementation of more complicated physics such as gas physics significantly raises the complexity and hence degrades the resolution again. Therefore, complementary to modelling baryonic processes via numerical integration of the hydrodynamics equations we plan to engage in the discipline of “semi-analytical galaxy formation”. Such a method combines our current understanding of galaxy formation with the predictions from dissipationless CDM simulations such as the ones presented in this thesis. It utilizes the merger trees of dark matter haloes found in the simulations and adds analytical prescriptions for galaxy formation. The parameters of these recipes are gauged by observations of galaxies in the local Universe. This technique has recently been extremely successful in explaining the intriguing result that *all* satellites of the Milky Way have the same mass interior to 300 parsec, i.e. $M \approx 10^7 M_\odot$ while spanning almost four orders of magnitude in luminosity (Strigari *et al.*, 2008; Li *et al.*, 2008b; Maccio’ *et al.*, 2008). However, at present, it remains unclear whether the luminosity function of the satellites of the Milky Way and their peculiar spatial distribution are unique to the Galaxy, or whether these are generic features that arise during the formation of a typical galaxy. For instance, we found that there exists a prominent population of “backsplash” subhaloes outside the (virial) radius of even galactic host haloes. Therefore, we should be able to detect these objects also about the Milky Way. But to allow for a comparison with observation predictions for their luminosities and/or morphologies are required, too. Therefore, the future plan is to couple the semi-analytical code GalICS (Hatton *et al.*, 2003) to our suite of dark matter haloes (cf. Section IV) and derive observable properties for the satellite galaxy population orbiting within them. We plan to address the question of the (putative) backsplash population and their possible relation to the rather peculiar spatial distribution of satellites on a so-called “disk of satellites” (Metz *et al.*, 2007, 2008). We further like to know what actually determines the number of Milky Way satellites and what shapes their luminosity function.

Galaxies at high-redshift Besides of the discrepancies between simulations of hierarchical structure formation and observations at *low* redshift (cf. Section III) there also

appear to be problems related to our understanding of structure formation at *high* redshift. There is a divergence between the predictions of analytic models and the results of computer simulations that follow the formation of the first objects in our Universe: while Jenkins *et al.* (2001) showed that the mass function of dark matter haloes appears to be universal, the recent years have seen a number of studies indicating that this universality actually breaks down in the high-redshift universe (Springel *et al.*, 2005; Reed *et al.*, 2005; Heitmann *et al.*, 2006; Betancort-Rijo and Montero-Dorta, 2006; Reed *et al.*, 2007). However, can we be certain to actually model and simulate the mass function at those high-redshifts accurately? While a lot of efforts have been directed towards modeling haloes as accurately as possible at low redshifts, high redshift simulations, however, suffer from their own set of systematic issues as quantified by Lukić *et al.* (2007). But as haloes forming at redshifts around $z \approx 15 - 20$ will host the first galaxies and stars that (presumably) re-ionized the Universe, a precise and quantitative understanding of those objects (and their abundance) is crucial for a comprehension of the subsequent structure formation. Further, the properties of those early objects can significantly differ from the particulars of their present day counterparts (Cohn and White, 2008; Knebe and Power, 2008) further pointing towards the necessity to study them in greater detail.

In that regards we plan to investigate the abundance of objects at redshifts $z \geq 10$ by utilizing extremely high-resolution cosmological simulations of hierarchical structure formation taking into account the criteria set by Lukić *et al.* (2007). This then allows us to establish the mass function of high redshift haloes. We shall further apply the technique of semi-analytical galaxy formation alluded to above to make predictions that can be tested by the next generation of 21cm missions such as LOFAR and the SKA that will observationally probe that redshift regime.

Cosmological Magneto-Hydrodynamics Magnetic fields play an important role in almost all astrophysical phenomena including star formation. But due to the difficulty in analytic modeling magnetic fields are still poorly understood; numerical simulation again is the major tool for studying their effects and impact.

When it comes to the local Universe, it has been well established that there are widespread magnetic fields in the intracluster medium (e.g. Carilli and Taylor, 2002; Govoni, 2006, for a recent review). There has also been tantalizing evidence for magnetic fields in the wider intergalactic medium. The origin of these large-scale magnetic fields is still unknown. Furthermore, it is presently mostly unknown whether these magnetic fields have played an important role or not in systems ranging from large-scale structure formation over galaxy clusters to cluster core regions and to galaxy formation itself. There have only been a few studies aiming at investigating the role of magnetic fields in the intracluster and intergalactic medium to date (e.g. Ryu *et al.*, 1998; Dolag *et al.*, 2002, 2005; Brüggén *et al.*, 2005; Li *et al.*, 2008a; Xu *et al.*, 2008), most of them *not* in a cosmological context.

With regards to the high-redshift Universe, preliminary investigations of the relevance of magnetic fields for cosmic structure formation scenarios reveal that their effects cannot be neglected (Sethi *et al.*, 2008). The presence of magnetic fields in the early Universe can significantly change the standard history of star formation and they can further seed early formation of structures (Sethi and Subramanian, 2005).

We therefore went one step further than simply adding gas physics to our simulation code described in Section II.6; we added the equations of magneto-hydrodynamics in su-

percomoving coordinates to MLAPM that are being solved by a conservative, divergence-free Godunov-type central scheme (Ziegler, 2005). And first test runs indicate that the presence of magnetic fields in the early universe will have an impact upon cosmic structure formation. We are currently in the process of confirming this finding with better resolved simulations and differing initial magnetic field configurations.

Cosmological Modified Newtonian Dynamics We just finished developing a novel solver for the analogue to Poisson’s equation in the framework of modified Newtonian dynamics (MOND)

$$\nabla \cdot \left[\mu \left(\frac{|\nabla \Phi_M|}{a^2 g_0} \right) \nabla \Phi_M \right] = \frac{4\pi G}{a} (\rho - \bar{\rho}) . \quad (\text{V.1})$$

This equation is (in contrast to the Newtonian Poisson’s equation) highly non-linear and hence standard codes based upon tree structures and/or FFT’s in general are not applicable to solve it; one needs to defer to multi-grid relaxation techniques. We will utilize this new code to revisit the issue of cosmic structure formation under MOND.¹⁴ And first steps in that direction show that, for instance, the probability of high-speed encounters between galaxy clusters (as, for instance, observed in the “Bullet cluster”, Markevitch (2006)) are more likely in MOND than in dark matter scenarios. Nevertheless, structure formation in a MONDian universe appears to be more rapid with less structures at high redshift – possibly in contradiction to observations. We hope to clarify this and either rule out or confirm the venturesome theory of MOND.

¹⁴Note that for the study presented in Section III.4 we did not solve the MONDian Poisson’s equation but rather modified the Newtonian potential according to a prescription based upon various assumptions to account for the affects of MOND.

Bibliography

- Aarseth, S. J. (1963). Dynamical evolution of clusters of galaxies, I. *MNRAS*, **126**, 223–+.
- Agertz, O., Moore, B., Stadel, J., Potter, D., Miniati, F., Read, J., Mayer, L., Gawryszczak, A., Kravtsov, A., Nordlund, Å., Pearce, F., Quilis, V., Rudd, D., Springel, V., Stone, J., Tasker, E., Teyssier, R., Wadsley, J., and Walder, R. (2007). Fundamental differences between SPH and grid methods. *MNRAS*, **380**, 963–978.
- Agustsson, I. and Brainerd, T. G. (2006). The Orientation of Satellite Galaxies: Evidence of Elongation in the Direction of the Host. *ApJ*, **644**, L25–L28.
- Akerib, D. S., Armel-Funkhouser, M. S., Attisha, M. J., Bailey, C. N., Baudis, L., Bauer, D. A., Brink, P. L., Bunker, R., Cabrera, B., Caldwell, D. O., Chang, C. L., Crisler, M. B., Cushman, P., Daal, M., Dixon, R., Dragowsky, M. R., Driscoll, D. D., Duong, L., Ferril, R., Filippini, J., Gaitskill, R. J., Hennings-Yeomans, R., Holmgren, D., Huber, M. E., Kamat, S., Lu, A., Mahapatra, R., Mandic, V., Martinis, J. M., Meunier, P., Mirabolfathi, N., Nelson, H., Nelson, R., Ogburn, R. W., Perera, T. A., Issac, M. C., Ramberg, E., Rau, W., Reisetter, A., Ross, R. R., Saab, T., Sadoulet, B., Sander, J., Savage, C., Schnee, R. W., Seitz, D. N., Serfass, B., Sundqvist, K. M., Thompson, J.-P. F., Wang, G., Yellin, S., and Young, B. A. (2005). Exclusion limits on the WIMP-nucleon cross section from the first run of the Cryogenic Dark Matter Search in the Soudan Underground Laboratory. *Phys. Rev. D*, **72**(5), 052009–+.
- Allgood, B., Flores, R. A., Primack, J. R., Kravtsov, A. V., Wechsler, R. H., Faltenbacher, A., and Bullock, J. S. (2006). The shape of dark matter haloes: dependence on mass, redshift, radius and formation. *MNRAS*, **367**, 1781–1796.
- Avila-Reese, V., Colín, P., Valenzuela, O., D’Onghia, E., and Firmani, C. (2001). Formation and Structure of Halos in a Warm Dark Matter Cosmology. *ApJ*, **559**, 516–530.
- Baertschiger, T., Joyce, M., and Sylos Labini, F. (2002). Power-Law Correlation and Discreteness in Cosmological N-Body Simulations. *ApJ*, **581**, L63–L66.
- Bahcall, N. A., Fan, X., and Cen, R. (1997). Constraining Omega with Cluster Evolution. *ApJ*, **485**, L53+.
- Bahcall, N. A., Ostriker, J. P., Perlmutter, S., and Steinhardt, P. J. (1999). The Cosmic Triangle: Revealing the State of the Universe. *Science*, **284**, 1481–+.

- Bailin, J. and Steinmetz, M. (2005). Internal and External Alignment of the Shapes and Angular Momenta of Λ CDM Halos. *ApJ*, **627**, 647–665.
- Bardeen, J. M., Bond, J. R., Kaiser, N., and Szalay, A. S. (1986). The statistics of peaks of Gaussian random fields. *ApJ*, **304**, 15–61.
- Barnes, J. and Efstathiou, G. (1987). Angular momentum from tidal torques. *ApJ*, **319**, 575–600.
- Barnes, J. and Hut, P. (1986). A Hierarchical $O(N \log N)$ Force-Calculation Algorithm. *Nature*, **324**, 446–449.
- Barriga, J., Gaztanaga, E., Santos, M. G., and Sarkar, S. (2001). Evidence for an inflationary phase transition from the LSS and CMB anisotropy data. *Nuclear Physics B Proceedings Supplements*, **95**, 66–69.
- Begeman, K. G., Broeils, A. H., and Sanders, R. H. (1991). Extended rotation curves of spiral galaxies - Dark haloes and modified dynamics. *MNRAS*, **249**, 523–537.
- Bekenstein, J. and Milgrom, M. (1984). Does the missing mass problem signal the breakdown of Newtonian gravity? *ApJ*, **286**, 7–14.
- Bekki, K. and Chiba, M. (2005). Formation and evolution of the Magellanic Clouds - I. Origin of structural, kinematic and chemical properties of the Large Magellanic Cloud. *MNRAS*, **356**, 680–702.
- Belokurov, V., Zucker, D. B., Evans, N. W., Gilmore, G., Vidrih, S., Bramich, D. M., Newberg, H. J., Wyse, R. F. G., Irwin, M. J., Fellhauer, M., Hewett, P. C., Walton, N. A., Wilkinson, M. I., Cole, N., Yanny, B., Rockosi, C. M., Beers, T. C., Bell, E. F., Brinkmann, J., Ivezić, Ž., and Lupton, R. (2006). The Field of Streams: Sagittarius and Its Siblings. *ApJ*, **642**, L137–L140.
- Bento, M. C., Bertolami, O., Rosenfeld, R., and Teodoro, L. (2000). Self-interacting dark matter and the Higgs boson. *Phys. Rev. D*, **62**(4), 041302–+.
- Bertschinger, E. and Gelb, J. M. (1991). Cosmological N-body simulations. *Computers in Physics*, **5**, 164–175.
- Betancort-Rijo, J. E. and Montero-Dorta, A. D. (2006). Understanding the Cosmic Mass Function High-Mass Behavior. *ApJ*, **650**, L95–L98.
- Bett, P., Eke, V., Frenk, C. S., Jenkins, A., Helly, J., and Navarro, J. (2007). The spin and shape of dark matter haloes in the Millennium simulation of a Λ cold dark matter universe. *MNRAS*, **376**, 215–232.
- Binney, J. and Knebe, A. (2002). Two-body relaxation in cosmological simulations. *MNRAS*, **333**, 378–382.
- Bode, P. and Ostriker, J. P. (2003). Tree Particle-Mesh: An Adaptive, Efficient, and Parallel Code for Collisionless Cosmological Simulation. *ApJS*, **145**, 1–13.
- Bode, P., Ostriker, J. P., and Turok, N. (2001). Halo Formation in Warm Dark Matter Models. *ApJ*, **556**, 93–107.

- Bond, J. R. and Szalay, A. S. (1983). The collisionless damping of density fluctuations in an expanding universe. *ApJ*, **274**, 443–468.
- Brandt, A. (1977). Multi-Level Adaptive Solutions to Boundary-Value Problems. *Math. of Comp.*, **31**, 333–390.
- Brown, T. M., Smith, E., Guhathakurta, P., Rich, R. M., Ferguson, H. C., Renzini, A., Sweigart, A. V., and Kimble, R. A. (2006). Deep Photometry of Andromeda Reveals Striking Similarities in the Tidal Stream and Spheroid Populations. *ApJ*, **636**, L89–L92.
- Brüggen, M., Ruszkowski, M., Simionescu, A., Hoeft, M., and Dalla Vecchia, C. (2005). Simulations of Magnetic Fields in Filaments. *ApJ*, **631**, L21–L24.
- Bryan, G. L. and Norman, M. L. (1998). Statistical Properties of X-Ray Clusters: Analytic and Numerical Comparisons. *ApJ*, **495**, 80–+.
- Buchert, T. and Domínguez, A. (2005). Adhesive gravitational clustering. *A&A*, **438**, 443–460.
- Bullock, J. S. (2001). Tilted CDM versus WDM in the Subgalactic Scuffle. *ArXiv Astrophysics e-prints (0111005)*.
- Bullock, J. S., Kolatt, T. S., Sigad, Y., Somerville, R. S., Kravtsov, A. V., Klypin, A. A., Primack, J. R., and Dekel, A. (2001). Profiles of dark haloes: evolution, scatter and environment. *MNRAS*, **321**, 559–575.
- Carilli, C. L. and Taylor, G. B. (2002). Cluster Magnetic Fields. *ARA&A*, **40**, 319–348.
- Chapman, S. and Cowling, T. G. (1991). *The Mathematical Theory of Non-uniform Gases*. The Mathematical Theory of Non-uniform Gases, by Sydney Chapman and T. G. Cowling and Foreword by C. Cercignani, pp. 447. ISBN 052140844X. Cambridge, UK: Cambridge University Press, January 1991.
- Chung, D. J. H., Kolb, E. W., Riotto, A., and Tkachev, I. I. (2000). Probing Planckian physics: Resonant production of particles during inflation and features in the primordial power spectrum. *Phys. Rev. D*, **62**(4), 043508–+.
- Clowe, D., Gonzalez, A., and Markevitch, M. (2004). Weak-Lensing Mass Reconstruction of the Interacting Cluster 1E 0657-558: Direct Evidence for the Existence of Dark Matter. *ApJ*, **604**, 596–603.
- Cohn, J. D. and White, M. (2008). Dark matter halo abundances, clustering and assembly histories at high redshift. *MNRAS*, **385**, 2025–2033.
- Colín, P., Avila-Reese, V., and Valenzuela, O. (2000). Substructure and Halo Density Profiles in a Warm Dark Matter Cosmology. *ApJ*, **542**, 622–630.
- Connors, T. W., Kawata, D., and Gibson, B. K. (2006). N-body simulations of the Magellanic stream. *MNRAS*, **371**, 108–120.

- Cortese, L., Marcillac, D., Richard, J., Bravo-Alfaro, H., Kneib, J.-P., Rieke, G., Covone, G., Egami, E., Rigby, J., Czoske, O., and Davies, J. (2007). The strong transformation of spiral galaxies infalling into massive clusters at $z \sim 0.2$. *MNRAS*, **376**, 157–172.
- Couchman, H. M. P. (1991). Mesh-refined P3M - A fast adaptive N-body algorithm. *ApJ*, **368**, L23–L26.
- Croft, R. A. C., Weinberg, D. H., Bolte, M., Burles, S., Hernquist, L., Katz, N., Kirkman, D., and Tytler, D. (2002). Toward a Precise Measurement of Matter Clustering: Ly α Forest Data at Redshifts 2-4. *ApJ*, **581**, 20–52.
- Dahle, H., Pedersen, K., Lilje, P. B., Maddox, S. J., and Kaiser, N. (2003). Weak Gravitational Lensing by a Sample of X-Ray-luminous Clusters of Galaxies. III. Serendipitous Weak Lensing Detections of Dark and Luminous Mass Concentrations. *ApJ*, **591**, 662–676.
- Dalal, N. and Kochanek, C. S. (2002). Direct Detection of Cold Dark Matter Substructure. *ApJ*, **572**, 25–33.
- Davis, M., Efstathiou, G., Frenk, C. S., and White, S. D. M. (1985). The evolution of large-scale structure in a universe dominated by cold dark matter. *ApJ*, **292**, 371–394.
- Dehnen, W. (2001). Towards optimal softening in three-dimensional N-body codes - I. Minimizing the force error. *MNRAS*, **324**, 273–291.
- Dicke, R. H., Peebles, P. J. E., Roll, P. G., and Wilkinson, D. T. (1965). Cosmic Black-Body Radiation. *ApJ*, **142**, 414–419.
- Diemand, J., Moore, B., Stadel, J., and Kazantzidis, S. (2004). Two-body relaxation in cold dark matter simulations. *MNRAS*, **348**, 977–986.
- Diemand, J., Moore, B., and Stadel, J. (2005). Earth-mass dark-matter haloes as the first structures in the early Universe. *Nature*, **433**, 389–391.
- Dolag, K., Bartelmann, M., and Lesch, H. (2002). Evolution and structure of magnetic fields in simulated galaxy clusters. *A&A*, **387**, 383–395.
- Dolag, K., Grasso, D., Springel, V., and Trachev, I. (2005). Simulating the Magnetic Field in the Local Supercluster. In L. O. Sjouwerman and K. K. Dyer, editors, *X-Ray and Radio Connections (eds. L.O. Sjouwerman and K.K Dyer) Published electronically by NRAO, <http://www.aoc.nrao.edu/events/xraydio> Held 3-6 February 2004 in Santa Fe, New Mexico, USA, (E8.10) 6 pages.*
- Domínguez, A. (2000). Hydrodynamic approach to the evolution of cosmological structures. *Phys. Rev. D*, **62**(10), 103501–+.
- Doroshkevich, A. G., Sunyaev, R. A., and Zeldovich, I. B. (1974). The formation of galaxies in Friedmannian universes. In M. S. Longair, editor, *Confrontation of Cosmological Theories with Observational Data*, volume 63 of *IAU Symposium*, pages 213–225.

- Efstathiou, G., Davis, M., White, S. D. M., and Frenk, C. S. (1985). Numerical techniques for large cosmological N-body simulations. *ApJS*, **57**, 241–260.
- Eisenstein, D. J. and Hu, W. (1998). Baryonic Features in the Matter Transfer Function. *ApJ*, **496**, 605–+.
- El-Zant, A. A. (2006). Two-body relaxation in simulated cosmological haloes. *MNRAS*, **370**, 1247–1256.
- Faltenbacher, A., Li, C., Mao, S., van den Bosch, F. C., Yang, X., Jing, Y. P., Pasquali, A., and Mo, H. J. (2007). Three Different Types of Galaxy Alignment within Dark Matter Halos. *ApJ*, **662**, L71–L74.
- Faltenbacher, A., Jing, Y. P., Li, C., Mao, S., Mo, H. J., Pasquali, A., and van den Bosch, F. C. (2008). Spatial and Kinematic Alignments between Central and Satellite Halos. *ApJ*, **675**, 146–155.
- Freeman, K. and Bland-Hawthorn, J. (2002). The New Galaxy: Signatures of Its Formation. *ARA&A*, **40**, 487–537.
- Frenk, C. S., White, S. D. M., Davis, M., and Efstathiou, G. (1988). The formation of dark halos in a universe dominated by cold dark matter. *ApJ*, **327**, 507–525.
- Frenk, C. S., White, S. D. M., Bode, P., Bond, J. R., Bryan, G. L., Cen, R., Couchman, H. M. P., Evrard, A. E., Gnedin, N., Jenkins, A., Khokhlov, A. M., Klypin, A., Navarro, J. F., Norman, M. L., Ostriker, J. P., Owen, J. M., Pearce, F. R., Pen, U.-L., Steinmetz, M., Thomas, P. A., Villumsen, J. V., Wadsley, J. W., Warren, M. S., Xu, G., and Yepes, G. (1999). The Santa Barbara Cluster Comparison Project: A Comparison of Cosmological Hydrodynamics Solutions. *ApJ*, **525**, 554–582.
- Gardiner, L. T. and Noguchi, M. (1996). N-body simulations of the Small Magellanic Cloud and the Magellanic Stream. *MNRAS*, **278**, 191–208.
- Gardner, J. P. (2001). Dependence of Halo Properties on Interaction History, Environment, and Cosmology. *ApJ*, **557**, 616–625.
- Gelb, J. M. and Bertschinger, E. (1994). Cold dark matter. 1: The formation of dark halos. *ApJ*, **436**, 467–490.
- Gentile, G., Tonini, C., and Salucci, P. (2007). Λ CDM halo density profiles: where do actual halos converge to NFW ones? *A&A*, **467**, 925–931.
- Ghigna, S., Moore, B., Governato, F., Lake, G., Quinn, T., and Stadel, J. (1998). Dark matter haloes within clusters. *MNRAS*, **300**, 146–162.
- Gill, S. P. D., Knebe, A., and Gibson, B. K. (2004a). The evolution of substructure - I. A new identification method. *MNRAS*, **351**, 399–409.
- Gill, S. P. D., Knebe, A., Gibson, B. K., and Dopita, M. A. (2004b). The evolution of substructure - II. Linking dynamics to environment. *MNRAS*, **351**, 410–422.
- Gingold, R. A. and Monaghan, J. J. (1977). Smoothed particle hydrodynamics - Theory and application to non-spherical stars. *MNRAS*, **181**, 375–389.

- Gnedin, N. Y. (1995). Softened Lagrangian hydrodynamics for cosmology. *ApJS*, **97**, 231–257.
- Goetz, M., Huchra, J. P., and Brandenberger, R. H. (1998). Group Identification in N-Body Simulations: SKID and DENMAX Versus Friends-of-Friends. *ArXiv Astrophysics e-prints*.
- Gottlöber, S. and Yepes, G. (2007). Shape, Spin, and Baryon Fraction of Clusters in the MareNostrum Universe. *ApJ*, **664**, 117–122.
- Govoni, F. (2006). Observations of magnetic fields in regular and irregular clusters. *Astronomische Nachrichten*, **327**, 539–+.
- Grillmair, C. J. (2006). Substructure in Tidal Streams: Tributaries in the Anticenter Stream. *ApJ*, **651**, L29–L32.
- Groth, E. J., Peebles, P. J. E., Seldner, M., and Soneira, R. M. (1977). The clustering of galaxies. *Scientific American*, **237**, 76–78.
- Gunn, J. E. and Gott, J. R. I. (1972). On the Infall of Matter Into Clusters of Galaxies and Some Effects on Their Evolution. *ApJ*, **176**, 1–+.
- Hannestad, S., Hansen, S. H., and Villante, F. L. (2001). Probing the power spectrum bend with recent cosmic microwave background data. *Astroparticle Physics*, **16**, 137–144.
- Hatton, S., Devriendt, J. E. G., Ninin, S., Bouchet, F. R., Guiderdoni, B., and Vibert, D. (2003). GALICS- I. A hybrid N-body/semi-analytic model of hierarchical galaxy formation. *MNRAS*, **343**, 75–106.
- Hawley, D. L. and Peebles, P. J. E. (1975). Distribution of observed orientations of galaxies. *AJ*, **80**, 477–491.
- Hayashi, E. and White, S. D. M. (2006). How rare is the bullet cluster? *MNRAS*, **370**, L38–L41.
- Hayashi, E., Navarro, J. F., Taylor, J. E., Stadel, J., and Quinn, T. (2003). The Structural Evolution of Substructure. *ApJ*, **584**, 541–558.
- Heitmann, K., Lukić, Z., Habib, S., and Ricker, P. M. (2006). Capturing Halos at High Redshifts. *ApJ*, **642**, L85–L88.
- Heitmann, K., Lukic, Z., Fasel, P., Habib, S., Warren, M. S., White, M., Ahrens, J., Ankeny, L., Armstrong, R., O’Shea, B., Ricker, P. M., Springel, V., Stadel, J., and Trac, H. (2007). The Cosmic Code Comparison Project. *ArXiv e-prints*, **706**.
- Helmi, A. (2004). Is the dark halo of our Galaxy spherical? *MNRAS*, **351**, 643–648.
- Helmi, A. and de Zeeuw, P. T. (2000). Mapping the substructure in the Galactic halo with the next generation of astrometric satellites. *MNRAS*, **319**, 657–665.
- Helmi, A. and White, S. D. M. (2001). Simple dynamical models of the Sagittarius dwarf galaxy. *MNRAS*, **323**, 529–536.

- Hockney, R. W. and Eastwood, J. W. (1988). *Computer simulation using particles*. Bristol: Hilger, 1988.
- Holmberg, E. (1969). A study of physical groups of galaxies. *Arkiv for Astronomi*, **5**, 305–343.
- Hubble, E. and Humason, M. L. (1931). The Velocity-Distance Relation among Extra-Galactic Nebulae. *ApJ*, **74**, 43–+.
- Ibata, R., Irwin, M., Lewis, G., Ferguson, A. M. N., and Tanvir, N. (2001). A giant stream of metal-rich stars in the halo of the galaxy M31. *Nature*, **412**, 49–52.
- Ibata, R. A., Gilmore, G., and Irwin, M. J. (1994). A Dwarf Satellite Galaxy in Sagittarius. *Nature*, **370**, 194–+.
- Ibata, R. A., Irwin, M. J., Lewis, G. F., Ferguson, A. M. N., and Tanvir, N. (2003). One ring to encompass them all: a giant stellar structure that surrounds the Galaxy. *MNRAS*, **340**, L21–L27.
- Icke, V. (1985). Distant encounters between disk galaxies and the origin of S 0 spirals. *A&A*, **144**, 115–123.
- Jenkins, A., Frenk, C. S., White, S. D. M., Colberg, J. M., Cole, S., Evrard, A. E., Couchman, H. M. P., and Yoshida, N. (2001). The mass function of dark matter haloes. *MNRAS*, **321**, 372–384.
- Johnston, K. V., Spergel, D. N., and Hernquist, L. (1995). The Disruption of the Sagittarius Dwarf Galaxy. *ApJ*, **451**, 598–+.
- Johnston, K. V., Hernquist, L., and Bolte, M. (1996). Fossil Signatures of Ancient Accretion Events in the Halo. *ApJ*, **465**, 278–+.
- Johnston, K. V., Law, D. R., and Majewski, S. R. (2005). A Two Micron All Sky Survey View of the Sagittarius Dwarf Galaxy. III. Constraints on the Flattening of the Galactic Halo. *ApJ*, **619**, 800–806.
- Kasun, S. F. and Evrard, A. E. (2005). Shapes and Alignments of Galaxy Cluster Halos. *ApJ*, **629**, 781–790.
- Klypin, A. and Holtzman, J. (1997). Particle-Mesh code for cosmological simulations. *ArXiv Astrophysics e-prints*.
- Klypin, A., Gottlöber, S., Kravtsov, A. V., and Khokhlov, A. M. (1999a). Galaxies in N-Body Simulations: Overcoming the Overmerging Problem. *ApJ*, **516**, 530–551.
- Klypin, A., Kravtsov, A. V., Valenzuela, O., and Prada, F. (1999b). Where Are the Missing Galactic Satellites? *ApJ*, **522**, 82–92.
- Klypin, A. A. and Shandarin, S. F. (1983). Three-dimensional numerical model of the formation of large-scale structure in the Universe. *MNRAS*, **204**, 891–907.
- Knebe, A. and Gibson, B. K. (2004). Galactic haloes in MONDian cosmological simulations. *MNRAS*, **347**, 1055–1064.

- Knebe, A. and Power, C. (2008). On the Correlation between Spin Parameter and Halo Mass. *ApJ*, **678**, 621–626.
- Knebe, A., Green, A., and Binney, J. (2001). Multi-level adaptive particle mesh (MLAPM): a c code for cosmological simulations. *MNRAS*, **325**, 845–864.
- Knebe, A., Devriendt, J. E. G., Mahmood, A., and Silk, J. (2002). Merger histories in warm dark matter structure formation scenarios. *MNRAS*, **329**, 813–828.
- Knebe, A., Gill, S. P. D., Gibson, B. K., Lewis, G. F., Ibata, R. A., and Dopita, M. A. (2004). Anisotropy in the Distribution of Satellite Galaxy Orbits. *ApJ*, **603**, 7–11.
- Knebe, A., Gill, S. P. D., Kawata, D., and Gibson, B. K. (2005). Mapping substructures in dark matter haloes. *MNRAS*, **357**, L35–L39.
- Knebe, A., Domínguez, A., and Domínguez-Tenreiro, R. (2006). Hydrodynamic approach to the evolution of cosmic structures - II. Study of N-body simulations at $z = 0$. *MNRAS*, **371**, 1959–1974.
- Knebe, A., Draganova, N., Power, C., Yepes, G., Hoffman, Y., Gottlöber, S., and Gibson, B. K. (2008a). On the relation between the radial alignment of dark matter subhaloes and host mass in cosmological simulations. *MNRAS*, **386**, L52–L56.
- Knebe, A., Yahagi, H., Kase, H., Lewis, G., and Gibson, B. K. (2008b). The radial alignment of dark matter subhalos: from simulations to observations. *ArXiv e-prints*, **805**.
- Komatsu, E., Dunkley, J., Nolta, M. R., Bennett, C. L., Gold, B., Hinshaw, G., Jarosik, N., Larson, D., Limon, M., Page, L., Spergel, D. N., Halpern, M., Hill, R. S., Kogut, A., Meyer, S. S., Tucker, G. S., Weiland, J. L., Wollack, E., and Wright, E. L. (2008). Five-Year Wilkinson Microwave Anisotropy Probe (WMAP) Observations: Cosmological Interpretation. *ArXiv e-prints*, **803**.
- Kravtsov, A. V., Klypin, A. A., and Khokhlov, A. M. (1997). Adaptive Refinement Tree: A New High-Resolution N-Body Code for Cosmological Simulations. *ApJS*, **111**, 73–+.
- Kravtsov, A. V., Gnedin, O. Y., and Klypin, A. A. (2004). The Tumultuous Lives of Galactic Dwarfs and the Missing Satellites Problem. *ApJ*, **609**, 482–497.
- Kuhlen, M., Diemand, J., and Madau, P. (2007). The Shapes, Orientation, and Alignment of Galactic Dark Matter Subhalos. *ApJ*, **671**, 1135–1146.
- Larson, R. B., Tinsley, B. M., and Caldwell, C. N. (1980). The evolution of disk galaxies and the origin of S0 galaxies. *ApJ*, **237**, 692–707.
- Leeuwin, F., Combes, F., and Binney, J. (1993). N-body simulations with perturbation particles. I - Method and tests. *MNRAS*, **262**, 1013–1022.
- Lesgourgues, J., Polarski, D., and Starobinsky, A. A. (1998). CDM models with a BSI step-like primordial spectrum and a cosmological constant. *MNRAS*, **297**, 769–776.

- Li, S., Li, H., and Cen, R. (2008a). CosmoMHD: A Cosmological Magnetohydrodynamics Code. *ApJS*, **174**, 1–12.
- Li, Y.-S., Helmi, A., De Lucia, G., and Stoehr, F. (2008b). On the common mass scale of the Milky Way satellites. *ArXiv e-prints*.
- Lin, D. N. C., Jones, B. F., and Klemola, A. R. (1995). The motion of the Magellanic clouds, origin of the Magellanic Stream, and the mass of the Milky Way. *ApJ*, **439**, 652–671.
- Little, B., Knebe, A., and Islam, R. R. (2003). Warm dark matter versus bumpy power spectra. *MNRAS*, **341**, 617–622.
- Lucy, L. B. (1977). A numerical approach to the testing of the fission hypothesis. *AJ*, **82**, 1013–1024.
- Lukić, Z., Heitmann, K., Habib, S., Bashinsky, S., and Ricker, P. M. (2007). The Halo Mass Function: High-Redshift Evolution and Universality. *ApJ*, **671**, 1160–1181.
- Macciò, A. V., Dutton, A. A., van den Bosch, F. C., Moore, B., Potter, D., and Stadel, J. (2007). Concentration, spin and shape of dark matter haloes: scatter and the dependence on mass and environment. *MNRAS*, **378**, 55–71.
- Maccio’, A. V., Kang, X., and Moore, B. (2008). Central mass and luminosity of Milky Way satellites in the LCDM model. *ArXiv e-prints*.
- Majewski, S. R., Skrutskie, M. F., Weinberg, M. D., and Ostheimer, J. C. (2003). A Two Micron All Sky Survey View of the Sagittarius Dwarf Galaxy. I. Morphology of the Sagittarius Core and Tidal Arms. *ApJ*, **599**, 1082–1115.
- Markevitch, M. (2006). Chandra Observation of the Most Interesting Cluster in the Universe. In A. Wilson, editor, *The X-ray Universe 2005*, volume 604 of *ESA Special Publication*, pages 723–+.
- Martin, J., Riazuelo, A., and Sakellariadou, M. (2000). Nonvacuum initial states for cosmological perturbations of quantum-mechanical origin. *Phys. Rev. D*, **61**(8), 083518–+.
- Martínez-Delgado, D., Gómez-Flechoso, M. Á., Aparicio, A., and Carrera, R. (2004). Tracing Out the Northern Tidal Stream of the Sagittarius Dwarf Spheroidal Galaxy. *ApJ*, **601**, 242–259.
- Mastropietro, C., Moore, B., Mayer, L., Wadsley, J., and Stadel, J. (2005). The gravitational and hydrodynamical interaction between the Large Magellanic Cloud and the Galaxy. *MNRAS*, **363**, 509–520.
- McGaugh, S. S. and de Blok, W. J. G. (1998). Testing the Hypothesis of Modified Dynamics with Low Surface Brightness Galaxies and Other Evidence. *ApJ*, **499**, 66–+.
- McGaugh, S. S., de Blok, W. J. G., Schombert, J. M., Kuzio de Naray, R., and Kim, J. H. (2007). The Rotation Velocity Attributable to Dark Matter at Intermediate Radii in Disk Galaxies. *ApJ*, **659**, 149–161.

- Merritt, D. (1983). Relaxation and tidal stripping in rich clusters of galaxies. I - Evolution of the mass distribution. *ApJ*, **264**, 24–48.
- Merritt, D. (1984). Relaxation and tidal stripping in rich clusters of galaxies. II - Evolution of the luminosity distribution. *ApJ*, **276**, 26–37.
- Metz, M., Kroupa, P., and Jerjen, H. (2007). The spatial distribution of the Milky Way and Andromeda satellite galaxies. *MNRAS*, **374**, 1125–1145.
- Metz, M., Kroupa, P., and Libeskind, N. I. (2008). The Orbital Poles of Milky Way Satellite Galaxies: A Rotationally Supported Disk of Satellites. *ApJ*, **680**, 287–294.
- Milgrom, M. (1983). A modification of the Newtonian dynamics as a possible alternative to the hidden mass hypothesis. *ApJ*, **270**, 365–370.
- Milgrom, M. (1994). Modified dynamics predictions agree with observations of the HI kinematics in faint dwarf galaxies contrary to the conclusions of Lo, Sargent, and Young. *ApJ*, **429**, 540–544.
- Milgrom, M. (1998). Galaxy Groups and Modified Dynamics. *ApJ*, **496**, L89+.
- Monaghan, J. J. (1992). Smoothed particle hydrodynamics. *ARA&A*, **30**, 543–574.
- Moore, B., Katz, N., Lake, G., Dressler, A., and Oemler, A. (1996). Galaxy harassment and the evolution of clusters of galaxies. *Nature*, **379**, 613–616.
- Moore, B., Ghigna, S., Governato, F., Lake, G., Quinn, T., Stadel, J., and Tozzi, P. (1999). Dark Matter Substructure within Galactic Halos. *ApJ*, **524**, L19–L22.
- Mortlock, D. J. and Turner, E. L. (2001). Gravitational lensing in modified Newtonian dynamics. *MNRAS*, **327**, 557–566.
- Navarro, J. F., Hayashi, E., Power, C., Jenkins, A. . R., Frenk, C. S., White, S. D. M., Springel, V., Stadel, J., and Quinn, T. R. (2004). The inner structure of Λ CDM haloes - III. Universality and asymptotic slopes. *MNRAS*, **349**, 1039–1051.
- Newberg, H. J., Yanny, B., Rockosi, C., Grebel, E. K., Rix, H.-W., Brinkmann, J., Csabai, I., Hennessy, G., Hindsley, R. B., Ibata, R., Ivezić, Z., Lamb, D., Nash, E. T., Odenkirchen, M., Rave, H. A., Schneider, D. P., Smith, J. A., Stolte, A., and York, D. G. (2002). The Ghost of Sagittarius and Lumps in the Halo of the Milky Way. *ApJ*, **569**, 245–274.
- Oh, K. S., Lin, D. N. C., and Aarseth, S. J. (1995). On the tidal disruption of dwarf spheroidal galaxies around the galaxy. *ApJ*, **442**, 142–158.
- Okamoto, T. and Habe, A. (1999). Formation and Evolution of Galactic Halos in Clusters of Galaxies. *ApJ*, **516**, 591–603.
- Peñarrubia, J., Benson, A. J., Martínez-Delgado, D., and Rix, H. W. (2006). Modeling Tidal Streams in Evolving Dark Matter Halos. *ApJ*, **645**, 240–255.
- Peebles, P. J. E. (1969). Origin of the Angular Momentum of Galaxies. *ApJ*, **155**, 393–+.

- Peebles, P. J. E. (1970). Structure of the Coma Cluster of Galaxies. *AJ*, **75**, 13–+.
- Peebles, P. J. E. (1982). Large-scale background temperature and mass fluctuations due to scale-invariant primeval perturbations. *ApJ*, **263**, L1–L5.
- Penzias, A. A. and Wilson, R. W. (1965). A Measurement of Excess Antenna Temperature at 4080 Mc/s. *ApJ*, **142**, 419–421.
- Pereira, M. J. and Kuhn, J. R. (2005). Radial Alignment of Cluster Galaxies. *ApJ*, **627**, L21–L24.
- Pereira, M. J., Bryan, G. L., and Gill, S. P. D. (2008). Radial Alignment in Simulated Clusters. *ApJ*, **672**, 825–833.
- Pohlen, M., Martínez-Delgado, D., Majewski, S., Palma, C., Prada, F., and Balcells, M. (2004). Tidal Streams around External Galaxies. In F. Prada, D. Martinez Delgado, and T. J. Mahoney, editors, *ASP Conf. Ser. 327: Satellites and Tidal Streams*, pages 288–+.
- Powell, W. L., Lauchner, A., Wilhelm, R., and McWilliam, A. (2006). Globular Cluster Tidal Streams: An Observational Study. In *Bulletin of the American Astronomical Society*, volume 38 of *Bulletin of the American Astronomical Society*, pages 940–+.
- Power, C., Navarro, J. F., Jenkins, A., Frenk, C. S., White, S. D. M., Springel, V., Stadel, J., and Quinn, T. (2003). The inner structure of Λ CDM haloes - I. A numerical convergence study. *MNRAS*, **338**, 14–34.
- Prada, F., Klypin, A. A., Simonneau, E., Betancort-Rijo, J., Patiri, S., Gottlöber, S., and Sanchez-Conde, M. A. (2006). How Far Do They Go? The Outer Structure of Galactic Dark Matter Halos. *ApJ*, **645**, 1001–1011.
- Press, W. H., Teukolsky, S. A., Vetterling, W. T., and Flannery, B. P. (1992). *Numerical recipes in C. The art of scientific computing*. Cambridge: University Press, —c1992, 2nd ed.
- Primack, J. R. (2003). Status of cold dark matter cosmology. *Nuclear Physics B Proceedings Supplements*, **124**, 3–12.
- Qin, B., Wu, X. P., and Zou, Z. L. (1995). An attempt to empirically evaluate the gravitational deflection of light in the modified Newtonian dynamics. *A&A*, **296**, 264–+.
- Reed, D., Governato, F., Verde, L., Gardner, J., Quinn, T., Stadel, J., Merritt, D., and Lake, G. (2005). Evolution of the density profiles of dark matter haloes. *MNRAS*, **357**, 82–96.
- Reed, D. S., Bower, R., Frenk, C. S., Jenkins, A., and Theuns, T. (2007). The halo mass function from the dark ages through the present day. *MNRAS*, **374**, 2–15.
- Ryu, D., Miniati, F., Jones, T. W., and Frank, A. (1998). A Divergence-free Upwind Code for Multidimensional Magnetohydrodynamic Flows. *ApJ*, **509**, 244–255.

- Sahni, V. and Coles, P. (1995). Approximation methods for non-linear gravitational clustering. *Phys. Rep.*, **262**, 1–135.
- Sanders, R. H. (1996). The Published Extended Rotation Curves of Spiral Galaxies: Confrontation with Modified Dynamics. *ApJ*, **473**, 117–+.
- Sanders, R. H. (1999). The Virial Discrepancy in Clusters of Galaxies in the Context of Modified Newtonian Dynamics. *ApJ*, **512**, L23–L26.
- Sanders, R. H. (2001). The Formation of Cosmic Structure with Modified Newtonian Dynamics. *ApJ*, **560**, 1–6.
- Sanders, R. H. and McGaugh, S. S. (2002). Modified Newtonian Dynamics as an Alternative to Dark Matter. *ARA&A*, **40**, 263–317.
- Scarpa, R., Marconi, G., and Gilmozzi, R. (2003). Using globular clusters to test gravity in the weak acceleration regime. *A&A*, **405**, L15–L18.
- Seljak, U. and Zaldarriaga, M. (1996). A Line-of-Sight Integration Approach to Cosmic Microwave Background Anisotropies. *ApJ*, **469**, 437–+.
- Sethi, S. K. and Subramanian, K. (2005). Primordial magnetic fields in the post-recombination era and early reionization. *MNRAS*, **356**, 778–788.
- Sethi, S. K., Nath, B. B., and Subramanian, K. (2008). Primordial magnetic fields and formation of molecular hydrogen. *ArXiv e-prints*, **804**.
- Spergel, D. N. and Steinhardt, P. J. (2000). Observational Evidence for Self-Interacting Cold Dark Matter. *Physical Review Letters*, **84**, 3760–3763.
- Spergel et al., D. N. (2003). First-Year Wilkinson Microwave Anisotropy Probe (WMAP) Observations: Determination of Cosmological Parameters. *ApJS*, **148**, 175–194.
- Spergel et al., D. N. (2007). Three-Year Wilkinson Microwave Anisotropy Probe (WMAP) Observations: Implications for Cosmology. *ApJS*, **170**, 377–408.
- Springel, V. (2005). The cosmological simulation code GADGET-2. *MNRAS*, **364**, 1105–1134.
- Springel, V., Yoshida, N., and White, S. D. M. (2001). GADGET: a code for collisionless and gasdynamical cosmological simulations. *New Astronomy*, **6**, 79–117.
- Springel, V., White, S. D. M., Jenkins, A., Frenk, C. S., Yoshida, N., Gao, L., Navarro, J., Thacker, R., Croton, D., Helly, J., Peacock, J. A., Cole, S., Thomas, P., Couchman, H., Evrard, A., Colberg, J., and Pearce, F. (2005). Simulations of the formation, evolution and clustering of galaxies and quasars. *Nature*, **435**, 629–636.
- Steinmetz, M. and Navarro, J. F. (1999). The Cosmological Origin of the Tully-Fisher Relation. *ApJ*, **513**, 555–560.

- Steinmetz, M., Zwitter, T., Siebert, A., Watson, F. G., Freeman, K. C., Munari, U., Campbell, R., Williams, M., Seabroke, G. M., Wyse, R. F. G., Parker, Q. A., Bienaymé, O., Roeser, S., Gibson, B. K., Gilmore, G., Grebel, E. K., Helmi, A., Navarro, J. F., Burton, D., Cass, C. J. P., Dawe, J. A., Fiegert, K., Hartley, M., Russell, K. S., Saunders, W., Enke, H., Bailin, J., Binney, J., Bland-Hawthorn, J., Boeche, C., Dehnen, W., Eisenstein, D. J., Evans, N. W., Fiorucci, M., Fulbright, J. P., Gerhard, O., Jauregi, U., Kelz, A., Mijović, L., Minchev, I., Parmentier, G., Peñarrubia, J., Quillen, A. C., Read, M. A., Ruchti, G., Scholz, R.-D., Siviero, A., Smith, M. C., Sordo, R., Veltz, L., Vidrih, S., von Berlepsch, R., Boyle, B. J., and Schilbach, E. (2006). The Radial Velocity Experiment (RAVE): First Data Release. *AJ*, **132**, 1645–1668.
- Strigari, L. E., Bullock, J. S., Kaplinghat, M., Simon, J. D., Geha, M., Willman, B., and Walker, M. G. (2008). A common mass scale for satellite galaxies of the Milky Way. *Nature*, **454**, 1096–1097.
- Suginohara, T. and Suto, Y. (1992). Properties of galactic halos in spatially flat universes dominated by cold dark matter - Effects of nonvanishing cosmological constant. *ApJ*, **396**, 395–410.
- Suisalu, I. and Saar, E. (1995). An adaptive multigrid solver for high-resolution cosmological simulations. *MNRAS*, **274**, 287–299.
- Suto, Y., Cen, R., and Ostriker, J. P. (1992). Statistics of the cosmic Mach number from numerical simulations of a cold dark matter universe. *ApJ*, **395**, 1–20.
- Taffoni, G., Mayer, L., Colpi, M., and Governato, F. (2003). On the life and death of satellite haloes. *MNRAS*, **341**, 434–448.
- Tasitsiomi, A., Kravtsov, A. V., Gottlöber, S., and Klypin, A. A. (2004). Density Profiles of Λ CDM Clusters. *ApJ*, **607**, 125–139.
- Teyssier, R. (2002). Cosmological hydrodynamics with adaptive mesh refinement. A new high resolution code called RAMSES. *A&A*, **385**, 337–364.
- Thompson, L. A. (1976). The Angular Momentum Properties of Galaxies in Rich Clusters. *ApJ*, **209**, 22–34.
- Tormen, G. (1997). The rise and fall of satellites in galaxy clusters. *MNRAS*, **290**, 411–421.
- Tormen, G., Diaferio, A., and Syer, D. (1998). Survival of substructure within dark matter haloes. *MNRAS*, **299**, 728–742.
- Tsuchiya, T. and Shimada, M. (2000). Orbital Deformation of Satellites by Dynamical Friction in Spherical Halos with Anisotropic Velocity Dispersion. *ApJ*, **532**, 294–301.
- van Kampen, E. (1995). Improved numerical modelling of clusters of galaxies. *MNRAS*, **273**, 295–327.
- Villumsen, J. V. (1989). A new hierarchical particle-mesh code for very large scale cosmological N-body simulations. *ApJS*, **71**, 407–431.

- Vitvitska, M., Klypin, A. A., Kravtsov, A. V., Wechsler, R. H., Primack, J. R., and Bullock, J. S. (2002). The Origin of Angular Momentum in Dark Matter Halos. *ApJ*, **581**, 799–809.
- Wang, J. and White, S. D. M. (2007). Discreteness effects in simulations of hot/warm dark matter. *MNRAS*, **380**, 93–103.
- Warnick, K. and Knebe, A. (2006). The sense of rotation of subhaloes in cosmological dark matter haloes. *MNRAS*, **369**, 1253–1266.
- Warnick, K., Knebe, A., and Power, C. (2008). The Tidal Streams of Disrupting Subhaloes in Cosmological Dark Matter Haloes. *MNRAS*, **999**, 0–0.
- Warren, M. S., Quinn, P. J., Salmon, J. K., and Zurek, W. H. (1992). Dark halos formed via dissipationless collapse. I - Shapes and alignment of angular momentum. *ApJ*, **399**, 405–425.
- Wehner, E. H., Gallagher, J. S., Papaderos, P., Fritze-von Alvensleben, U., and Westfall, K. B. (2006). NGC 3310 and its tidal debris: remnants of galaxy evolution. *MNRAS*, **371**, 1047–1056.
- Weinberg, D. H., Hernquist, L., and Katz, N. (1997). Photoionization, Numerical Resolution, and Galaxy Formation. *ApJ*, **477**, 8–+.
- West, M. J. and Blakeslee, J. P. (2000). The Principal Axis of the Virgo Cluster. *ApJ*, **543**, L27–L30.
- White, S. D. M. (1996). Formation and Evolution of Galaxies. In R. Schaeffer, J. Silk, M. Spiro, and J. Zinn-Justin, editors, *Cosmology and Large Scale Structure*, pages 349–+.
- White, S. D. M. and Rees, M. J. (1978). Core condensation in heavy halos - A two-stage theory for galaxy formation and clustering. *MNRAS*, **183**, 341–358.
- White, S. D. M., Frenk, C. S., and Davis, M. (1983). Clustering in a neutrino-dominated universe. *ApJ*, **274**, L1–L5.
- Xu, H., Collins, D. C., Norman, M. L., Li, S., and Li, H. (2008). A Cosmological AMR MHD Module for Enzo. In *First Stars III*, volume 990 of *American Institute of Physics Conference Series*, pages 36–38.
- Yanny, B., Newberg, H. J., Grebel, E. K., Kent, S., Odenkirchen, M., Rockosi, C. M., Schlegel, D., Subbarao, M., Brinkmann, J., Fukugita, M., Ivezić, Ž., Lamb, D. Q., Schneider, D. P., and York, D. G. (2003). A Low-Latitude Halo Stream around the Milky Way. *ApJ*, **588**, 824–841.
- Yoshizawa, A. M. and Noguchi, M. (2003). The dynamical evolution and star formation history of the Small Magellanic Cloud: effects of interactions with the Galaxy and the Large Magellanic Cloud. *MNRAS*, **339**, 1135–1154.
- Zaritsky, D., Smith, R., Frenk, C. S., and White, S. D. M. (1997). Anisotropies in the Distribution of Satellite Galaxies. *ApJ*, **478**, L53+.

-
- Zel'dovich, Y. B. (1970). Gravitational instability: An approximate theory for large density perturbations. *A&A*, **5**, 84–89.
- Ziegler, U. (2005). Self-gravitational adaptive mesh magnetohydrodynamics with the NIRVANA code. *A&A*, **435**, 385–395.

Acknowledgment

I want to thank all persons, who contributed to this thesis by some means or the other. The list is way too long to be summarized here and includes basically all co-authors on my publications.

The only person I like to mention by name is my ex-wife Anne Christin Knebe; she has been with me through all the ups and downs during the time that was required to collate the research that eventually made it into this Habilitation.

*“I wish I would have known, wish I would have seen,
I wish I’d had some lines to read between”
(The Perishers)*

Erklärungen

Hiermit erkläre ich, dass die vorliegende Habilitationsschrift von mir selbst und ohne fremde Hilfe verfasst wurde. Alle benutzten Quellen sind im Literaturverzeichnis angegeben.

Die Arbeit hat in gleicher oder ähnlicher Form noch keiner Prüfungsbehörde vorgelegen. Ich versichere weiterhin, dass von mir kein früherer Habilitationsantrag gestellt wurde.

Desweiteren erkläre ich, von der Habilitationsordnung der Universität Potsdam vom 25.11.1999 Kenntnis genommen zu haben.

Dr. Alexander Knebe

Potsdam, 5. November 2008